Metabolic support of regulatory T cells by lactic acid

by

McLane J. Watson

Bachelor of Sciences, Hope College, 2015

Submitted to the Graduate Faculty of the

School of Medicine in partial fulfillment

of the requirements for the degree of

Doctor of Philosophy

University of Pittsburgh

2021

UNIVERSITY OF PITTSBURGH

SCHOOL OF MEDICINE

This thesis was presented

by

McLane J. Watson

It was defended on

October 26, 2021

and approved by

Heth R. Turnquist, Associate Professor, Department of Surgery

Dario A.A. Vignali, Professor, Department of Immunology

Amanda C. Poholek, Assistant Professor, Department of Pediatrics

Stacy G. Wendell, Associate Professor, Department of Pharmacology and Chemical Biology

Dissertation Director: Greg Delgoffe, Associate Professor, Department of Immunology

Metabolic support of tumor infiltrating regulatory T cells by lactic acid

McLane J. Watson, PhD

University of Pittsburgh, 2021

Regulatory T (T_{reg}) cells, although vital for immune homeostasis, also represent a major barrier to anti-cancer immunity, as the tumor microenvironment (TME) promotes the recruitment, differentiation, and activity of these cells[1,2]. Tumor cells show deregulated metabolism, leading to a metabolite-depleted, hypoxic and acidic TME[3], which places infiltrating effector T cells in competition with the tumor for metabolites and impairs their function[4–6]. At the same time, T_{reg} cells maintain a strong suppression of effector T cells within the TME[7,8]. As previous studies suggested that T_{reg} cells possess a distinct metabolic profile from effector T cells[9–11], we hypothesized that the altered metabolic landscape of the TME and increased activity of intratumoral T_{reg} cells are linked. Here we show that T_{reg} cells display broad heterogeneity in their metabolism of glucose within normal and transformed tissues and can engage an alternative metabolic pathway to maintain suppressive function and proliferation. Glucose uptake correlates with poorer suppressive function and long-term instability, and high-glucose conditions impair the function and stability of T_{reg} cells in vitro. T_{reg} cells instead upregulate pathways involved in the metabolism of the glycolytic by-product lactic acid. T_{reg} cells withstand high-lactate conditions, and treatment with lactate prevents the destabilizing effects of high-glucose conditions, generating intermediates necessary for proliferation. Lactic acid also contributes directly to epigenetic modifications through histone lactylation which may support the expression of T_{reg} cell signature genes. Deletion of MCT1—a lactate

transporter—in T_{reg} cells reveals that lactate uptake is dispensable for the function of peripheral T_{reg} cells but required intratumorally, resulting in slowed tumor growth and an increased response to immunotherapy. Thus, T_{reg} cells are metabolically flexible: they can use ‘alternative’ metabolites in the TME to maintain their suppressive identity. Further, our results suggest that tumors avoid destruction by not only depriving effector T cells of nutrients, but also metabolically supporting regulatory populations.

Table of Contents

List of Figures

Preface

Acknowledgements

The authors wish to thank Amanda Burton and Creg Workman for the generation and gift of the *Foxp3*$^{\text{FlpO-Ametrine}}$ mice and Geoffrey Camirand for the gift of OT-II Foxp3RFP Thy1.1 spleens. This work was supported by the Sidney Kimmel Foundation, an NIH Director's New Innovator Award (DP2AI136598), the Hillman Fellows for Innovative Cancer Research Program, a Stand Up to Cancer-American Association for Cancer Research Innovative Research Grant (SU2C-AACR-IRG-04-16), Swim Across America/Alliance for Cancer Gene Therapy Young Investigator Award, the UPMC Hillman Cancer Center Melanoma/Skin Cancer and Head and Neck Cancer SPOREs (P50CA121973-09 and P50CA097190), R21AI135367, and the Sy Holzer Endowed Immunotherapy Fund (all to G.M.D.). D.A.A.V is supported by R01DK089125, R01CA203689 and P01AI108545. Trainees on this manuscript were supported by T32CA082084 (to M.J.W., P.D.A.V., A.E.O.D., and K.D.), F31AI149971 (to M.J.W.), F30CA247034 (to P.D.A.V.), T32AI089443 (to R.M.P and S.G.), F31AI147638 (to S.G.), and a Damon Runyon Cancer Research Fellowship (A.E.O.D.). Mass spectrometry was supported by S10OD023402 (to S.G.W.), and floxed animal generation was supported by R01NS099320 (to J.D.R., and B.M.M). as well as R01 NS086818 (to B.M.M.). Sequencing was supported by the Samuel and Emma Winters Foundation and a Grand Prize Award Grant (2017) from the Immuno-Oncology Young Investigators' Forum (both to G.M.D.) and was performed at the University of Pittsburgh Health Sciences Sequencing Core at Children's Hospital of Pittsburgh. RNA sequencing analysis was

supported in part by the University of Pittsburgh Center for Research Computing through the resources provided. This work utilized the UPMC Hillman Cancer Center Flow Cytometry and Animal Facilities, supported in part by P30CA047904.

1.0 Introduction: “Toxic” Metabolites and implications for immunotherapy

1.1 Foreword

This chapter was adapted from an accepted review in JCI: McLane J. Watson, Greg M. Delgoffe. “Fighting in a wasteland: deleterious metabolites and antitumor immunity” *JCI* 2021.

1.2 Toxic metabolites in the tumor microenvironment

Cancer immunotherapy has revolutionized the treatment of cancer, unlocking the door to durable disease-free states in a subset of patients. Accompanying this major advancement is an improved understanding of the interaction of the immune system and cancer as well as major barriers preventing successful anti-tumor immunity. One such barrier is the harsh metabolic landscape of the tumor microenvironment (TME). It is well appreciated that tumor cells are metabolically deranged [3] resulting in a hypoxic, acidic, glucose- and amino acid-deprived environment. Many tumors undergo “Warburg metabolism” or “aerobic glycolysis”, the process of performing glycolysis despite the presence of adequate oxygen, to meet their biosynthetic and energetic needs [12–14]. In addition, rapid proliferation and aberrant cell signaling results in inadequate vasculature and thus poor oxygenation of the TME (more on how tumor cells deplete metabolites can be found here [15,16]). Many have investigated and discussed how the lack of these

metabolites inhibits infiltrating effector immune cells, such as NK cells, macrophages, $CD8^+$ and $CD4^+$ T cells. While these perspectives are incredibly important, the tumor is not a metabolic vacuum, only consuming and never producing. Therefore, while tumor cells deplete glucose, oxygen, and amino acids, the metabolites they produce are equally, if not more, important in shaping immune cell function and response to immunotherapy. The rules of the game are changing as technology and methods allow us to probe deeper into the true interactions between immune cell metabolism and the TME in vivo. We can no longer rely on the simple model of tumors starving immune cells but must also consider the impact of the "toxic" catabolites produced in shaping immune cell function. Moreover, the metabolic landscape of the TME, while distinct, is not unique as catabolites such as lactic acid, kynurenine, adenosine, and ROS are regularly encountered in various tissues and immunologic contexts. It is these non-tumor contexts that have evolutionarily shaped the immune cell-catabolite interactions that play out in the TME. Therefore, it is important to view the TME as one of many metabolic contexts immune cells may find themselves and to seek metabolic insight about tumor infiltrating lymphocytes from non-tumor contexts. This perspective will be crucial when implementing metabolic strategies to improve immunotherapy by understanding how these therapies may impact typical immunity.

Tumor cells both deplete vital nutrients and produce "toxic" catabolites. From glucose to lactic acid, tryptophan to kynurenine, molecular oxygen to ROS, the tumor produces metabolites that shape immune cell function (**Figure 1**), and this may be therapeutically targeted. Here we review the metabolic landscape of the tumor from the perspective of metabolite abundance rather than scarcity, discussing how lactic acid,

kynurenine, ROS, and adenosine shape immune cell function and how these are being targeted to improve immunotherapy.

1.3 Lactic acid

A study analyzing metabolomics data from over 900 samples spanning seven different cancer types identified lactic acid as a consistently upregulated metabolite [17]. Within the TME lactic acid is derived from highly glycolytic tumor cells fermenting glucose to pyruvate then lactate via Lactate dehydrogenase (LDH). Lactate and protons are then co-exported producing extracellular lactic acid. In normal serum, lactate concentrations range from 1.5-3 mM [18], while tumor concentrations can range from 10-30 mM, reaching extremely high levels (50 mM) within necrotic tumor cores [19]. Indeed, elevated levels of lactic acid indicate poor prognosis in several cancer types including cervical [18], breast [20], head and neck cancer [19,21], high grade gliomas [22], and non-small cell lung cancer [23].Therefore, it comes as no surprise that lactic acid especially at tumor-equivalent concentrations, has profound effects on infiltrating immune cells (**Figure 1**). Emerging is lactate's role as a major carbon source for many cell types in a homeostatic state [24]. This is a prime example of how a toxic metabolite within the tumor is encountered in non-tumor contexts. Using infusions of ^{13}C-labeled glucose and lactate into live mice, Hui et al demonstrated that lactate, more than glucose, extensively contributes to the TCA cycle in all tissues examined. Indeed, even T cells, both effectors and T_{reg} cells, can utilize lactate to feed the TCA cycle [25,26]. By studying effector T cell metabolism through in vitro culture in glucose-rich medias, the field has likely overestimated the importance of

glycolysis for effector functions. In vivo carbon tracing has revealed that physiologically activated $CD8^+$ T cells display an increased oxidative metabolism, in addition to a high glycolytic rate, compared to their in vitro activated counterparts, opening the possibility that smaller carbon substrates like lactate play a larger role in effector $CD8^+$ T cell metabolism than previously appreciated [27]. These studies highlight the importance of lactate in shaping immune cell metabolism far before they enter the TME. Further detail on lactate-immune cell interaction in non-tumor tissues can be found here[28–30]. Understanding how immune cells metabolize in vivo under physiological conditions will be key to developing successful metabolism-targeted therapies for the improvement of immunotherapy.

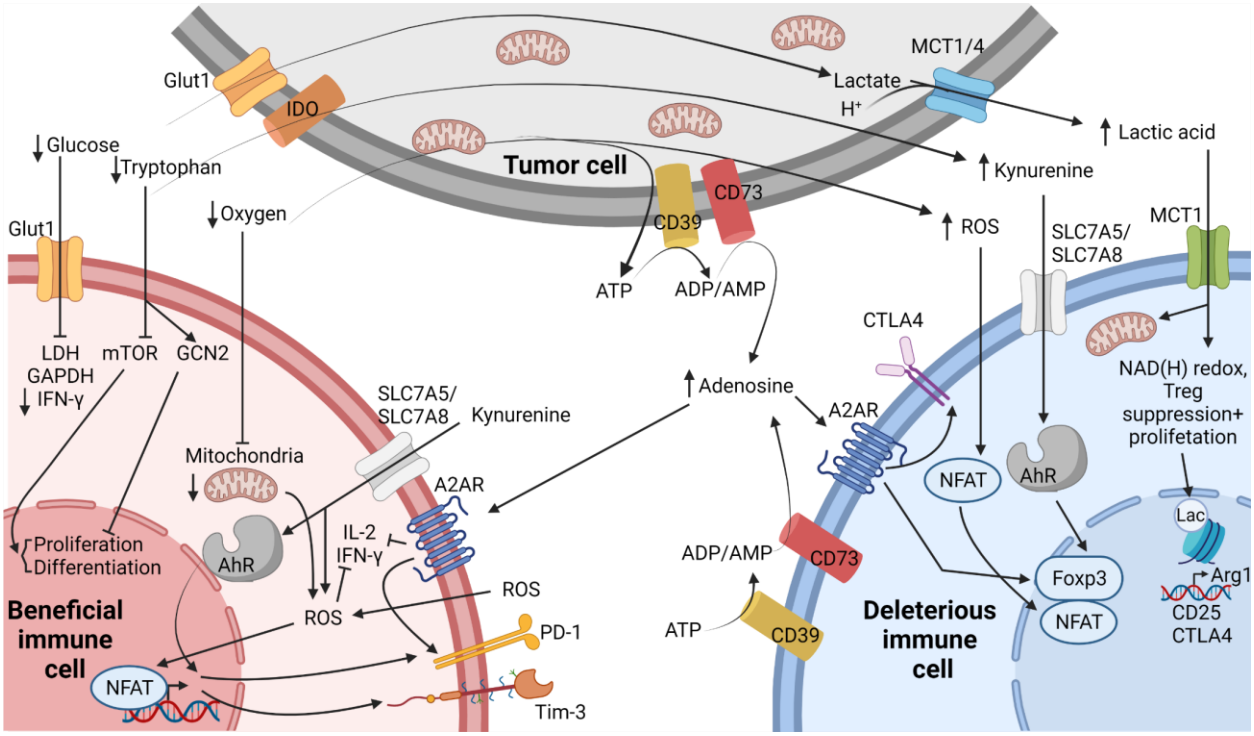

Figure 1. Depletion of key nutrients and production of toxic byproducts impair effector cells but support regulatory cells. Depletion of key nutrients in the TME leads to accumulation of "toxic" metabolites adding to the immunosuppression of nutrient deprivation alone. Beneficial cells, such as CD8+ and CD4+ effector T cells (Teff) are depicted left, with deleterious cells, including T_{reg} cells and TAMs, depicted right. Highly glycolytic tumor cells import glucose via GLUT1 and ferment it to lactate, which is co-exported with protons into the TME via MCT1/4. Glucose deprivation impairs Teff cell glycolytic capacity, key for their proliferation and translation of IFN-γ protein. Lactic acid impairs Teff cell proliferation by altering NAD(H) redox balance. Import and utilization of lactic acid via MCT1 supports T_{reg} proliferation and suppressive function. Lactic acid contributes to histone lactylation which supports the expression of M2-like genes such as Arg1 in macrophages. Tryptophan is depleted via IDO expressed by MDSCs, TAMs, and tumor cells. Depletion of tryptophan triggers the stress response kinase GCN2 and suppresses the mTOR pathway, reducing proliferation, altering memory differentiation, reducing activation of Teff cells, and inducing a regulatory phenotype in naïve T cells. Kynurenine is imported via SLC7A5/8 where it engages with AhR to increase PD-1 and Foxp3 expression. Kynurenine induced ROS inhibits IL-2 signaling critical for T cell survival. Depletion of oxygen in the TME inhibits oxidative metabolism and decreases

mitochondrial mass of CD8 T cells. ROS both intra- and extra-cellularly drives partnerless Nuclear factor of activated T cells (NFAT) signaling and expression of PD-1 and Tim-3 in CD8 T cells while promoting NFAT/Foxp3 signaling in T_{reg} cells. Oxygen depletion promotes extracellular accumulation of ATP which is broken down to adenosine by cell surface ectonucleotidases CD39 and CD73. Adenosine acts through the adenosine A2A receptor (A2AR) to impair IL-2 and IFN-γ production and increase PD-1 expression in Teff cells, while activating Foxp3 and CTLA4 expression to promote the development of T_{reg} cells. (Created with Biorender.com)

In general, lactate/lactic acid acts as an immunosuppressive metabolite. Indeed, activating effector CD8+ and CD4+ T cells in vitro in tumor equivalent concentrations of lactic acid reduces their proliferation and capacity to produce cytokine [25,26,31]. The presence of tumor-derived lactic acid acts as a double-edge sword, for where there is lactic acid there is glucose deprivation, both of which independently impact effector T cell function. As mentioned above, effector CD8 and CD4 T cells rely on glycolysis for translation of IFN-γ and proliferation [27,32–35]. While restricting glucose uptake helps promote CD8+ T cell memory formation, glucose is still critical for short-lived effector CD8+ T cells [36]. However, tumor infiltrating T cells experience glucose deprivation and lactic acid simultaneously. Several studies demonstrate that both lactate and lactic acid impair CD8+ and CD4+ effector T cell proliferation and cytokine production even in the presence of sufficient glucose [25,26]. Deeper mechanistic studies revealed lactate works to limit T cell proliferation via the NAD(H) redox state, reducing NAD+ to NADH in lactate-rich conditions, resulting in altered NAD+-dependent enzymatic reactions and thus decreased glycolytic intermediates needed for proliferation [37]. These data reveal a balance, as T cells are in constant contact with serum lactate and thus have a threshold for withstanding some lactate impairment. This threshold is likely determined at the level

of lactate transport via solute carries, like monocarboxylate transporter 1 (MCT1, encoded by *Slc16a1*). MCT1 is a bi-directional proton assisted transporter with highest affinity for lactate [38]. Directionality of transport is determined by both substrate and H^+ ion concentration, thus T cells entering the TME likely experience an influx of lactic acid followed by changes in redox balance and impairment in proliferation and effector function, reducing tumor control [39]. Of note, succinate, another MCT1 substrate [40,41], can also be found at high levels within tumors and can mediate tumor associated macrophage (TAM) polarization, metastasis, and angiogenesis suggesting short chain fatty acids act similarly within the TME[42,43].

Recent findings suggest that glucose may not be as limited in the TME as previously thought, meaning lactic acid could be contributing more to T cell dysfunction than lack of glucose [44]. Pulsing mice bearing MC38 tumors (an immunogenic colon tumor model) with ^{18}F-fluorodeoxyglucose (FDG) then measuring uptake directly ex vivo revealed that tumor infiltrating CD3+ T cells had similar FDG avidity to the MC38 cancer cells. While CD3+ T cells were not the highest FDG consumers, these data suggest T cells have adequate access to and can compete for glucose within the TME. In addition, glycolysis was still occurring within the tumor and myeloid cell compartment, suggesting T cells were experiencing lactic acid.

Not all immune cells respond negatively to tumor-derived lactic acid. The TME actively recruits and promotes the differentiation of T_{reg} cells, a subset of CD4+ T cells that express the transcription factor Foxp3[1,2]. T_{reg} cells are potent suppressors of the immune system, tasked with maintaining immune homeostasis and preventing autoimmunity. Unlike effector cells, T_{reg} cells do not rely on glycolysis to meet their

metabolic demands[9,10,25,26,45], but rely more heavily on oxidative metabolism including lipid synthesis and signaling[11,46]. The diminished glucose metabolism and reliance on alternative metabolites primes T_{reg} cells to thrive in the glucose-depleted TME and exert their immunosuppressive function. In contrast to effector T cells, lactic acid was shown to be critical for tumor infiltrating T_{reg} proliferation and function [26]. Carbon tracing experiments revealed that lactic acid-supported proliferation was dependent upon the generation of phosphoenolpyruvate (PEP), the starting intermediate for gluconeogenesis[26]. Tumor-infiltrating T_{reg} proliferation also likely relies on NAD(H) redox state, as Angelin et al observed an increased NAD/NADH ratio in the presence of lactate in Foxp3+ iT_{reg} cells compared to Foxp3- T_{conv} cells[25]. Additionally, lactate influenced NAD/NADH ratio may play a role in T_{reg} suppressive function, as genetic impairment of complex I of the electron transport chain can lower NAD/NADH ratios and reduce T_{reg} suppressive function[25]. Consistent with these data is the observation that T_{reg}-specific loss of the lactate transporter MCT1 reduced their suppressive capacity and proliferation within the tumor microenvironment[26]. Interestingly, T_{reg} suppressive function positively correlated with the glycolytic activity of the tumors from which they were isolated, suggesting that lactic acid can enhance T_{reg} suppressive capacity. Further research is needed to identify how NAD(H) redox balance in T_{reg} cells influences suppression and proliferation and whether this is the main mechanism by which lactic acid bolsters T_{reg} cells within the tumor.

Lactic acid also impacts innate immune cells. Lactic acid was found to polarize macrophages towards an M2-like/TAM-like state, including increased Arginase 1 (Arg1) expression [47]. Not only was lactic acid polarizing, but TAMs were found to have increased

utilization of lactic acid. M2-like macrophages are known to be immunosuppressive [48], supporting the idea that cells that share a metabolism share a function. A potential mechanism for lactic acid's influence on macrophage and T_{reg} function may come through its contribution to histone lactylation and thus altered epigenetics [49]. Zhang et al identified that histones can undergo modification by lactylation, a histone mark with distinct dynamics compared to acetylation[49]. Increasing histone lactylation late in M1 macrophage polarization resulted in increased Arg1 and other wound-healing associated gene expression, suggesting a shift to the immunosuppressive M2 macrophage phenotype. Lactylation may play a similar role in T_{reg} cells to induce or fortify the expression of immunosuppressive genes. Further research into lactate utilization by immune cells and its ability to drive a suppressive phenotype is warranted.

1.4 Kynurenine

Another metabolite consistently upregulated across multiple tumor types is kynurenine [17]. Like lactic acid, kynurenine (kyn) is an immunosuppressive byproduct derived from the depletion of a critical metabolite, in this case tryptophan. Tryptophan is one of nine essential amino acids required by humans and plays roles in protein synthesis, serotonin production, and immune cell regulation [50,51]. Depletion of tryptophan and production of kyn is driven by three rate-limiting enzymes, IDO1 (indoleamine 2,3-dioxygenase 1), IDO2, and TDO (tryptophan 2,3-dioxygenase). Many studies have focused on IDO1 as the main contributor to tryptophan depletion because TDO tissue expression is relatively restricted [52–54], and while IDO2 is widely expressed, it has a

reduced capacity for breaking down tryptophan and its role in inflammation is debated [55–58]. IDO1 is expressed by many cell types, including immune cells, epithelial cells, cancer cells, and fibroblasts. IDO1 expression is greatly enhance by IFN-γ generated during tissue inflammation and acts as a negative feedback loop to curb excessive inflammation [59–61]. This explains the paradoxical expression of IDO1 on some pro-inflammatory cells such as M1 macrophages [62].

Beyond the tumor, kynurenine plays a role in shaping the immune cell function. Kynurenine was found to be key in regulating maternal fetal tolerance, as pharmacological inhibition of IDO in mice resulted in maternal T cell-mediated rejection of allogeneic fetuses [63]. In addition, kyn plays a role in the maintenance of immune privileged sites, such as the eyes and the brain (reviewed in [50]). While the TME takes advantage of the immunosuppressive nature of IDO1 and kyn, tumors did not “patent” this mechanism, but rather utilized what evolved to maintain immune privilege. This perspective is critical as new in vivo techniques shift our understanding of the TME metabolic landscape and we identify new or underappreciated metabolites with a large physiological role in shaping immune function [27,44].

Like glucose and lactic acid, tryptophan depletion and kyn production have independent immunosuppressive effects (**Figure 1**). Depletion of tryptophan triggers the stress response kinase GCN2 (general control nondepressible 2) and suppresses the mTOR pathway resulting in reduced proliferation and activation of effector T cells as well as inducing a regulatory phenotype in naïve T cells [64,65]. Independently, kyn can suppress through several mechanisms including a) promoting tolerogenic antigen presenting cell differentiation [66,67] b) promoting T_{reg} differentiation via the aryl hydrocarbon receptor

(AhR) [68,69], c) and inhibiting IL-2 signaling [70]. It is well established that many tumor types express IDO1, with high expression associated with poor prognosis and increased presence of tumor infiltrating T_{reg} cells [71–75]. Kyn can also have a direct impact on effector T cells as T cell receptor (TCR) stimulation can increase kyn uptake via *Slc7a5/Slc7a8*, leading to increased PD-1 expression induced by AhR ligation [76,77]. Of note, many in vitro experiments use much higher concentrations of kyn to impair T cells than what is found in vivo [78,79] putting into question its clinical significance. However, the kynurenine pathway produces several different metabolites, with kyn itself able to be further metabolized, making it difficult to understand kyn's full impact in vivo. Treating mice with a specific kyn depleting enzyme improve tumor growth and enhanced immunotherapy indicating in vivo concentrations of kyn may still be clinically relevant [79]. Ultimately, lack of tryptophan and production of kyn impair activation of tumor infiltrating effector T cells critical for clearing tumors and promote the presence of immunosuppressive T_{reg} cells. Tryptophan depletion and kyn production are employed to create an immunosuppressive environment, which at steady state maintains immune tolerance, but in tumors is exploited to evade immune destruction.

1.5 ROS and adenosine

Many tumors, if not all, experience some level of oxygen depletion (hypoxia) [80]. Oxygen depletion occurs from the poor vascularization and high metabolic demand of the tumor outpacing the available oxygen supply. As with glucose and tryptophan depletion, oxygen depletion is accompanied by the production of "toxic" byproducts such as ROS

and adenosine, which have been a heavy focus in cancer research [81,82]. ROS is produced as a normal part of oxidative metabolism and is important for normal cell survival, signaling, and homeostasis [83]. However, cancer takes advantage of ROS using its overproduction, among other things, to drive mitogenic signaling pathways, metastasis, and survival [84,85]. In addition to ROS, tumor hypoxia drives the accumulation of extracellular ATP, which is broken down to the immunosuppressive metabolite adenosine [86,87]. ATP release and adenosine generation can act on purinergic receptors to impair immune cell infiltration and activation, thus decreasing anti-tumor immunity [88,89]. While tumor-derived ROS and adenosine have been extensively investigated, there remains a deep interest in understanding and manipulating their impact on immune cells to improve cancer therapies.

As with lactic acid and kyn, ROS plays an important role in shaping immune cell function in non-tumor contexts. For example, upon encounter with microbial invaders, innate immune cells utilize NADPH oxidase (NOX)-derived superoxide to disrupt iron-sulfur centers and kill microorganisms [90]. ROS can also act in chemotaxis, signaling neutrophils and other immune cells to sites of injury or infection and even activate and mature dendritic cells [91–94]. In fact, even T cell activation requires some level of mitochondrial ROS (mROS) production [95]. In contrast, ROS can also play an anti-inflammatory role, as ROS produced by antigen presenting cells is critical for suppressing autoreactive T cells in a model of arthritis [96,97]. In humans, mutations in NOX2 (NADPH oxidase) leads to chronic granulomatous disease (CGD) in which recurrent and severe infections are associated with an increased and prolonged inflammatory gene profile in neutrophils compared to healthy controls [98]. These findings highlight that innate and

adaptive immune systems are tuned by ROS far before entering the TME. What makes the TME distinct is the continuous and high levels of ROS compared to normal tissue, pushing infiltrating immune cells to respond at the extreme end of their previous attunement.

Like other toxic byproducts discussed, high levels of ROS impair effector T cells within the TME (**Figure 1**). The metabolic fitness and anti-tumor efficacy of CD8 T cells relies heavily on oxidative metabolism. CD8 T cells that infiltrate the TME experience a loss of mitochondrial mass and decreased cytokine production which can be rescued by over-expressing the regulator of mitochondrial biogenesis PGC1α (PPAR-gamma coactivator 1 alpha) [4]. Further, more oxidative (thus more hypoxic) TMEs are associated with increased CD8 T cell exhaustion and decreased response to anti-PD1 immunotherapy [5,99]. Recent mechanistic insight revealed that continuous TCR stimulation and hypoxia drive increased mROS production by CD8 T cells which is sufficient to induce an exhaustion-like phenotype [100]. Overexpression of Gpx1, a glutathionine peroxidase capable of acting on a variety of ROS, reduced ROS accumulation and increased IFN-γ production by tumor infiltrating CD8 T cells. These data are consistent with T cell response to macrophage-derived ROS, as this also impairs IFN-γ production [96]. In addition, myeloid derived suppressor cells (MDSCs), an abundant suppressive cell population within tumors, can impair antigen recognition by CD8 T cells in a ROS-dependent manner [101].

In addition to impairing effector cells, high levels of ROS can support regulatory populations (**Figure 1**). Some evidence suggests macrophage derived ROS may induce the formation of peripheral T_{reg} cells [102]. Consistent with this is the finding that ROS,

including tumor-derived ROS, can trigger the accumulation of SENP3 (SUMO-specific protease 3), a protein crucial for deSUMOlylation of BACH2, in T_{reg} cells, which results in the repression of effector CD4 T cell associated genes [103]. In addition to T_{reg} cells, MDSCs represent a major immunosuppressive population within the TME. Like T_{reg} cells, MDSC formation appears to be supported by oxidative stress-prone tissues [104]. MDSCs display a high level of oxidative metabolism which is key to their suppressive capacity [105]. Nuclear factor (erythroid-derived 2)-like 2 (Nrf2), a key antioxidant protein, was identified as key player in promoting and maintaining MDSC identity by balancing redox levels within the cell [105]. MDSCs also utilize ROS to suppress effector T cell responses. In particular, expression of NOX2, a generator of extracellular ROS, was found to be required on MDSCs for the suppression of T cells and maintenance of MDSC identity [106]. Taken together, ROS at low levels is vital for normal immune functioning but at high levels in the TME promote the dysfunction of effector cells and the presence of regulatory populations.

Adenosine is a potent immunosuppressive metabolite both impairing effector cells and supporting regulatory cells (**Figure 1**). Within the TME, adenosine is derived via the cell surface ectonucleotidases CD39 and CD73 expressed by both tumor cells and infiltrating immune cells. Hypoxia drives HIF1A activity which in turn upregulates CD39, CD73, and the adenosine receptor A2BR [107–109]. Extracellular ATP is converted to ADP and/or AMP by CD39 while AMP is converted to adenosine by CD73 [82]. Adenosine then binds to one of four receptors, A1R, A2AR, A2BR, or A3R, to exert its regulatory functions. While A1R, A2AR, and A3R have high affinity for adenosine, A2AR and A2BR signal through cyclic AMP (cAMP), which is associated with profound immunosuppression [110–112]. Signaling through A2AR and A2BR can decrease IFN-γ and IL-2 production and

increase the inhibitory molecule PD-1 in effector cells, and can activate Foxp3, CTLA4, and Lag3, promoting the development of T_{reg} cells [82].

It is important to note that co-expression of CD39 and CD73 on the same cell is not required to produce adenosine. While cells such as T_{reg} cells, regulatory dendritic cells (DCs), and tumor cells can certainly express both CD39 and CD73, it may be that one cell expresses CD39 while a neighboring cell expresses CD73 inducing local adenosine production[82]. This may be the case with "exhausted" CD8 T cells, which express high amounts of CD39[113]. High expression of CD39 may confer a suppressive capacity to exhausted T cells by creating a pool of AMP that can be converted to adenosine by the T cells themselves or by neighboring cells expressing CD73. Indeed, production of adenosine is a known suppressive tactic of T_{reg} cells[114]; therefore, work into the immunosuppressive capacity of exhausted T cells is warranted.

Of note, all the "toxic" byproducts discussed here tend to negatively impact effector cells while supporting regulatory immune cells. This suggests that regulatory immune cell populations have evolved to be metabolically out-of-sync with their effector cell counterparts, utilizing the metabolites effector cells and inflamed tissues produce to reign in immune responses and prevent tissue damage. Selective pressures on the TME have pushed tumors to utilize these toxic byproducts to maintain immune tolerance. While each toxic byproduct is not unique to the TME, the combination and high production of these byproducts makes it distinct.

1.6 Implications for immunotherapy

Recognition of the abundance and immunomodulatory impacts of lactic acid, kynurenine, ROS, and adenosine have led to the development of therapies targeting their production in hopes of improving cancer immunotherapies. The benefit of targeting these toxic metabolites is their abundance across multiple tumor types offering a broad range therapy. However, it will be important to understand how inhibiting lactic acid, kynurenine, or ROS will interact with a range of immunotherapies. Further understanding of how limiting these toxic metabolites to alter immune cell function will help the field utilize the proper immunotherapy to see maximal efficacy. Here we approach metabolic therapies from two perspectives: altering the metabolic landscape of the tumor versus altering infiltrating immune cell metabolism to overcome the TME.

1.6.1 Altering the metabolic landscape of the tumor

Many strategies exist for altering the metabolic landscape of the tumor (**Figure 2**). For example, lactic acid production can be targeted by inhibiting LDH, the enzyme responsible for converting pyruvate to lactate, or inhibiting glycolysis at an earlier point in the pathway. LDH levels in the blood and TME are associated with poor outcomes for cancer patients and are used in determining tumor staging in melanoma [115]. For melanoma patients, high LDH levels are predictive of poor response to anti-PD1 immunotherapy [116,117]. To date, glycolytic inhibitors are still in the pre-clinical phase so their impact on human patients is unknown. Despite this, pre-clinical models provide compelling evidence that blocking lactic acid production enhances immunotherapy. One

study demonstrated that knocking down LDHA in 4T1 and B16 tumors increased response to anti-CTLA4 treatment, in part by shifting T_{reg} cells away from lactate metabolism and increasing T_{reg} glucose uptake [26,118]. Utilizing a pharmaceutical approach, another study showed inhibition of patient-derived and B16 melanoma LDHA with the inhibitor GSK2837808A enhanced T cell killing both in vitro and in vivo and enhanced adoptive cell therapy [119]. While specific LDH and glycolytic inhibitors have not fully made it into the clinic, we could potentially repurpose old drugs that have glycolysis inhibiting effects. For example, diclofenac, a common non-steroidal anti-inflammatory drug (NSAID), has been shown to modulate glycolysis independent of COX inhibition and could be used to improve anti-PD-1 immunotherapy [120,121]. While we have focused discussion on immune cells, we appreciate that inhibiting tumor cell glycolysis directly impacts the fitness of tumor cells. Therapeutically, this is ideal as inhibiting tumor cell glycolysis can both kill tumors and promote immune cells. A more detailed discussion on how inhibiting glycolysis impacts the fitness of tumor cells can be found here [122].

Lactic acid can also be decreased within the TME by targeting its export. Lactic acid is transported via MCTs[38]. MCT1, almost ubiquitously expressed, has the highest affinity for lactate and can both import and export lactate based on concentration gradient of substrate and protons. MCT4 is more heavily expressed by highly glycolytic tissues, including tumor cells, and while it is also a bidirectional transporter, it mainly participates in the export of lactate [38]. While many small molecule inhibitors of MCT1/MCT4 have been developed for preclinical use, only AstraZeneca's AZD3965 compound is currently being tested for in-human use (NCT01791595). Preclinical work has shown AZD3965 can lower lactic acid secretion into the TME and increase tumor immune cell infiltration [123]. However,

these findings should be taken cautiously, as data were generated from Raji xenograft-bearing SCID mice looking only at NK and myeloid cells. In fact, this is a limitation of many of the preclinical studies using MCT inhibitors, and further work on how MCT inhibitors impact adaptive immune cells, especially within the TME, is warranted [124–126]. In light of this, deletion of MCT1 specifically on T_{reg} cells was shown to slow tumor growth and synergize with anti-PD-1 therapy, suggesting that pharmacological inhibition of MCT1 may play a dual role, both to inhibit lactate secretion by tumor cells and to impair immunosuppressive T_{reg} cells[26].

Lactic acid creates a low pH environment which can be targeted to improve cancer therapy. To counteract acidity, bicarbonate has been employed, administering it through a variety of methods (reviewed in[127]). Bicarbonate administration has been shown to control Yumm1.1 melanoma growth and increase CD8 T cell infiltration, NK, and B cell activation, as well as improve anti-CTLA4, anti-PD-1 therapy, and adoptive cell therapy in B16 melanoma-bearing mice[128,129]. In addition, bicarbonate can act to alter cancer cell mTORC signaling which may help to limit lactic acid production[130].

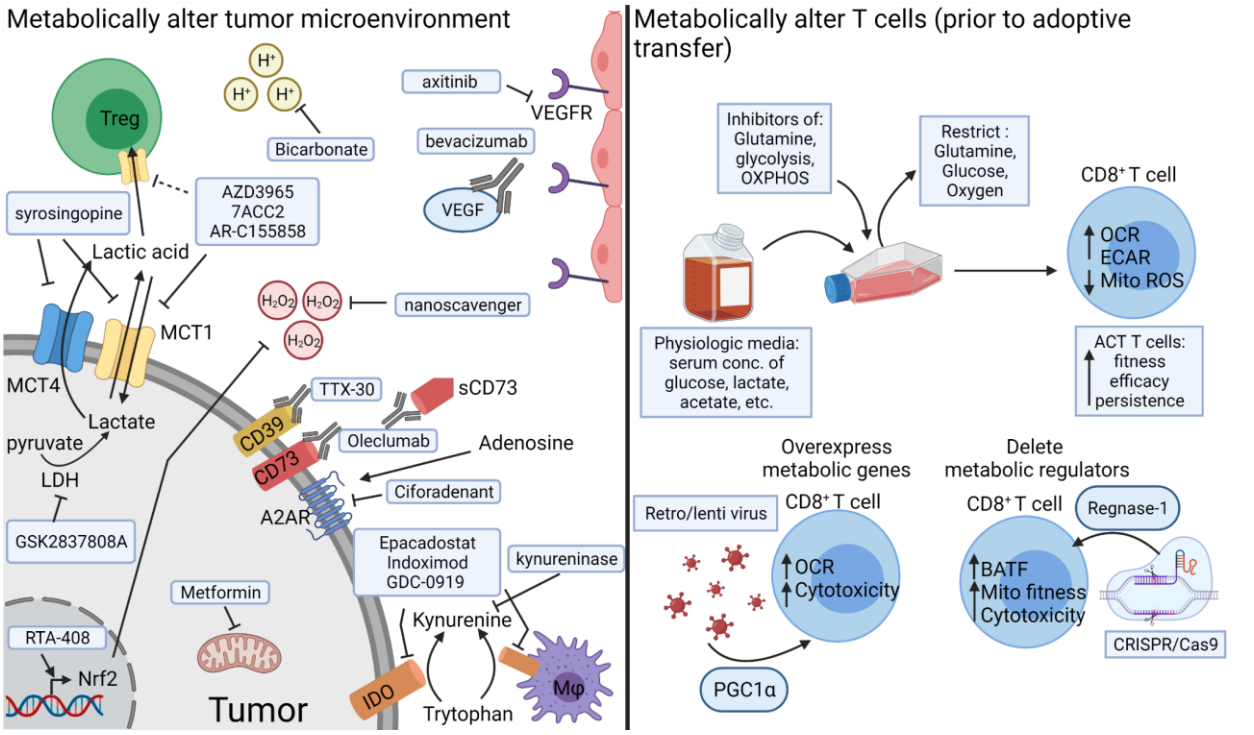

Figure 2. Metabolically altering the TME versus metabolically bolstering T cells to improve cancer immunotherapy. Altering the metabolic landscape of the tumor can be accomplished in many ways. Lactic acid production by tumor cells can be targeted by using an inhibitor of LDH (GSK2837808A). Alternatively, lactic acid export by tumor cells could be targeted using MCT1 inhibitors (AZD3965 in clinical trials, 7ACC2 and AR-C155858 pre-clinical) or MCT4/MCT1 dual inhibitors (syrosingopine). MCT1 inhibitors may also block T_{reg} import and usage of lactic acid, leading to diminished suppressive function and proliferation. Lactic acid lowers the pH of the TME which can be counteracted through bicarbonate treatment. Tryptophan depletion and kynurenine production can be targeted by inhibiting IDO found on tumor cells and TAMs (Epacadostat, indoximod, GDC-0919). Alternatively, kynurenine alone can be depleted using an enzyme engineered for its degradation (PEGylated kynureninase). Oxygen depletion can be targeted using VEGF inhibitors (bevacizumab) or VEGFR inhibitors (axitinib) to normalize tumor vasculature and improve tumor oxygenation. Metformin, a common diabetes drug, can be used to decrease tumor hypoxia potentially through its action as a mitochondrial complex I inhibitor. ROS can be targeted through drugs promoting endogenous ROS scavengers (RTA-408 promoting Nrf2) or by addition of exogenous engineered ROS nano-scavengers. The production of adenosine can be targeted using

monoclonal antibodies against CD39 (TTX-30) and CD73 (both membrane bound and soluble (sCD73), Oleclumab) or by small molecule inhibition of A2AR (Ciforadenant). Instead of altering the TME, T cells used for cellular therapies (CAR-T cells or adoptive cell therapy) can be metabolically bolstered prior to patient re-infusion. During the in vitro expansion phase of cellular therapies, limiting metabolites such as glucose, glutamine, or oxygen in the media or using a media with physiologic metabolite concentrations may better prepare T cells for survival and efficacy in the metabolically dearth TME. Alternatively, T cells can be engineered to either overexpress key metabolic genes, such as *PGC1α*, to improve mitochondrial fitness, or delete metabolic regulators, such as REGNASE-1 which negatively regulates mitochondrial fitness, to give T cells a metabolic edge within the TME. (Created with Biorender.com)

Kynurenine metabolism can also be targeted at several points (**Figure 2**). Much of the work targeting kynurenine has been through the inhibition of IDO1[131]. Theoretically, in the context of the TME, inhibition of IDO1 is the best of both worlds, stopping tryptophan depletion and kynurenine production. Indeed, pre-clinical models targeting IDO1 strongly enhanced B16 and 4T1 tumor response to both anti-CTLA4 and anti-PD-1 therapy, and demonstrated efficacy regardless of tumor IDO1 expression[132,133]. As a result, several IDO inhibitors are in clinical trials (NCT04049669, NCT03432676, NCT02471846). Unfortunately, Incyte's trial of Epacadostat in combination with Pembrolizumab (anti-PD-1) was stopped after intermediary analysis revealed no added benefit of IDO1 inhibition (NCT03432676). While this has certainly dampened enthusiasm for targeting IDO1, it highlights the complexity of targeting the IDO pathway. It may be that some level of tryptophan catabolism is required to create an optimally tuned anti-tumor immune response. Lack of tryptophan catabolism could lead to a buildup of serotonin, which has been shown to have pro-tumor effects and modulate immune cell function and

mitochondrial metabolism [134,135]. While preclinical models suggested synergy between IDO inhibition and checkpoint blockade, in humans a better synergy may be found between CAR-T therapy, oncolytic viruses, or cytokine treatment. More work is needed to identify if IDO1 inhibitors will truly boost immunotherapies.

Kynurenine can also be targeted directly, leaving IDO and tryptophan catabolism intact. Using a pharmacologically optimized enzyme, PEGylated kynureninase, one study demonstrated that peritumoral injection slowed B16 and CT26 tumor growth in a CD8 T cell-dependent manner [79]. Administration of PEGylated kynureninase improved anti-PD-1 efficacy in B16 tumors, anti-CTLA4 in 4T1 tumors, and a cancer vaccine in CT26 tumors. These findings suggest that kyn, rather than tryptophan depletion, is playing a larger role in inhibiting anti-tumor immune response, supporting the idea that the toxic byproducts rather than the depletion of key nutrients drive metabolic immunosuppression in the TME.

Due to the variety of ROS-generating mechanisms, ROS production can be targeted in many ways (**Figure 2**). One promising method is through the reduction of tumor hypoxia. In preclinical models, metformin, a common type II diabetes drug that can act as a weak mitochondrial complex I inhibitor, reduced tumor hypoxia and promoted B16 tumor clearance when combined with anti-PD-1 [99]. While not statistically significant, a retrospective cohort study revealed a trend toward improved outcomes of melanoma patients on metformin being treated with checkpoint blockade [136]. Tumor hypoxia can also be targeted through the inhibition of VEGF. In an attempt to oxygenate the TME, tumors secrete VEGF and promote angiogenesis, but the blood vessels formed are highly disorganized and leaky, providing inadequate oxygen [3,137,138]. Low doses of

antiangiogenic antibodies (anti-VEGFR2) have been shown to normalize the tumor vasculature, which improves M1-like macrophage polarization, T cell tumor infiltration, and whole cancer cell vaccine therapy in murine breast cancer models [139]. In addition, many others (reviewed in [138]) have shown in preclinical models that antiangiogenic treatments can improve anti-PD-L1 therapy. Clinically, antiangiogenic and immunotherapy combinations have shown the best efficacy in Renal Cell Carcinoma (RCC) and Hepatocellular carcinoma (HCC). Patients with previously untreated metastatic RCC were given pembrolizumab and axitinib (VEGFR1, 2, and 3 inhibitor) combination therapy, which statistically improved progression-free survival over sunitinib monotherapy, leading to FDA approval for treatment-naïve RCC patients [140]. Likewise, combination of atezolizumab (anti-PD-L1) and bevacizumab (anti-VEGF-A), saw improvements in progression-free and overall survival compared to standard of care in unresectable HCC patients [141].

Another way tumor-derived ROS can be targeted is using scavengers. ROS production in the TME is finely tuned by ROS generators and ROS scavengers to maintain optimal levels for signaling, growth, and survival [85]. However, this finely tuned balance can be disrupted by addition of exogenous ROS scavengers or induced expression of endogenous ones. One group developed an extracellular matrix-targeting, pH-sensitive ROS nanoscavenger which can target to the TME, decrease ROS, and improve anti-tumor immunity in several tumor models [142]. This study provides proof of principle for use of a manufactured ROS scavenger in the improvement of immunotherapy. Alternatively, endogenous ROS scavengers could be induced, for example using the drug RTA-408, also known as omaveloxolone. RTA-408 was shown to induce Nrf2, a major protein

involved in oxidative stress protection, and resulted in suppression of ROS in tumor xenograft models [143–145]. In 2019, a Phase 1b/2 clinical trial completed combining anti-CTLA4 and anti-PD-1 with RTA-408 in melanoma patients, but results have not been formally posted (NCT02259231).

In addition to the hypoxia-reducing methods above, adenosine production can be targeted directly. These drugs take the form of small molecule inhibitors or blocking antibodies mainly targeting CD73, CD39, and A2AR (reviewed in [146]). While these drugs have shown pre-clinical efficacy in reducing adenosine production and even preventing the ectonucleotidase of soluble forms of CD73 (MEDI9447 aka Oleclumab [147]), most are awaiting results from Phase I/II clinical trials [146]. Interestingly, treating tumor-bearing mice intraperitoneally with antisense oligonucleotides targeting CD39 augmented CD8 T cell proliferation, reduced CD39 expression by tumor and T_{reg} cells, and enhanced anti-PD-1 treatment [148]. These results are encouraging and hopefully a similar efficacy is achieved in human trials.

While we have discussed targeting a single toxic metabolite in combination with immunotherapy, we appreciate that many tumors undergo multiple metabolic changes and thus produce a collection of toxic metabolites. Thus, it may be necessary to target several sources of toxic metabolites in combination with immunotherapy to yield the best therapeutic efficacy.

1.6.2 Altering infiltrating immune cell metabolism

Chimeric antigen receptor (CAR) T and adoptive T cell therapies provide a way to metabolically bolster T cells to function in the harsh TME (**Figure 2**). These therapies require taking the patients' blood, enriching for T cells, then activating, expanding, and (depending) genetically altering via viral or non-viral methods. In vitro expansion and transduction provide a window in which T cell functioning can be enhanced to better compete in the TME. One method of bolstering CAR T cells is to overexpress or delete genes that regulate metabolism. For example, overexpression of PGC1α, a transcriptional co-activator key for mitochondrial biogenesis, prevented the loss of mitochondrial mass and improved anti-tumor efficacy in an adoptive cell therapy model [4]. Conversely, deletion of *Regnase-1*, a gene identified to negatively regulate the transcription factor BATF and mitochondrial metabolism in CD8 T cells, improved the efficacy of adoptive cell transfer [149]. While these are two targets of many, they represent a means of genetically altering T cells to improve efficacy against solid tumors.

Adoptive T cell therapies can also be metabolically bolstered through their expansion media. Commonly used media such as RPMI, DMEM, and AIM-V contain high amounts of glucose and reduced metabolite levels compared to serum, poorly preparing them for the harsh metabolic landscape of the tumor [150]. As T cells are highly sensitive to their metabolic environment [27,151], expanding T cells in media containing or lacking certain metabolites may improve their persistence and efficacy in vivo. Consistent with this, glutamine restriction in vitro either by nutrient starvation or metabolic inhibitor enhanced the efficacy of adoptively transferred T cells in mice [152]. Restricting metabolites or adding

metabolic inhibitors to expansion media is an attractive method of improving adoptive cell therapies due to its relative simplicity, making it a hot area of investigation.

1.7 Conclusions

Tumors not only consume essential metabolites but simultaneously produce toxic byproducts, which persist in the TME due to its poor perfusion. Both the consumption of metabolites such as glucose, amino acids, and oxygen and the production of lactic acid, kynurenine, ROS, and adenosine negatively regulate effector immune cells and support regulatory immune populations. While the TME is not unique in its production of these toxic metabolites, it is distinct with its high persistent levels of them. As we further investigate immunometabolism in the TME and how best to modulate it to improve immunotherapy, it is critically important to remember that depletion and production of metabolites both have independent impacts on immune cell function. As in the failed IDO1 inhibitor trial, there may be a more finely tuned balance between depletion of essential metabolites and production of toxic ones than we appreciate. Ultimately, understanding the physiologic balance between essential metabolites and their toxic byproducts and the subsequent impact on immune cells will be key to developing approaches to fuel curative immunotherapy for cancer.

2.0 Regulatory T cells are metabolically distinct from effector T cells with glucose avidity associated with reduced functionality

2.1 Foreword

This chapter was adapted from a previously published manuscript in *Nature*: **Watson MJ**, Vignali PDA, Mullett SJ, Overacre-Delgoffe AE, Peralta RM, Grebinoski S, Menk AV, Rittenhouse NL, DePeaux K, Whetstone RD, Vignali DAA, Hand TW, Poholek AC, Morrison BM, Rothstein JD, Wendell SG, Delgoffe GM. "Metabolic support of tumour-infiltrating regulatory T cells by lactic acid." *Nature*. 2021 Mar;591(7851):645–51.

2.2 Introduction

Regulatory T cells (T_{reg}) are a subset of $CD4^+$ T cells expressing the lineage defining transcription factor Foxp3[1,2]. T_{reg} cells are vital for maintaining immune homeostasis and preventing autoimmunity. Both mice and humans lacking Foxp3 develop severe systemic autoimmunity and have shortened lifespans, demonstrating the vital importance of T_{reg} cells and their potent immunosuppressive function[153]. However, cancer exploits T_{reg} cell's suppressive nature and consequently T_{reg} cells are overrepresented in the tumor microenvironment (TME) compared to lymphoid tissues[154]. T_{reg} cells are critical for supporting tumor growth as deletion of these cells using a mouse

expressing diphtheria toxin receptor (DTR) from the Foxp3 locus (Foxp3^{DTR}), results in dramatic tumor clearance[8].

Previously, T_{reg} cells and effector T cells, both T_{conv} (CD4$^+$ Foxp3$^-$) and CD8$^+$ T cells, have been shown to have distinct metabolic profiles[9–11,25]. These studies described effector T cells as having higher Glut1 expression, a glucose transporter, and displaying high glycolytic rates. These high glycolytic rates in effector cells are induced by T cell receptor (TCR) stimulation and are required for the translation of IFN-γ and for proliferation[27,32,33]. In contrast, T_{reg} cells are more dependent on oxidative metabolism, with Foxp3 actively antagonizing glycolytic metabolism[9,10]. Overexpression of Glut1 or deletion of mitochondrial complex III protein in T_{reg} cells both leads to impaired suppressive function, suggesting glucose metabolism is detrimental, while oxidative metabolism is required for T_{reg} cell suppressive capacity[10,11]. However, how T_{reg} cells behave metabolically within the TME and how this contributes to their presence and function is poorly understood. In this chapter we show T_{reg} cells possess a distinct metabolic profile from T_{conv} cells in both normal and transformed tissues.

2.3 Results

Having previously shown heightened tumor cell metabolism correlates with decreased effector T cell function[5], we sought to determine the relationship of heighted tumor metabolism with T_{reg} cell function. Using mice that report *Foxp3*[155,156], we implanted them with syngeneic tumor lines displaying increasing glycolytic capacity from B16 (melanoma) to Clone24 (PTEN-deficient, BRAF mutant melanoma) to MEER (head and

neck). Glycolytic capacity (Extracellular acidification rate: ECAR) of the tumor cells was determined using an extracellular flux analyzer (Seahorse). Tumor infiltrating T_{reg} cells from each tumor were isolated (gating strategy **Fig. 4a**) and measured for their suppressive function in a miniaturized *in vitro* suppression assay. Remarkably, increased glycolytic capacity of tumor cells correlated with increased suppressive function of the intratumoral T_{reg} cells (**Fig. 3a**). Expectedly, T_{reg} cells were enriched within tumors (**Fig. 3b, 4b**) and were actively proliferating compared to their T_{conv} cell ($CD4^+$ $Foxp3^-$) counterparts suggesting that they were not metabolically suppressed (**Fig. 3c**). Given the relationship between tumor glycolysis and T_{reg} cell function, we determined the glycolytic capacity of T_{reg} cells directly *ex vivo* and immediately after activation, a reprogramming event occurring downstream of the TCR in T cells[32]. This was achieved by simultaneously measuring ECAR while exposing the cells to streptavidin-complexed anti-CD3-biotin ("in seahorse activation"). As T_{reg} cells are thought to arise from a pool of cells with self-reactive TCRs[157–159], at steady state most T_{reg} cells are antigen experienced ($CD44^+$) in contrast to T_{conv} cells. To compare TCR induced glycolysis more adequately between T_{reg} and T_{conv} cells we divided T_{conv} cells into naïve ($CD44^-$ $CD62L^+$) and antigen experience ($CD44^+$ $CD62L^-$). TCR triggering induced less glycolysis in T_{reg} cells compared to naïve or antigen-experienced conventional T cells and highly glycolytic $CD8^+$ T cells (**Fig. 3d**). Even under strong activating stimuli (anti-CD3, CD28, and IL-2 for 48 h) to normalize activation status of bulk T_{reg} and T_{conv} cells, this resistance to glycolysis persisted, with tumor-derived T_{reg} cells displaying even lower glycolytic activity (**Fig. 4c**). Of note, oligomycin treatment showed T_{reg} cells are resistant to engaging glycolysis even when

oxidative metabolism is inhibited, suggesting glucose transport may be limiting in T_{reg} cells (**Fig. 4c**).

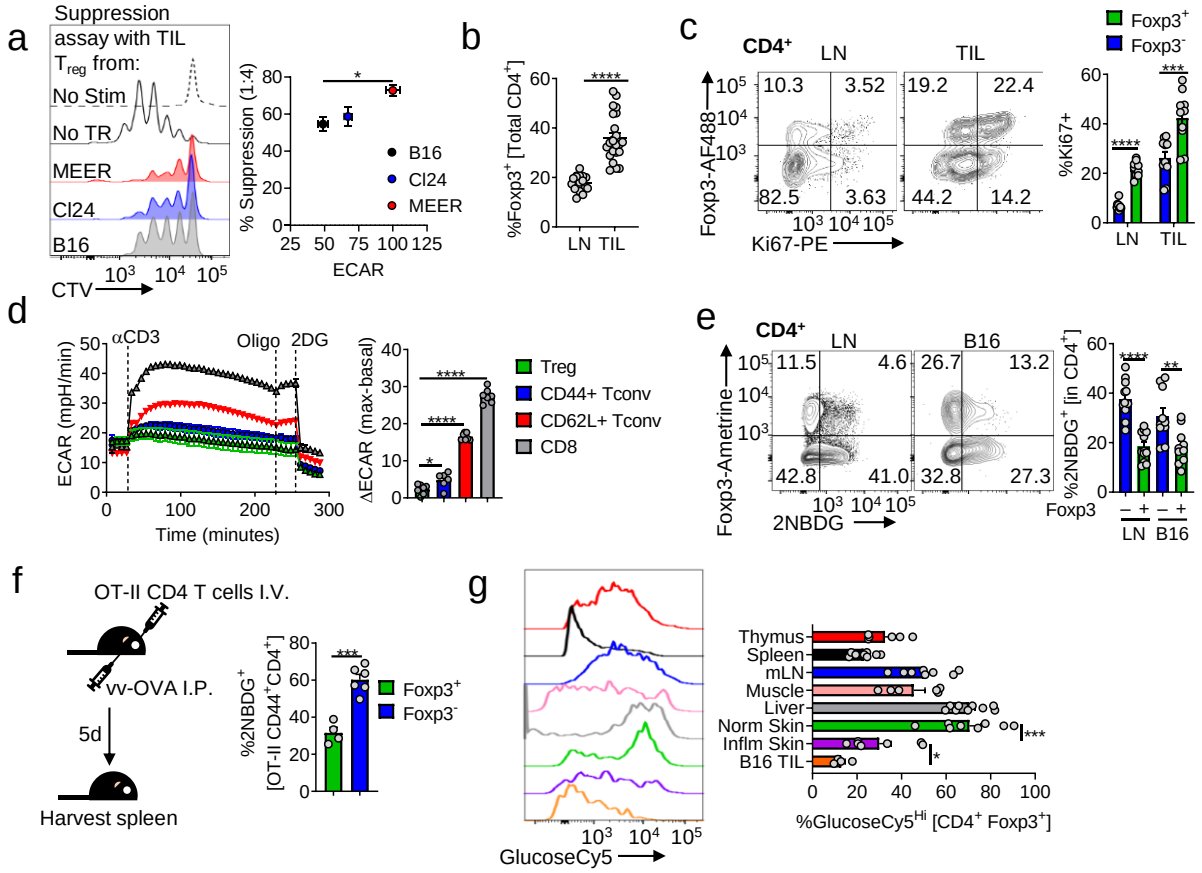

Figure 3. Regulatory T cells possess a distinct metabolic profile from conventional T cells in normal and transformed tissues. (a) (left) Representative histogram of T_{conv} responder cell proliferation dye dilution after 72hrs of co-culture with T_{reg} cells isolated from B16, Cl24 (melanoma), or MEER (HPV+ HNSCC) tumors. (right) Capacity of T_{reg} cells to suppress the proliferation of CellTrace Violet (CTV) labelled T_{conv} cells as a function of the glycolytic extracellular acidification rate (ECAR) of the tumors from which they were isolated (*p=0.047) . (b) Percent T_{reg} cells ($CD4^+$ $Foxp3^+$) of total $CD4^+$ T cells from lymph node (LN) and tumor infiltrating lymphocyte (TIL) preparations from C57BL/6 mice bearing B16 melanoma tumors (14 d post intradermal injection) (c) Percent proliferating ($Ki67^+$) T_{reg} and T_{conv} cells ($CD4^+$ $Foxp3^-$) from mice as in (b). (d) ECAR of in-Seahorse activated T_{reg}, CD8+, CD44+CD62L- and CD44-CD62L+ T_{conv} cells sorted from LN and spleen of Foxp3 reporter mice. Oligo = oligomycin, 2-DG = 2-deoxy-D-glucose, ΔECAR = max reading after αCD3 minus basal ECAR. (*p=0.022) (e) Flow cytogram depicting *ex vivo* 2NBDG uptake by T_{reg} and T_{conv} cells from the LN and

B16 TIL of *Foxp3* reporter mice. Representative plots gated on CD4+ cells. (p=0.006) (f) Diagram of experimental procedure and quantification of *ex vivo* 2NBDG uptake by CD44$^+$ OT-II T_{reg} and T_{conv} cells isolated 5 days after transfer into congenically mismatched hosts infection with Vaccinia-OVA. (g) Representative histogram and quantification of *ex vivo* GlucoseCy5 uptake by T_{reg} cells isolated from various tissues (*p=0.047). Results are representative of five (b), three (a,c,e, and g) or two (d,f) independent experiments. (*p< 0.05, **p <0.01, ***p < 0.001 ****p<0.0001) by unpaired two-tailed t test (a,b,d,f,g) or two-way ANOVA with Sidak's multiple comparisons test (c,e). Data presented as mean values ±SEM.**

To test glucose transport directly we used the fluorescent glucose tracer 2NBDG, and indeed T_{reg} cells had significant reductions in glucose uptake compared to T_{conv} cells directly *ex vivo* (**Fig. 3e, Fig. 4d**), regardless of CD44/CD62L expression (notably, the largest difference was observed between CD62L^{hi} populations) (**Fig. 4e**). To compare activation-induced glucose uptake of T_{reg} and T_{conv} cells more directly and in a physiological setting, we adoptively transferred congenically marked OT-II CD4$^+$ T cells from *Foxp3*^{RFP} mice into *Vaccinia*^{OVA}-infected hosts. Day five post infection spleens were harvested and pulsed with 2NBDG. Activated (CD44$^+$) OT-II T_{reg} cells took up significantly less 2NBDG than their Foxp3$^-$ counterparts, despite sharing the same TCR and undergoing robust activation (**Fig. 3f**). While T_{reg} cells are not thymically selected on the OT-II TCR, activation by the same antigen *in vivo* under the same inflammatory context results in disparate metabolic phenotypes if Foxp3 is expressed.

To determine if low glucose uptake was a universal phenotype of T_{reg} cells, we interrogated the infiltrate of various tissues at normal and inflammatory states. 2NBDG is not only incompatible with YFP and GFP employed in *Foxp3*-driven Cre lines, but may have limited utility in some cells as a glucose tracer[160]. Thus, we synthesized a novel

fluorescent glucose tracer (Cy5-linked 1amino-glucose; GlucoseCy5[161]), recapitulating our findings with 2NBDG while demonstrating superior specificity and sensitivity (**Fig. 4f-h**). Of note, T_{reg} cells that were GlucoseCy5 avid displayed decreased Nrp1 expression, a gene key for T_{reg} cell stability[8,162], consistent with previous findings that glucose uptake is detrimental to T_{reg} cell function[10] (**Fig. 4h**). T_{reg} cell glucose uptake was quite heterogeneous in tissues of *Foxp3*^{YFP}-iCre mice. Notably, T_{reg} cells displayed a stepwise decrease in glucose uptake going from non-inflamed to imiquimod-inflamed skin to B16 (**Fig. 3g**), suggesting inflammation may drive lower glucose uptake in T_{reg} cells. Conventional T cells possessed far less heterogeneity in glucose avidity when assayed from the same environments (**Fig. 4i**).

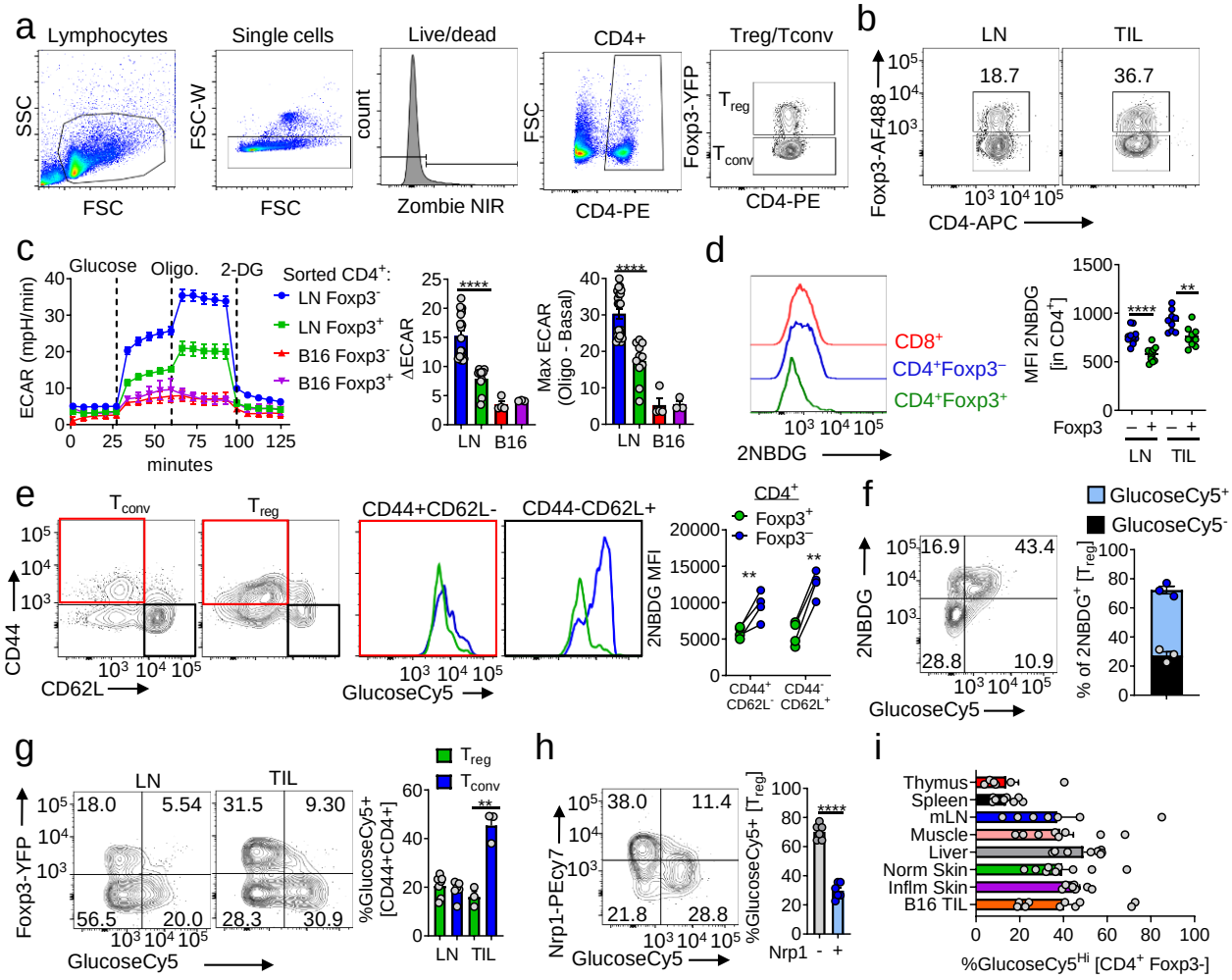

Figure 4. 1-amino-Cy5-glucose (GlucoseCy5) can act as a surrogate for 2NBDG in GFP/YFP Treg reporter mice.Gating strategy for T_{reg} and T_{conv} cells (b) Representative plot of percent T_{reg} ($CD4^+$ $Foxp3^+$) in the lymph node (LN) and tumor (TIL) of B16 bearing C57Bl/6 mice day 14 post tumor inoculation. Representative plots gated on total CD4+ cells. (c) Glycolytic extracellular acidification rates (ECAR) of T_{reg} and T_{conv} cells sorted from LN and B16 TIL preparations as in (b) 48hrs after activation with αCD3/CD28 and IL-2. Oligo = oligomycin, 2-DG = 2-deoxy-D-glucose, ΔECAR = max reading after glucose minus basal ECAR. Max ECAR = max reading at after oligo minus basal ECAR. (d) *Ex vivo* 2NBDG uptake mean fluorescence intensity (MFI) by T_{reg}, T_{conv}, and $CD8^+$ T cells from the LN and B16 TIL (p=0.0045). (e) *Ex vivo* 2NBDG uptake by CD44+CD62L- and CD44-CD62L+ T_{reg} and Tconv cells isolated from the LN of Foxp3-Amt reporter mice. (f) Lymphocytes from Foxp3-Ametrine reporter mice were simultaneously pulsed with 2NBDG and GlucoseCy5. Representative plot is**

gated $CD4^+$ $Foxp3^+$ with tabulation of percent $GlucoseCy5^+$ of $2NBDG^+$ T_{reg}. (g) *Ex vivo* GlucoseCy5 uptake by $CD44^+$ T_{reg} and T_{conv} cells from the LN and B16 TIL. Representative plots gated on $CD44^+$ $CD4^+$ cells (p=0.0025). (h) GlucoseCy5 positivity in Nrp1 negative and positive T_{reg} cells. (i) *Ex vivo* GlucoseCy5 uptake by T_{conv} cells isolated from various tissues. Results are representative of three (a-d,f-i) or two (e) independent experiments. Significance (*p< 0.05, **p <0.01, ***p < 0.001, ****p<0.0001) was determined by paired two-tailed t test (e), unpaired two-tailed t test (d,f,g,h) or two-way ANOVA with Sidak's multiple comparisons test (c). Data are presented as mean values ±SEM.**

While the majority of lymph node and tumor infiltrating T_{reg} cells took up little of the glucose tracer 2NBDG, a subset was 2NBDG avid (**Fig. 5a**). Given that T_{reg} cells minimally engaged in glycolysis and were the least glucose avid in inflammatory environments, we hypothesized that glucose avid T_{reg} cells would have a decreased suppressive capacity. T_{reg} subsets of low and high glucose avidity were purified, and their function was measured using a micro-suppression assay. Regardless of tissue (lymph node or tumor), 2NBDG avid T_{reg} cells displayed significantly reduced suppressive capacity compared to $2NBDG^{lo}$ T_{reg} cells (**Fig. 5a, 6a**). This could be a result of reduced viability of $2NBDG^{hi}$ T_{reg} cells however, this was not the case as $2NBDG^{hi}$ T_{reg} cells were more viable after the assay (**Fig. 6b,c**), and retained their initial proclivities for glucose (**Fig. 6b,d**). Similarly, using the glucose tracer glucoseCy5, glucoseCy5 avid T_{reg} cells displayed reduced suppressive capacity regardless of tissue origin (**Fig. 6a**). Thus, within a tissue, avidity for glucose predicts poorly suppressive T_{reg} cells.

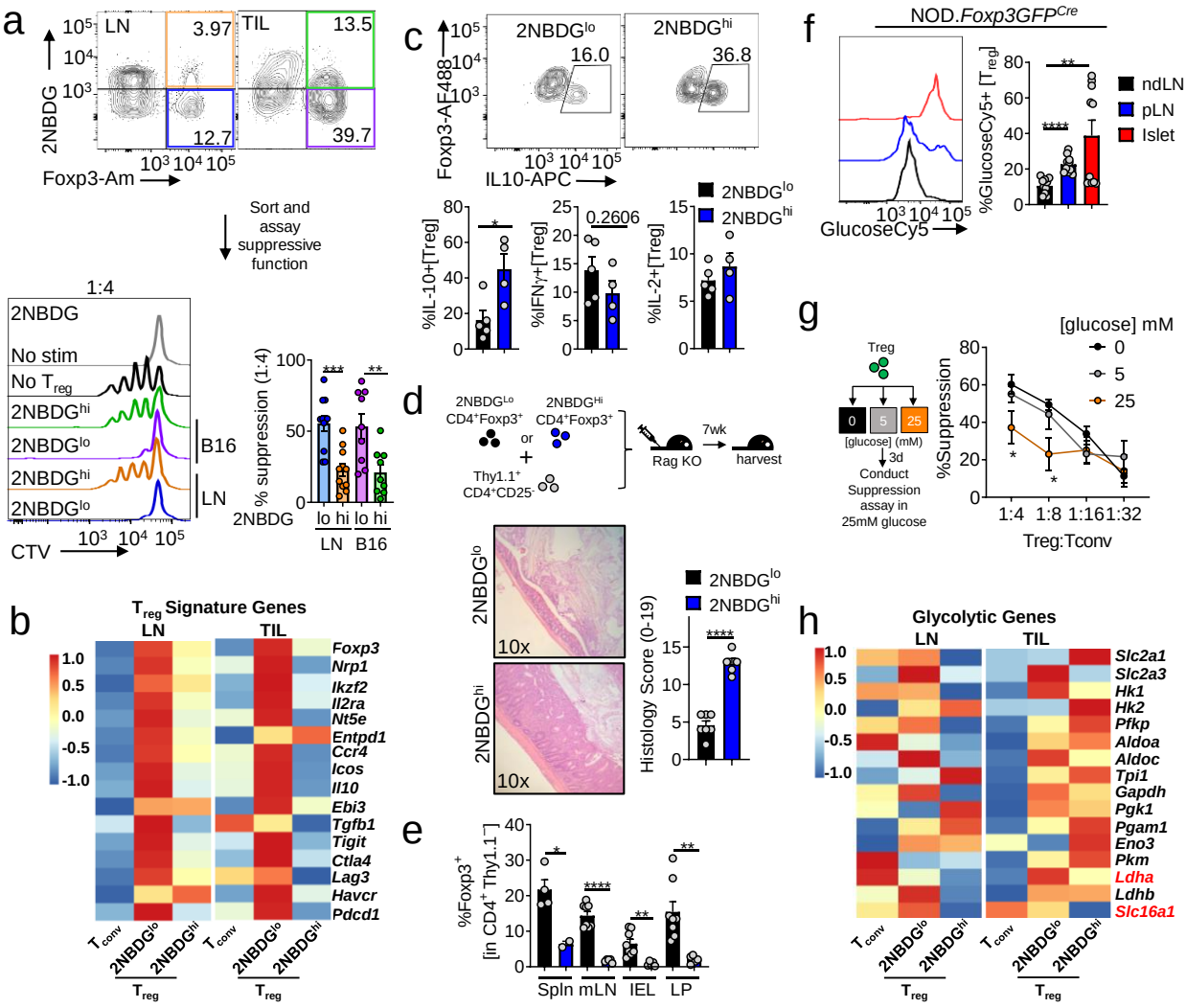

Figure 5. Glucose avidity is associated with reduced functionality of Treg cells. (a) Flow cytogram of CD4+ T cells from B16-bearing Foxp3Ametrine mice depicting sorting strategies for Treg cells based on their glucose uptake. Treg cells sorted based on 2NBDG uptake were assayed for their ability to suppress the proliferation of CellTrace Violet (CTV) labeled Tconv cells. Representative histogram shows 1:4 ratio of Treg to Tconv. (p=0.0056). (b) Treg cell signature gene expression in RNAseq analysis of 2NBDGhi or 2NBDGlo Treg cells sorted from lymph node (LN) or tumor (TIL) of B16 melanoma-bearing Foxp3 reporter mice as in (a). (c) Production of IL-10, IFN-γ, and IL-2 by sorted 2NBDGlo and 2NBDGhi Treg cells stimulated overnight with PMA/ionomycin and stained intracellularly (*p=0.02). (d) Diagram and colon histology Rag1–/– mice that received either 2NBDGlo or 2NBDGhi Thy1.2+ Treg cells plus Thy1.1+ Tconv cells I.V and followed for 7 wks. (e) Percent of**

transferred 2NBDGlo or 2NBDGhi Treg cells as in (d) expressing Foxp3 within the spleen (Spln), mesenteric lymph node (mLN), intraepithelial layer (IEL), and lamina propria (LP) (*p=0.02, **p=0.004). (f) Representative histogram and tabulation of GlucoseCy5 uptake by Treg cells isolated from the non-draining lymph node (ndLN), pancreatic lymph node (pLN), and the islet of 10-12-week-old NOD.Foxp3GFPCre mice (p=0.005). (g) (left) Diagram of experimental procedure and (right) capacity of Treg cells conditioned in 0,5, or 25mM glucose media to suppress the proliferation of CellTrace Violet (CTV) labelled Tconv cells. (1:4 *p=0.031, 1:8 *p=0.012 between 0 and 25 mM). (h) Glycolytic pathway gene expression as in (b). Results are representative of three (a,b,c,g,h), or two (d,e,f) independent experiments. Significance (*p< 0.05, **p <0.01, ***p < 0.001, ****p<0.0001) was determined by unpaired two-tailed t test (a,c,d,e,f), or two-way ANOVA with Tukey's multiple comparison test (g). Data presented as mean values ±SEM.**

We next sought to determine the transcriptional differences between 2NBDG low and high T_{reg} subsets. RNA sequencing of 2NBDG low and high lymph node and B16-infiltrating T_{reg} cells revealed reduced expression of *Foxp3*, *Ikzf2* (Helios), *Il2ra* (CD25), *Nrp1* (Neuropilin 1), and other T_{reg} signature genes in 2NBDG^{hi} T_{reg} cells. Flow cytometry of surface markers, as 2NBDG cannot be used with permeabilized cells, further confirmed the RNA sequencing data showing reduced expression of *Nrp1*, *CD73*, *Foxp3* (ametrine reporter), and *TIGIT* (**Fig. 5b, 6e**). These data suggested while glucose avid T_{reg} cells are still Foxp3^{+}, they harbor a 'weaker' T_{reg} cell signature. As 2NBDG^{hi} T_{reg} cells harbored some suppressor function, we measured cytokine production after a brief restimulation with PMA (phorbol myrisate acetate) and Ionomycin. 2NBDG^{hi} T_{reg} cells produced significantly more IL-10, but not IFN-γ or IL-2, suggesting distinct suppressive mechanisms between 2NBDG T_{reg} states, especially intriguing given the low IL-10 mRNA expression measured by RNA sequencing (**Fig. 5b,c**). Low IL-10 mRNA and high IL-10

protein expression may be driven by glycolysis which is tied to cytokine translation in conventional T cells[33]. To assess long-term stability and function of 2NBDG T_{reg} cell subsets under inflammation, Thy1.2^{+} Foxp3^{+} T_{reg} cells of high or low glucose avidity were transferred into *Rag1*-deficient animals, along with Thy1.1^{+} Foxp3^{-} T_{conv} cells to induce colitis. After 7 weeks, mice receiving glucose avid T_{reg} cells began to lose weight due to increased colitis compared to those receiving 2NBDG^{lo} T_{reg} cells, and transferred 2NBDG^{hi} T_{reg} cells lost *Foxp3* expression (**Fig. 5d,e, 6f**). These data suggest that while glucose avid T_{reg} cells initially display a T_{reg} signature, albeit weakened, they ultimately fail to suppress and maintain their T_{reg} cell characteristics in vivo. Taken together these data suggest that glucose avidity marks unstable and poorly suppressive T_{reg} cells.

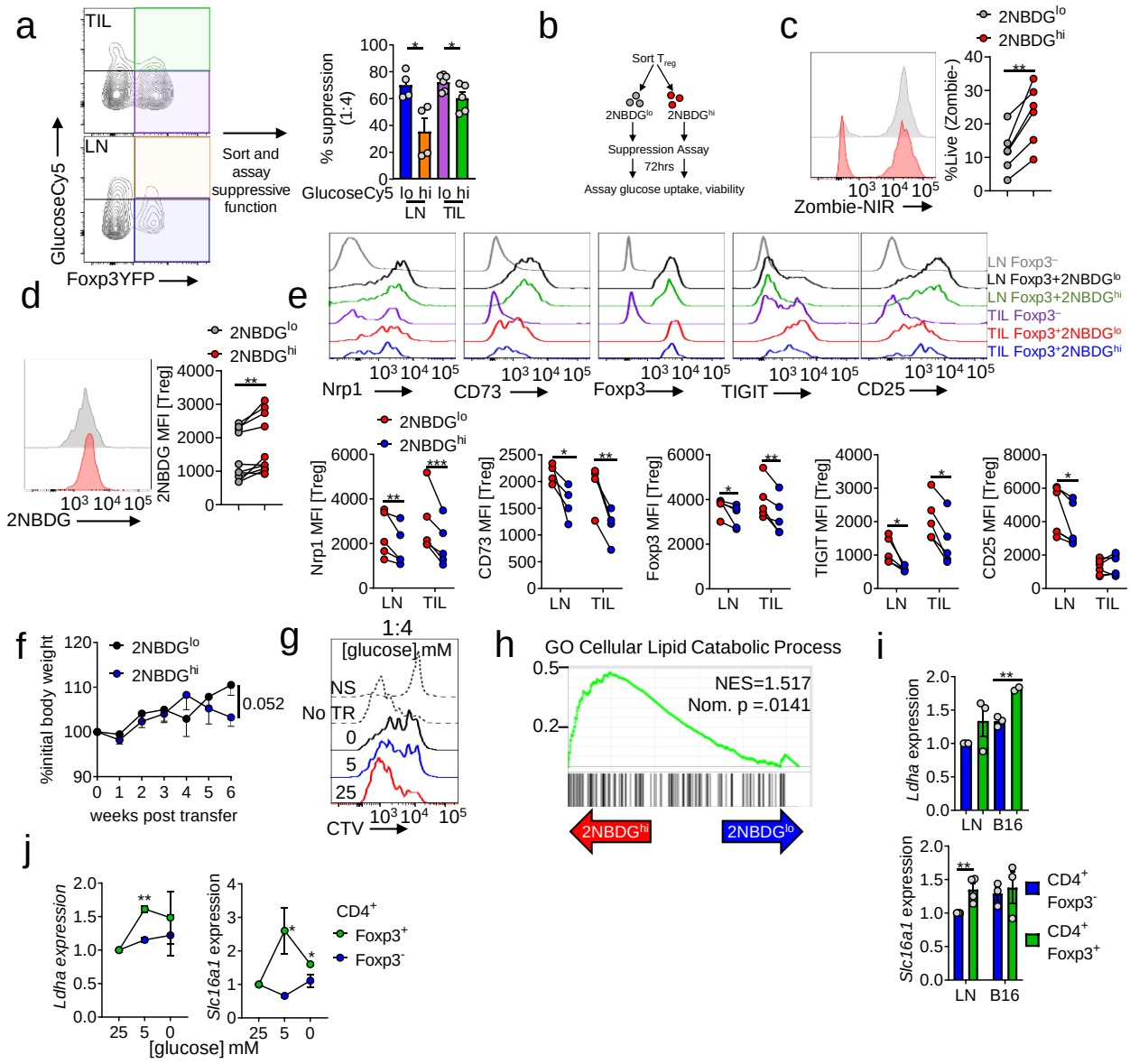

Figure 6. Glucose avid Treg cells harbor a weaker Treg cell signature but retain viability and some suppressor activity. (a) Treg cells were sorted based on GlucoseCy5 uptake and assayed for their ability to suppress the proliferation of CellTrace Violet (CTV) labeled Tconv cells at 1:4 (Treg:Tconv) (LN*p=0.02, TIL *p=0.041). (b) Experimental diagram for (c, d). (c) Representative histogram and quantification of viability of sorted 2NBDGhi and 2NBDGlo Treg cells after 72hrs in a suppression assay. (d) 2NBDG uptake by 2NBDGhi or 2NBDGlo Treg as in (b). (e) Representative flow cytometric histograms and tabulation of Treg signature gene expression between 2NBDG low and high Treg cell subsets (Nrp1 **p=0.0016, CD73 *p=0.029 **p=0.0076, TIGIT LN*p=0.04 TIL*p=0.016, CD25

***p=0.037). (f) Weights of Rag1–/– mice that received an adoptive transfer of either 2NBDGlo or 2NBDGhi Treg cells plus Thy1.1+ Tconv cells I.V. (g) Representative histogram of Tconv responder cell proliferation after 72hrs of co-culture with Treg cells (1:4) conditioned in 0, 5, or 25mM glucose for 3 days. The suppression assay occurred in 25 mM glucose conditions. (h) Geneset enrichment plot of cellular lipid catabolic process from TIL 2NBDGhi vs 2NBDGlo Treg cells. (i) mRNA expression of Slc16a1 and Ldha in LN- and B16-derived Treg and Tconv cells by qPCR (Ldha **p=0.004, Slc16a1 **p=0.009). (j) Slc16a1 and Ldha mRNA expression in Treg or Tconv cells activated overnight and conditioned in the glucose concentration indicated for 3 days (normalized to 25mM glucose, significance between Treg and Tconv) (Ldha **p=0.002 Slc16a1 5 *p=0.030, 0 *p=0.046). Results are representative of three (a,e,h,i,j), or two (c,d,f) independent experiments. Significance (*p< 0.05, **p <0.01, ***p < 0.001) determined by unpaired two-tailed t test (a,f,i,j) or paired two-tailed t test (c,d) or two-way ANOVA with Sidak's multiple comparisons test (e,). Data presented as mean values ±SEM.**

As the transfer colitis model is a contrived system, we also investigated whether increased glucose uptake could be observed in T_{reg} cells from an unmanipulated autoimmune setting. Using a model of non-obese type I diabetes, T_{reg} cells were isolated from pancreatic islets, draining lymph node (dLN), and non-draining lymph node (ndLN) of pre-diabetic NOD.*Foxp3*^{GFP} mice. Islet infiltrating T_{reg} cells are known to be dysfunctional in this model[163] and took up significantly more glucose than those from non-draining lymph node (ndLN) (**Fig. 5f**). Of note, there was a stepwise increase in glucose uptake as T_{reg} cells moved from ndLN to dLN to islets suggesting that the environment of the islet is responsible for this change. Thus, glucose avidity in T_{reg} cells correlates with poor suppressive capacity, even in a model of autoimmunity.

We next asked whether exposure to a high glucose environment would drive a less suppressive phenotype, regardless of glucose uptake status. T_{reg} cells were isolate,

activated overnight, then conditioned in 0-, 5-, or 25-mM glucose media for three days. After conditioning, T_{reg} cell's suppressive function was measured in a micro-suppression assay with 25mM glucose media. Remarkably, conditioning T_{reg} cells in 25mM glucose dampened suppressive function compared to those in 0- or 5-mM glucose (**Fig. 5g, 6g**). This suggests that glucose in the environment is enough to shift the suppressive capacity of T_{reg} cells, potentially by leading to more glucose avid T_{reg} cells within the population (see chapter 6 for more on this system).

We further interrogated the transcriptome of 2NBDG^{lo} T_{reg} cells to identify metabolic pathways that may support their function. Gene set enrichment analysis revealed 2NBDG^{lo} T_{reg} cells did not possess a transcriptome preferential to lipid metabolism; rather, lipid metabolism genes were enriched in the 2NBDG^{hi} subset (**Fig. 6h**). As these T_{reg} cell subsets were defined by their glucose uptake we interrogated glycolytic gene expression. Both subsets expressed upstream enzymes in glycolysis, suggesting proclivity for glucose was not regulated at the level of transporter or enzyme expression (**Fig. 5h**). The 2NBDG^{lo} subpopulation, however, had enriched expression for the terminal steps of glycolysis: specifically lactate dehydrogenase (*Ldha*), and the monocarboxylate transporter MCT1 (encoded by *Slc16a1*) (**Fig. 5h**), confirmed by qPCR (**Fig 6i**). While lactate is the end-product of glycolysis, it represents a significant fuel source for many cells[24]. Lactate uptake is mediated through MCT1, where it is converted by LDH to pyruvate[38]. T_{reg} cells (but not T_{conv} cells) conditioned in low or glucose-deficient media increased expression of *Ldh*a and *Slc16a1* (**Fig. 6j**) suggesting limiting environmental glucose may drive lactate metabolism. Taken together these data suggest that glucose is detrimental to T_{reg} cell suppressive function and stability and that T_{reg} cells

lacking glucose uptake or in glucose limiting environments upregulate lactate metabolism genes and have increased suppressive capacity. Specifically, these data suggest that lactate may be utilized by T_{reg} cells to maintain identity and suppressive function.

2.4 Discussion

In this chapter, we showed T_{reg} and T_{conv} cells possess a distinct metabolic profile in both normal and transformed tissues. In direct contrast to effector T cells, which display decreased functionality in highly energetic tumors[5,121], T_{reg} cells display increased suppressive capacity (**Fig. 3a**). This simple observation brings profound insight, suggesting that, at least in the context of the TME, T_{reg} cells are metabolically out-of-sync with the effector cell counterparts. While the TME environment drains effector T cell functionality, it fuels T_{reg} cell functionality. While this chapter focuses on T_{reg} cell's reduced glycolytic capacity and glucose uptake, a benefit in an environment where glucose is presumably limiting[6,44], it is unlikely that lack of glucose alone is maintaining T_{reg} cell functionality. Rather, as we will develop further in later chapters, the TME is likely providing an alternate fuel that supports T_{reg} cell functionality. This must be the case, as T_{reg} cells need some sort of fuel to maintain their high proliferative capacity in the TME (**Fig. 3c**), without consuming large amount of glucose and not relying on fatty acid oxidation (**Fig. 3e**, **Fig 4e-g**).

T_{reg} cell's low glucose avidity extends beyond the TME, an observation also made by others. As mentioned in the introduction, previous groups have described T_{reg} cells as

more oxidative and, in a way, anti-glycolytic with Foxp3 repressing glycolytic genes[9–11,25,45]. However, some studies using transcriptomic and proteomic analysis have suggested that T_{reg} cells are highly glycolytic[164–166]. As we observed in various mouse tissues (**Fig. 3g**) context is key for defining glucose avidity in T_{reg} cells. As many of these studies focused on human T_{reg} cells, both freshly isolated and in vitro cultured, the environmental context for these T_{reg} cells is vastly different than the mouse. As collection of human T_{reg} cells is mainly limited to the blood, it is difficult to gauge the heterogeneity of glucose usage by different tissue derived T_{reg} cells and in different states of inflammation. Despite these differences, our data suggests that strong activation and inflammatory contexts, environments where T_{reg} cells are at their most active, drive a reduction in glucose avidity and glycolytic capacity to support their functionality. These studies also heavily rely on gene and protein expression data which does not necessarily translate into functionality. As we will see in chapter two, glucose avid and non-avid T_{reg} cells display similar expression of glycolytic pathway genes despite differences in their glucose uptake. As many of the glycolytic enzymatic reactions are reversible, it may be that heightened glycolytic gene expression is a result of gluconeogenesis (making glucose from smaller carbon substrates) rather than glycolysis.

In this chapter we demonstrate that glucose avidity can predict T_{reg} cell function. While the glucose tracer 2NBDG has limited utility as a glucose tracer in some cells[160], we were able to identify two functionally distinct T_{reg} cell populations based on 2NBDG uptake and recapitulate these findings with a superior tracer, glucoseCy5 (**Fig. 5a, Fig. 6a**). Unlike previous studies which demonstrate associations between increased glycolysis and decreased suppressive function[9,10,25,45], we show directly that glucose

avidity characterizes poorly suppressive T_{reg} cells, or at least those suppressing via mechanisms not potent *in vitro* coculture (**Fig. 5a,c Fig. 6a**). It may be that 2NBDG^{hi} T_{reg} cells suppress via a different mechanism, as they produced significantly more IL-10 than their 2NBDG^{lo} counterparts (**Fig. 5c**). However, while IL-10 is widely considered an anti-inflammatory cytokine, it can also be inflammatory, especially if it has higher affinity for the IL-10 receptorβ (IL10-Rβ)[167]. Therapeutically, pegylated-IL-10 is used to enhance anti-tumor immune responses[168]. Therefore, while 2NBDG^{hi} T_{reg} cells express more IL-10, it may be acting in a proinflammatory manner rather than a suppressive one. This seems likely as mice receiving 2NBDG^{hi} T_{reg} cells had significantly more colitis suggesting that both in vitro and in vivo suppressive mechanisms were weakened (**Fig. 5d, e**).

Transcriptomic analysis revealed that 2NBDG^{hi} T_{reg} cells harbor a weak T_{reg} cell signature. While 2NBDG^{hi} T_{reg} cells still express Foxp3, and thus are still T_{reg} cells, the purpose/presence of this weakened T_{reg} subset is perplexing. It is unclear whether 2NBDG^{hi} T_{reg} cells exist as a state, a temporary phenotype that T_{reg} cells can freely move in and out of, or a fate, a permanent “differentiation” lineage. For example, if 2NBDG^{hi} was a state, T_{reg} cells may utilize glucose to regulate their suppressive capacity throughout infection. A study investigating salmonella infection demonstrated T_{reg} cells modulated their suppressive capacity over the course of infection[169], while another study revealed increases in blood glucose fueled inflammatory T cells at the height of ocular herpes simplex virus (HSV) infection[170]. Therapeutic treatment with the non-metabolizable glucose analog 2DG reduced HSV lesions and lead to a decrease in T_{conv} cells in the cornea. It may be that during peak inflammation, an influx of glucose reduces T_{reg} cell suppressive function (as we demonstrate in **Fig. 5g**) and allows for maximal

effector T cell response. After the pathogen is eliminated and glucose used up by the inflammatory cells, T_{reg} cells may decrease glucose uptake and exert their maximal suppressive capacity. This is a simple and attractive explanation for the purpose of $2NBDG^{hi}$ T_{reg} cells but is not fully supported by the data presented here. Namely, when assayed for glucose uptake after a suppression assay, $2NBDG^{hi}$ T_{reg} cells maintained their proclivity for glucose (**Fig. 6d**), and $2NBDG^{hi}$ T_{reg} cells failed to suppress colitis and maintain Foxp3 expression (**Fig 5d, e**). These data suggest that $2NBDG^{hi}$ is more of a fate than a state. Within the colitis model if $2NBDG^{hi}$ T_{reg} cells could freely move to $2NBDG^{lo}$ then we might expect an outgrowth of the stronger more suppressive and stable $2NBDG^{lo}$ T_{reg} cells. However, the lower Foxp3 percentage and increased colitis (**Fig. 5d, e**) suggest that this did not occur or at least did not occur very quickly suggesting $2NBDG^{hi}$ T_{reg} cells have more permanent qualities. Therefore, $2NBDG^{hi}$ T_{reg} cells may be a fate or more differentiated lineage. The purpose of this differentiated T_{reg} cell fate may be much harder to explain. It is possible that $2NBDG^{hi}$ T_{reg} cells are peripherally induced T_{reg} cells but reliable methods for determining this are lacking. One possible method is to use a mouse harboring a deletion of the conserved non-coding sequence 1 (CNS1) in the Foxp3 locus. Deletion of CNS1 in the Foxp3 locus impairs the development of peripheral T_{reg} cells, but not thymically derived[171], and could be used to determine a reduction or absence in $2NBDG^{hi}$ T_{reg} cells. The idea of state or fate of $2NBDG^{hi}$ T_{reg} cells is further explored in chapter 6 with more experimental evidence.

T_{reg} cells consuming low amounts of glucose still express glycolytic pathway genes (**Fig. 5h**). This was unexpected given that $2NBDG^{hi}$ and $2NBDG^{lo}$ T_{reg} cells are

distinguished by their glucose uptake. Interestingly, within the tumor 2NBDG^{lo} cells expressed the glucose transporter *Slc2a3* (*Glut3*) while 2NBDG^{hi} cells expressed *Slc2a1* (*Glut1*) (**Fig. 5h**) with *Glut3* having a higher affinity for transporting glucose[172]. Despite expressing a high affinity glucose transporter glucose^{lo} T_{reg} cells consume little 2NBDG or glucoseCy5 tracer either indicating that *Glut3* does not transport glucose tracers or may not be active in these cells. Given that these data are mRNA expression levels it may be that Glut3 protein expression is similar between the two subsets or that translated *Glut3* protein is not being trafficked and expressed on the cell surface[173]. Similarly, Hexokinase 1 and 2 (*Hk1*, *Hk2*) are inversely expressed by 2NBDG$^{lo/hi}$ subsets and may ultimately play a role in determining the impact of glucose uptake on T_{reg} cells. Despite this discrepancy, many other glycolytic pathway genes are expressed at a similar level between 2NBDG subsets, especially within the tumor (**Fig. 5h**). As most reactions in glycolysis are reversible, it is possible that 2NBDG^{lo} T_{reg} cells are building higher-order glycolytic intermediates from smaller carbon sources like lactate. Indeed, genes involved in lactate metabolism were consistently enriched in 2NBDG^{lo} T_{reg} cells suggesting an increased usage of lactate, a common source of carbon for many tissues[24] (**Fig. 5h**). This appears to be driven, in part, by low environmental glucose, as low glucose conditioning upregulated lactate metabolism genes in a bulk population of T_{reg} cells (**Fig. 6j**).

Taken together these data suggest that glucose uptake is detrimental to T_{reg} cell suppressive function and upregulation of lactate metabolism genes is associated with a more stable and suppressive T_{reg} cell. As we will explore in coming chapters, lactate is indeed utilized by T_{reg} cells to support their function within the tumor but not the peripheral tissues, at least at steady state. This suggests that lactate metabolism is not obligate for

function and survival but something that can be utilized especially when glucose is lacking. This metabolic flexibility also highlights how T_{reg} cells are exquisitely tuned to their metabolic environment, adapting their metabolism, and altering their suppressive function to best maintain immune homeostasis.

3.0 T_{reg} cells metabolize lactic acid to support their proliferation and suppressor function

3.1 Foreword

This chapter was adapted from a previously published manuscript in *Nature*: **Watson MJ**, Vignali PDA, Mullett SJ, Overacre-Delgoffe AE, Peralta RM, Grebinoski S, Menk AV, Rittenhouse NL, DePeaux K, Whetstone RD, Vignali DAA, Hand TW, Poholek AC, Morrison BM, Rothstein JD, Wendell SG, Delgoffe GM. "Metabolic support of tumour-infiltrating regulatory T cells by lactic acid." *Nature*. 2021 Mar;591(7851):645–51.

3.2 Introduction

The previous chapter demonstrated that glucose avidity predicts T_{reg} cell function. Using RNA sequencing we identified that T_{reg} cells with low glucose avidity upregulated genes involved in lactate metabolism. As described in the introduction to this thesis, lactic acid is highly enriched within many different tumor microenvironments, as are T_{reg} cells. This correlation, along with our findings of increased lactate metabolism genes, suggests that tumor derived lactic acid may act as a fuel source for tumor infiltrating T_{reg} cells. In this chapter, we demonstrate that T_{reg} cells can utilize lactic acid as a fuel to support their proliferation and suppressor function.

3.3 Results

Lactic acid is highly enriched in the TME of many human and murine malignancies[17,174]. Indeed, when we assayed the interstitial fluid of murine B16 melanoma we found lactic acid was significantly enriched (~9mM vs 3mM) compared to the spleen (**Fig. 7a**). Lactic acid is known to be immunosuppressive[25,31], and, indeed, it curbed the proliferation and IFN-γ production of conventional and $CD8^+$ T cells cultured in vitro in aB16 tumor-equivalent lactic acid concentrations (**Fig. 8a,b**). Conversely, both T_{reg} cell suppressor function and proliferation were resistant when cultured in tumor-equivalent concentrations of lactic acid (**Fig. 8a,c**). Lactate can stimulate cells via GPR81[175] and enter as a metabolite via monocarboxylate transporter 1 (MCT1), so we asked if T_{reg} cells could consume lactic acid by measuring intracellular pH changes[176]. Lymphocytes from *Foxp3*$^{YFP\text{-}Cre}$ reporter mice were loaded with intracellular pH dye, which at neutral pH does not fluoresce, but at lower pH fluoresces and incubated with lactic acid. T_{reg} cells, but not T_{conv} cells, took up lactic acid, evidenced by increased fluorescence (**Fig. 7b**). As this assay could readily detect lactic acid uptake in small numbers of cells, we determined whether T_{reg} cell lactic acid uptake was as heterogenous as glucose uptake across multiple tissues. Lactic acid uptake was also heterogeneous within various tissue derived T_{reg} cells, notably low in tissues where T_{reg} cells were glucose avid, such as the liver or vice versa such as inflamed skin (**Fig. 3g, 7c**). Indeed, most dye+ T_{reg} cells did not take up glucose, suggesting lactic acid avid T_{reg} cells have an increased suppressive capacity (**Fig. 8d**). We wondered whether this the inverse correlation between glucose and lactic acid uptake held true in autoimmune NOD mice and indeed, islet T_{reg} cells, with high glucose avidity, took up less lactic acid than those from the ndLN (non-draining lymph

node) or pLN (pancreatic lymph node) (**Fig. 7d**). pH dye+ T_{reg} cells from LN and B16 TIL possessed increased CD44 and Nrp1 expression, while maintaining similar Foxp3 expression to dye negative cells suggesting lactic acid uptake associates with more stable and active T_{reg} cells (**Fig. 7e**).

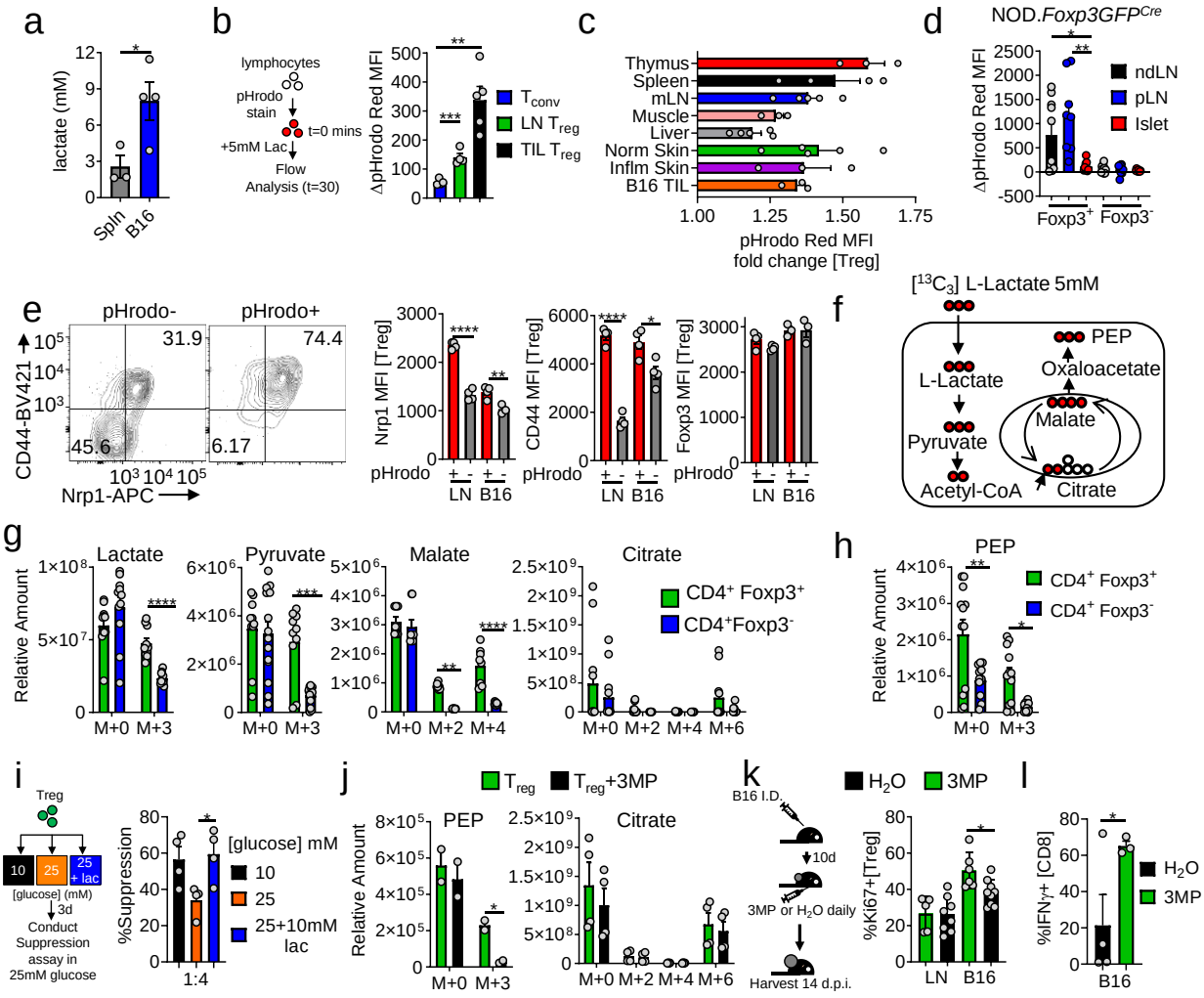

Figure 7. Treg cells metabolize lactic acid to support their proliferation and suppressor function.Lactate concentration in spleen or B16 melanoma interstitial fluid (*p=0.041). (b) Lymphocytes from Foxp3YFP-iCre mice were loaded with pHrodo Red (intracellular pH dye) and pulsed with 5mM lactic acid. Results are change of MFI from t=0 (p=0.0012). (c) Lactic acid uptake determined as in (b) by Treg cells infiltrating various tissues. (d) Lactic acid uptake from Treg and Tconv cells isolated from islets, non-draining (ndLN), and pancreatic lymph node (pLN) of 10-12-week-old NOD.Foxp3GFP mice (*p=0.017, **p=0.001). (e) Flow cytogram and tabulation depicting Nrp1 and CD44 expression in Treg cells based on lactate-elicited pH change (*p=0.018, **p=0.0097). (f) Diagram showing incorporation of 13C derived from lactate into downstream metabolites. (g) Relative abundance determined by mass spectrometry of intracellular lactate, pyruvate, malate, and citrate in Treg and Tconv cells were activated overnight then pulsed with uniformly labeled 13C-**

lactate (m+n equal to the number of incorporated heavy carbons) (p=0.0025). (h) Relative abundance of PEP derived from 13C-lactate as in (g) (*p=0.036, **p=0.0011). (i) Capacity of Treg cells conditioned for 3 days in 25mM glucose media ± 10mM lactic acid to suppress the proliferation of CellTrace Violet (CTV) labelled Tconv cells (*p=0.021). (j) As in (h) with the addition of PEPCK inhibitor 3MP (*p=0.018). (k) Ki67 expression in Treg cells of B16 tumor-bearing mice treated with 3MP or water for 3 days (*p=0.015). (l) IFN-γ expression by B16-infiltrating CD8+ T cells from mice treated as in (k) for 5 days. Results are representative of three (a,c,e,g,h,k), or two (b,d,i,j,l) independent experiments. Significance (*p< 0.05, **p <0.01, ***p < 0.001, ****p<0.0001) determined by unpaired two-tailed t test (a,b,d,e,i,j,k,l) or unpaired one-tail t test (l) or two-way ANOVA with Sidak's multiple comparisons test (g,h). Data presented as mean values ±SEM.**

To identify how T_{reg} cells were utilizing lactic acid, we performed high resolution mass spectrometry (MS) on activated T_{reg} and T_{conv} cells pulsed with [U^{13}C]-L-lactate (at pH 6.9) (**Fig. 7f**). We used LN-derived T_{reg} cells (which do readily take up lactate, **Fig. 7b**) to facilitate cellular input needed for MS analysis and confirmed T_{reg} cells took up significantly more lactate than T_{conv} cells (**Fig. 7g**). T_{reg} cells converted ^{13}C-lactate into pyruvate and subsequently into citrate and malate indicating mitochondrial import and entry to the TCA cycle (**Fig. 7g**). Further analysis revealed T_{reg} cells also incorporated lactate-derived carbon into phosphoenolpyruvate (PEP) (**Fig 7h**), formed by phosphoenolpyruvate carboxykinase (PEPCK) which converts oxaloacetate into PEP and CO_2. PEP contributes to upstream glycolytic intermediates in a process called gluconeogenesis. Gluconeogenesis involves making glucose from smaller carbon substrates, such as lactic acid, and is normally associated with liver and kidney cells[177]. It may be that lactate serves as a gluconeogenic fuel source, decreasing a T_{reg} cell's need for glucose. We hypothesized that rather than making glucose to break it back down via

glycolysis, T_{reg} cells shunted it into the pentose phosphate pathway which is essential for generating intermediates needed for proliferation[178].

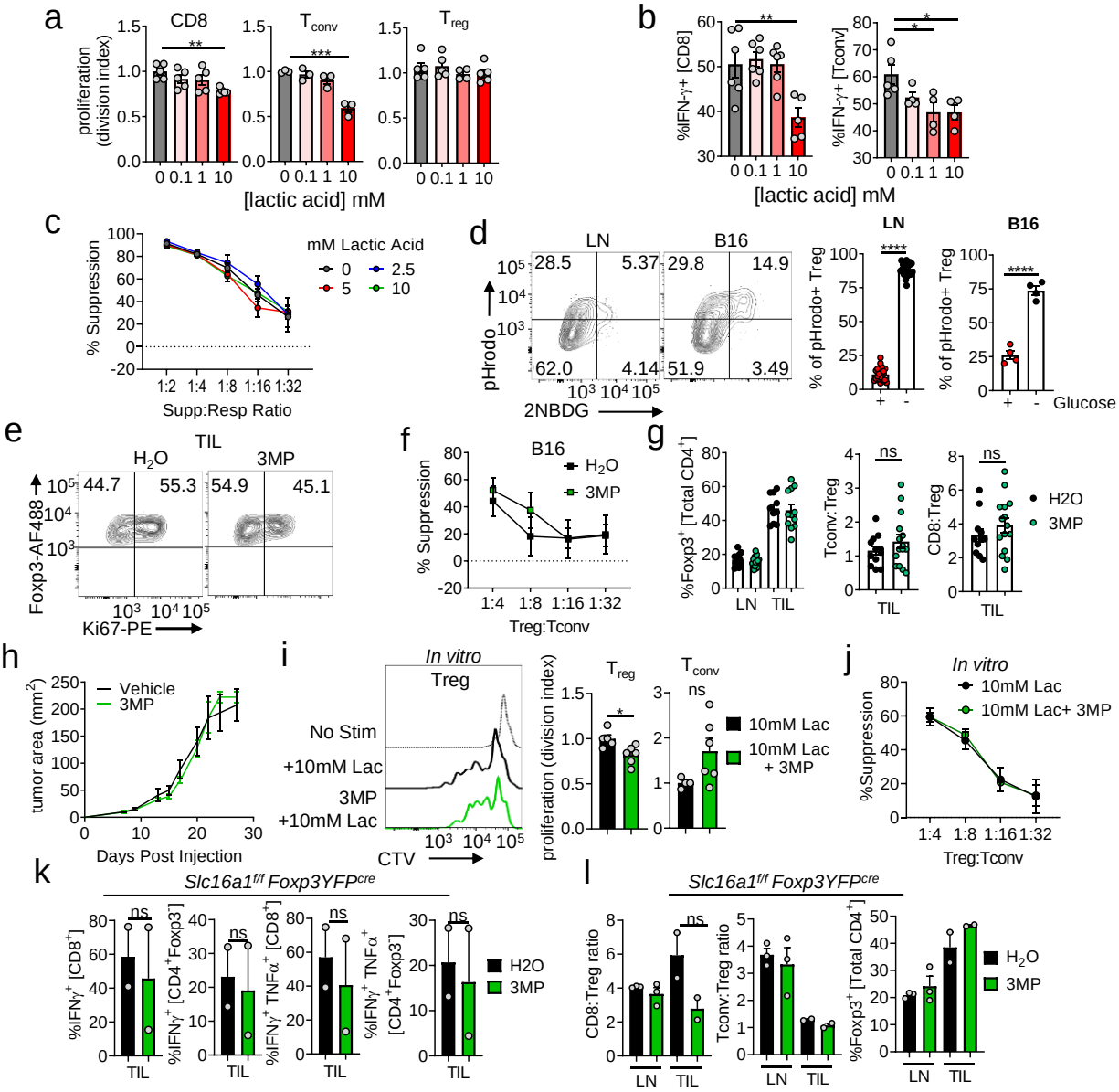

Figure 8. Treg cells are resistant to lactic acid and use PEPCK-mediated metabolic pathways to support their proliferation.Proliferation of CD8+, Tconv, and Treg cells labeled with CellTrace Violet (CTV) activated in media with lactic acid for 3 days (p=0.0058). (b) IFN-γ production of CD8 and Tconv cells conditioned as in (a) then re-stimulated overnight with PMA/ionomycin (CD8 **p=0.0042, Tconv *p=0.02). (c) Suppression assay using Treg cells conditioned as in (a) performed in absence of additional lactic acid. (d) Representative histogram and quantification of pHrodo+ Treg cells taking up 2NBDG. (e) Representative flow plot of Ki67 expression by B16-infiltrating Treg cells from mice treated ±3MP for 3 days. (f) Suppressive capacity of Treg cells, isolated from mice as in Fig.3k.**

(g) Percent Foxp3+ cells, Tconv to Treg ratio, and CD8 to Treg ratio within the TIL of mice treated as in (f). (h) Tumor growth curve of B16 in C57BL/6 mice treated with H2O or 3MP. (i) Proliferation of Treg and Tconv cells activated and cultured in 10mM lactic acid media ±3MP for 3 days (*p=0.016). (j) Capacity of activated Treg cells conditioned in 10mM lactic acid media ± 250μM 3MP for 3 days to suppress the proliferation of CTV labelled Tconv cells. (k) IFN-γ expression by CD8 and Tconv cells in Foxp3YFPcre or Slc16a1f/fFoxp3YFPCre mice treated as in (f). (l) Percent Foxp3+ cells, Tconv to Treg ratio, and CD8 to Treg ratio within LN and tumor of Slc16a1f/fFoxp3YFPCre mice treated as in (f). Results are representative of four (d), three (a,b,c,f,g,i), or two (h,j,k,l) independent experiments. Significance (*p< 0.05, **p <0.01, ***p < 0.001, ****p<0.0001) determined by unpaired two-tailed t test (d,e,g,i,k,l) or one-way ANOVA with Dunnett's multiple comparisons test (a,b) or two-way ANOVA with Sidak's multiple comparisons test (c,f,h,j). Data presented as mean values ±SEM.

As high environmental glucose can inhibit T_{reg} cell suppressor function (**Fig. 5g**), we asked whether lactic acid could mitigate the deleterious effects of glucose. Indeed, conditioning T_{reg} cells in high glucose plus tumor-equivalent concentrations of lactic acid rescued suppressor function (**Fig 7i**). Thus, T_{reg} cells are not only resistant to lactic acid but can take up this metabolite, in part to counteract deleterious effects of high glucose, and those that do display an activated T_{reg} cell signature and low glucose uptake.

To dissect the individual contributions of lactate uptake and oxidation from upstream gluconeogenic reactions dependent on lactate-derived PEP we used the PEPCK inhibitor 3-mercaptopicolinic acid (3MP)[179]. 3MP treatment of ^{13}C-lactate pulsed T_{reg} cells reduced PEP accumulation without impacting incorporation into the TCA cycle (**Fig 7j**). To simply assess the impact of inhibiting PEP formation on T_{reg} cells proliferation, T_{reg} cells were activated and cultured in 10 mM lactic acid with or without 3MP. As

hypothesized, T_{reg} cells in the presence of 3MP significantly reduced their proliferation but there was no change in T_{conv} cells assayed in the same conditions (**Fig. 8i**). However, 3MP did not impact the suppressive capacity of T_{reg} cells in vitro suggesting PEP formation mainly contributes to proliferation (**Fig. 8j**). To assess 3MP's impact on T_{reg} cell proliferation in vivo, B16 tumor bearing mice were treated for 3 days with 3MP. Mice that received 3MP decreased the proliferation of tumor-resident, but not LN, T_{reg} cells, and increased intratumoral CD8 IFN-γ production confirming our in vitro findings (**Fig. 7k,l**). This tumor specific impact on T_{reg} cells further confirms their utilization of lactic acid in lactic acid rich environments. The increase in CD8 IFN-γ production suggests a decrease T_{reg} cell suppressive capacity upon 3MP treatment, but this may be a consequence of decreased T_{reg} number. However, 3MP treatment did not overtly affect the intratumoral percentage of $Foxp3^+$ cells or T_{conv}/CD8:T_{reg} cells ratios (**Fig. 8g**). Consistent with our in vitro findings, 3MP treatment did not impact intratumoral T_{reg} cell suppressor function when interrogated ex vivo (**Fig. 8f**). As acute treatment of 3MP led to decreased T_{reg} cell proliferation, we investigated long term treatment on overall tumor growth. Starting seven days post tumor injection with B16, mice were treated daily with 3MP or water. 3MP treatment did not overtly impact tumor growth (**Fig. 8h**). Thus, T_{reg} cells utilize lactic acid to not only feed the TCA cycle, but to generate PEP, critical for fueling T_{reg} cell proliferation within the tumor.

3.4 Discussion

In this chapter we demonstrated that, in contrast to effector T cells, T_{reg} cells utilize lactic acid, a metabolite rich in the TME, to support their proliferation and counteract the deleterious effects of high glucose on their suppressive function. Lactic acid has been shown to be immunosuppressive to both CD8 and effector CD4 T cells[25,31]. As lactate is an organic acid with a pkA of 3.86 it may be that acidity alone is responsible for the impairment of effector cells. However, Angelin et al demonstrated that pH neutral lactate reduces effector T cell proliferation both in vitro and in vivo[25] without impacting T_{reg} cell proliferation or suppressive function, similar to our findings (**Fig. 8a-c**). This indicates that lactate alone is sufficient to impair effector T cells.

While the concept of using intracellular pH dyes to detect lactic acid uptake is not new[176], its application in flow cytometry is a powerful tool. The single cell resolution of flow cytometry allowed us to identify lactate uptake by T_{reg} cells in many different tissue types where their number is limiting or difficult to obtain (**Fig. 7c**). While measuring intracellular pH changes is not a perfect readout for lactic acid uptake, it did recapitulate our deeper mass spectrometry approach which requires a large cellular input (**Fig. 7g**). Moreover, the multidimensionality of flow cytometry allowed for simultaneous probing of glucose avidity and phenotypic markers revealing lactic acid avid T_{reg} cells were phenotypically more activated and took up little glucose **(Fig 7e, Fig. 8d**).

The simplicity and robustness of this assay could also be applied to other limiting cell populations, especially to identify if lactic acid uptake is common among other regulatory cell populations within the TME. This may be the case as lactic acid polarizes macrophages to an M2-like state, thought to harbor a more suppressive phenotype, and

increases protein and histone lactylation, a post-translational modification derived from lactate[47,49]. These findings suggest that regulatory populations may share a metabolism, begging the question does high lactate metabolism drive a suppressive phenotype or the suppressive phenotype drive high lactate metabolism? If lactate metabolism can drive a suppressive phenotype this would be extremely useful in generating T_{reg} cell therapies to treat various autoimmune conditions[180]. Like chimeric antigen receptor (CAR) T cell therapies, T_{reg} cell therapies involve expanding T_{reg} cells in vitro, allowing for an opportunity to either alter gene expression through viral vectors or alter the media in which they are expanded to bolster lactate metabolism and thus immunosuppression. Measuring lactic acid uptake via intracellular dyes and flow cytometry could prove a useful and simple readout if lactate metabolism was to be explored for T_{reg} cell therapies.

Lactate is often thought of as a waste product of glycolytic metabolism, but it represents an important metabolite for cellular function and a likely fuel source for tissues[24]. Our data suggest T_{reg} cells are endowed with metabolic flexibility to use this carbon source, both as fuel and as a means to protect their high suppressive capacity from negative effects of glucose (**Fig 7g-i**). Consequently, T_{reg} cells do not possess both high lactic acid and glucose uptake (**Fig. 3g, 5f, 7c,d, 8d**). Thus, we propose a glucose:lactate axis exists to fine-tune T_{reg} cell functioning depending on the nutrient milieu (**Fig 5g, 7i**). As discussed in the previous chapter, nutrient milieu likely acts as an immune cell extrinsic regulator during a pathogen response, where high environmental glucose at the beginning of the immune response[170] may drive effector cells and dampen T_{reg} cell function, then as the pathogen is cleared and glucose is metabolized to lactic acid, T_{reg} cell proliferation and suppression is bolstered to reign in the inflammation

(Chapter 2.4). As T_{reg} cells must be active when immune activity is at its lowest, they exist metabolically 'out-of-sync' with their conventional counterparts. This requires utilizing fuels prevalent in tissue environments to maintain suppressor function when their conventional T cell targets may be competing for nutrients.

We show that lactate not only fuels the TCA cycle but is also exported from the mitochondria, contributing to gluconeogenesis via PEP in T_{reg} cells. It has been previous demonstrated that lactate taken up by T_{reg} cells contributes to the TCA cycle but not that it contributes to the generation of PEP[25]. The formation of PEP from lactate derived carbons suggests T_{reg} cells are performing gluconeogenesis to produce glucose, offering a potential explanation as to their limited glucose avidity, especially in lactate rich environments (**Fig. 7c**). This gluconeogenic component of lactate metabolism supports T_{reg} cell proliferation, suggesting a shunting of carbons into the pentose phosphate pathway (PPP). The PPP is responsible for the generation of nucleotides, ribose, and amino acids all of which are critical for proliferation. As T_{reg} cells are critical for maintaining immune homeostasis, the use of lactate to supply carbon to the PPP may have evolutionarily arisen to protect T_{reg} function in situations where glucose was limiting. Unfortunately, this metabolic flexibility has provided high adaptability to the harsh TME. Blocking PEP formation using the inhibitor 3MP reduced T_{reg} cell proliferation both in vitro and in vivo in the presence of lactic acid (**Fig. 7k, 8i**). In vitro this was only observed in T_{reg} cells and not T_{conv} cells consistent with the carbon tracing data showing very little PEP derived from lactate carbons in T_{conv} cells (**Fig. 7h, 8i**). In vivo, 3MP treatment did not globally impair T_{reg} proliferation, as the lymph node T_{reg} cells remained unchanged, but specifically reduced the proliferation of those infiltrating the tumor (**Fig. 7k**). This suggests

that PEP formation from lactic acid is not required for T_{reg} cell proliferation, rather T_{reg} cells can use lactic acid, especially when it is abundant (**Fig. 7a**) to support their proliferation. The tumor specificity of blocking lactate metabolism is exciting as we can treat with a global inhibitor and only impact the T_{reg} cells within the tumor. Unfortunately, therapeutic treatment with 3MP did not impact overall tumor growth (**Fig. 8h**). As 3MP would block PEP formation in gluconeogenic tissues, such as the liver and kidneys, it is likely this altered overall blood glucose levels[181] and lowered the lactic acid output by the tumor making PEP formation less critical for T_{reg} cells. Altering blood glucose levels likely creates many confounding variables resulting in no change in overall tumor growth. Therapeutically, it would be more beneficial to target lactate metabolism far downstream of PEP because, as we will see in greater detail next chapter, lactic acid contributes to both proliferation and suppressive function of T_{reg} cells, while PEP formation contributes only to proliferation.

4.0 Tumor-infiltrating T_{reg} cells require lactate uptake to maintain their high suppressive function

4.1 Foreword

This chapter was adapted from a previously published manuscript in *Nature*: **Watson MJ**, Vignali PDA, Mullett SJ, Overacre-Delgoffe AE, Peralta RM, Grebinoski S, Menk AV, Rittenhouse NL, DePeaux K, Whetstone RD, Vignali DAA, Hand TW, Poholek AC, Morrison BM, Rothstein JD, Wendell SG, Delgoffe GM. "Metabolic support of tumour-infiltrating regulatory T cells by lactic acid." *Nature*. 2021 Mar;591(7851):645–51.

4.2 Introduction

In the previous chapter we demonstrated that T_{reg} cells can utilize lactic acid to support their proliferation and suppressive function. In addition, we revealed a glucose:lactate axis that fine tunes T_{reg} cell functioning depending on the nutrient milieu. However, left unanswered is whether T_{reg} cells require lactate metabolism within the tumor microenvironment and if this can be targeted to enhance anti-tumor immunity. Here we address this question using a mouse model harboring a T_{reg} cell specific deletion of the lactate transporter *Slc16a1* and several different tumor models. We reveal that indeed, T_{reg} cells require lactate metabolism within the tumor, but not in the periphery,

leading to delayed tumor growth and synergy with anti-PD-1 immunotherapy. These findings provide a rationale for combing lactate transporter inhibitors and anti-PD-1 therapy in human trials and reveal a fundamental mechanism of T_{reg} cell's persistence and functioning with the TME.

4.3 Results

To determine the significance of lactic acid utilization by T_{reg} cells in vivo, we generated a mouse with a constitutive, T_{reg}-specific deletion of MCT1 (*Slc16a1*$^{f/f}$*Foxp3*^{YFPCre}). qPCR confirmed *Slc16a1* deletion, lack of compensation by *Slc16a7*/MCT2 or *Slc16a3*/MCT4 upregulation, and no deletion in CD4^{+}Foxp3^{-} cells (**Fig. 9a,b**). Expectedly, deletion of *Slc16a1* resulted in loss of lactic acid uptake as measured by intracellular acidification (**Fig. 10a**). These mice did not show any overt signs of autoimmunity or lymphoproliferation (**Fig. 9c,d**). Rather, T_{reg} cells from the LN of *Slc16a1*$^{f/f}$*Foxp3*^{YFPCre} mice displayed similar suppressive capacity, proliferation, and expression of T_{reg} signature genes when assayed ex vivo (**Fig. 9e-h**). MCT1 deficiency in T_{reg} cells revealed no significant differences in percentage of Foxp3^{+} cells infiltrating various tissues, although several compartments (thymus, muscle p= 0.051) showed increases in glucose uptake at the steady-state, further supporting the existence of a glucose:lactate axis (**Fig. 9i,j**). To test the impact of inflammation on MCT1 deficient T_{reg} cells, ear skin was painted with Imiquimod (TLR7 agonist) over 6 days. Treatment resulted in no increased inflammatory ear thickness, nor loss of T_{reg} cell markers in *Slc16a1*$^{f/f}$*Foxp3*^{YFPCre} mice (**Fig. 9k,l**). We also determined long-term function and stability

of MCT1-deficient T_{reg} cells in transfer colitis. Unlike 2NBDG^{hi} T_{reg} cells, MCT1-deficient T_{reg} cells did not show reduced stability (**Fig. 9m**). However, they were not completely functional: at 7 weeks, mice receiving MCT1-deficient T_{reg} cells had more histologically severe colitis, although less severe than mice receiving 2NBDG^{hi} T_{reg} cells (**Fig. 9n,o**). Thus, MCT1 deficiency appeared dispensable for T_{reg} cell survival and function, although under highly inflammatory conditions they may have decreased activity.

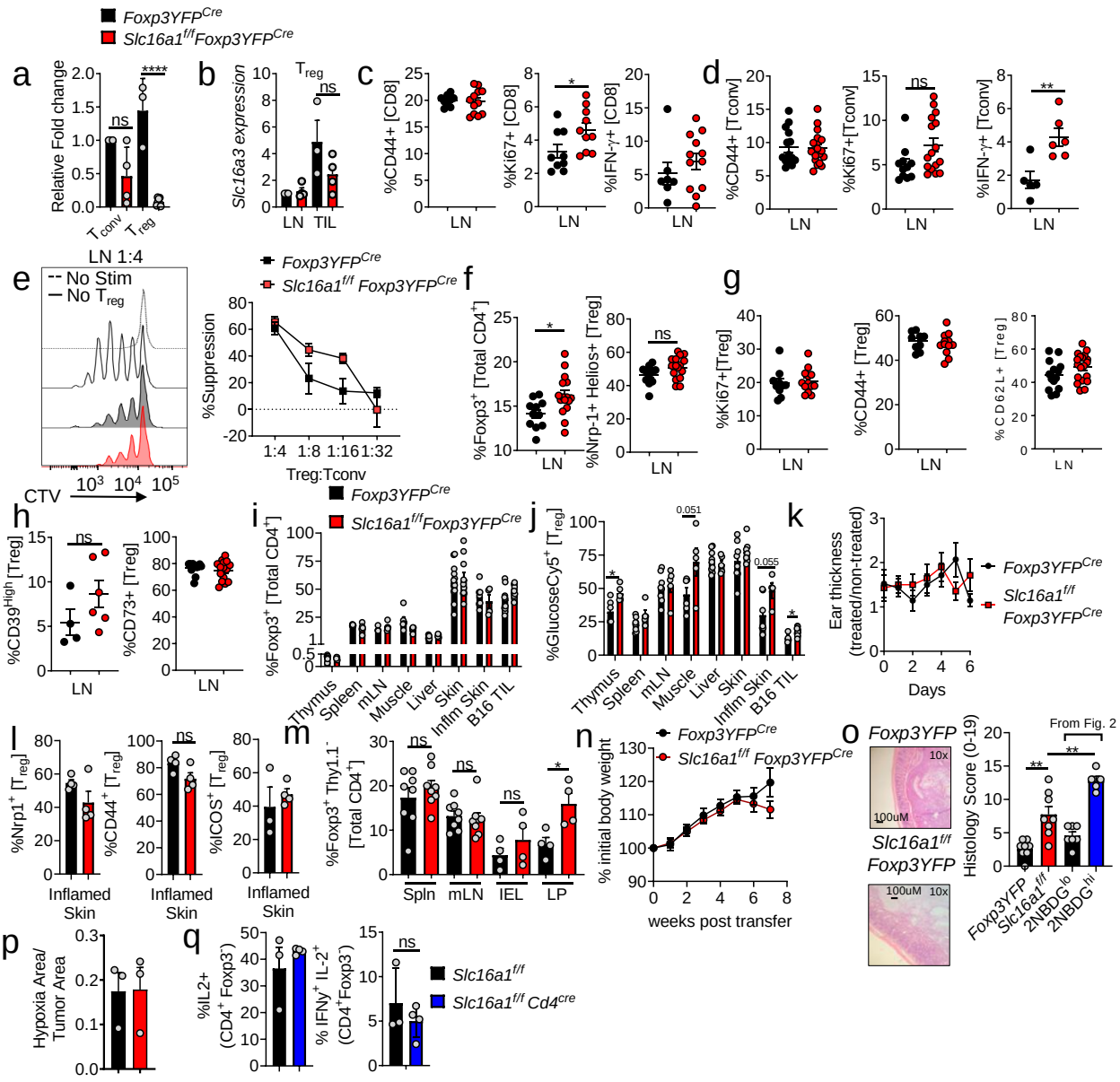

Figure 9. MCT1 is efficiently deleted in Treg cells of Slc16a1f/fFoxp3YFP-Cre mice and is not required for peripheral Treg cell function.Slc16a1 expression in Tconv and Treg cells from the lymph nodes (LN) of Foxp3YFPCre or Slc16a1f/fFoxp3YFPCre mice. (b) Treg cell mRNA expression of Slc16a3 (MCT4) from mice as in (a). CD44, Ki67, and IFN-γ production by LN CD8+ T cells (c, *p=0.039) or Tconv cells (d, **p=0.007) from mice as in (a). (e) Capacity of LN-derived Treg cells as in (a) to suppress proliferation of CellTrace Violet (CTV) labelled Tconv cells. (f) Percent Foxp3+ and Nrp1+Helios+ LN Treg cells from mice as in (a) (*p=0.013). (g) CD44, Ki67, and CD62L expression by LN Treg cells as in (a). (h) CD39 and CD73 expression by LN Treg cells as in (a). Percent of Foxp3+

cells (i) or GlucoseCy5+ Treg cells (j) from various tissues of mice as in (a) (thymus *p=0.014, B16 *p=0.019). (k) Normalized ear thickness of imiquimod treated mice as in (a). (l) Percent marker positive Treg cells from mice treated as in (k). (m) Foxp3 expression in transferred wild type or Slc16a1-deficient Treg infused with Thy1.1+ Tconv cells into Rag1–/– mice iv. (*p=0.02) (n) Weight of Rag1–/– mice over time from (m). (o) Representative sections of the colon and quantified histology scores 7 weeks post transfer from mice as in (m) and Fig.2d (p=0.001, **p=0.009). (p) Anti-pimonidazole area over tumor area (B16) calculated from immunofluorescence from Foxp3YFPcre and Slc16a1f/fFoxp3YFPCre mice. (q) IL-2 and IFN-γ expression by Slc16a1-deficient Tconv cells stimulated overnight with PMA/ionomycin. Results are representative of four (c,d,f,g), three (a,b,e,h,j,p,q), or two (k,l,m,i,o) independent experiments. Significance (*p< 0.05, **p <0.01, ****p < 0.0001) determined by unpaired two-tailed t test (a-d,f-q) or two-way ANOVA (e). Data presented as mean values ±SEM.**

However, we reasoned MCT1-mediated lactate uptake would be most important within lactate-rich tumor tissue. Inoculating *Slc16a1$^{f/f}$Foxp3^{YFPCre}* mice with B16 melanoma resulted in slowed tumor growth and prolonged survival (**Fig. 10b**). Characterizing the infiltrate when both genotypes harbored tumors of similar sizes (day 14) showed while CD8$^+$ T cells in *Slc16a1$^{f/f}$Foxp3^{YFPCre}* mice exhibited higher coinhibitory markers PD-1 and Tim-3, indicative of terminal differentiation (**Fig. 10c**), CD8$^+$ and T_{conv} cells were more proliferative and competent to produce IFN-γ, suggesting decreased suppressive function by MCT1-deficient T_{reg} cells (**Fig. 10d, e**). Indeed, intratumoral MCT1-deficient T_{reg} cells had reduced suppressive function *ex vivo* (**Fig. 10f**) and were less proliferative, resembling intratumoral T_{reg} cells from 3MP-treated mice (**Fig. 10g, 7k**). Analysis of 3MP-treated *Slc16a1$^{f/f}$Foxp3^{YFPCre}* mice suggested 3MP's effects on T_{reg} cells was mediated through MCT1, as tumor infiltrating effector cell cytokine production and

$CD8^+$- and T_{conv-} to T_{reg} cell ratios remained unchanged (**Fig. 8k,l**). Characterization of intratumoral MCT1-deficient T_{reg} cells revealed decreases in CD44 and Nrp1 staining, concomitant with elevated PD-1 staining, potentially indicating dysfunctional T_{reg} cells[182] (**Fig. 10h**). Metabolically, MCT1-deficient, tumor-resident T_{reg} cells compensated by becoming glucose avid (**Fig. 10i**). We found, as a consequence, that MCT1-deficient T_{reg} cells would no longer persist within the lactate rich hypoxic areas of tumors, as measured by pimonidazole staining, despite overall tumor hypoxia remaining similar (**Fig. 9p, 10j**).

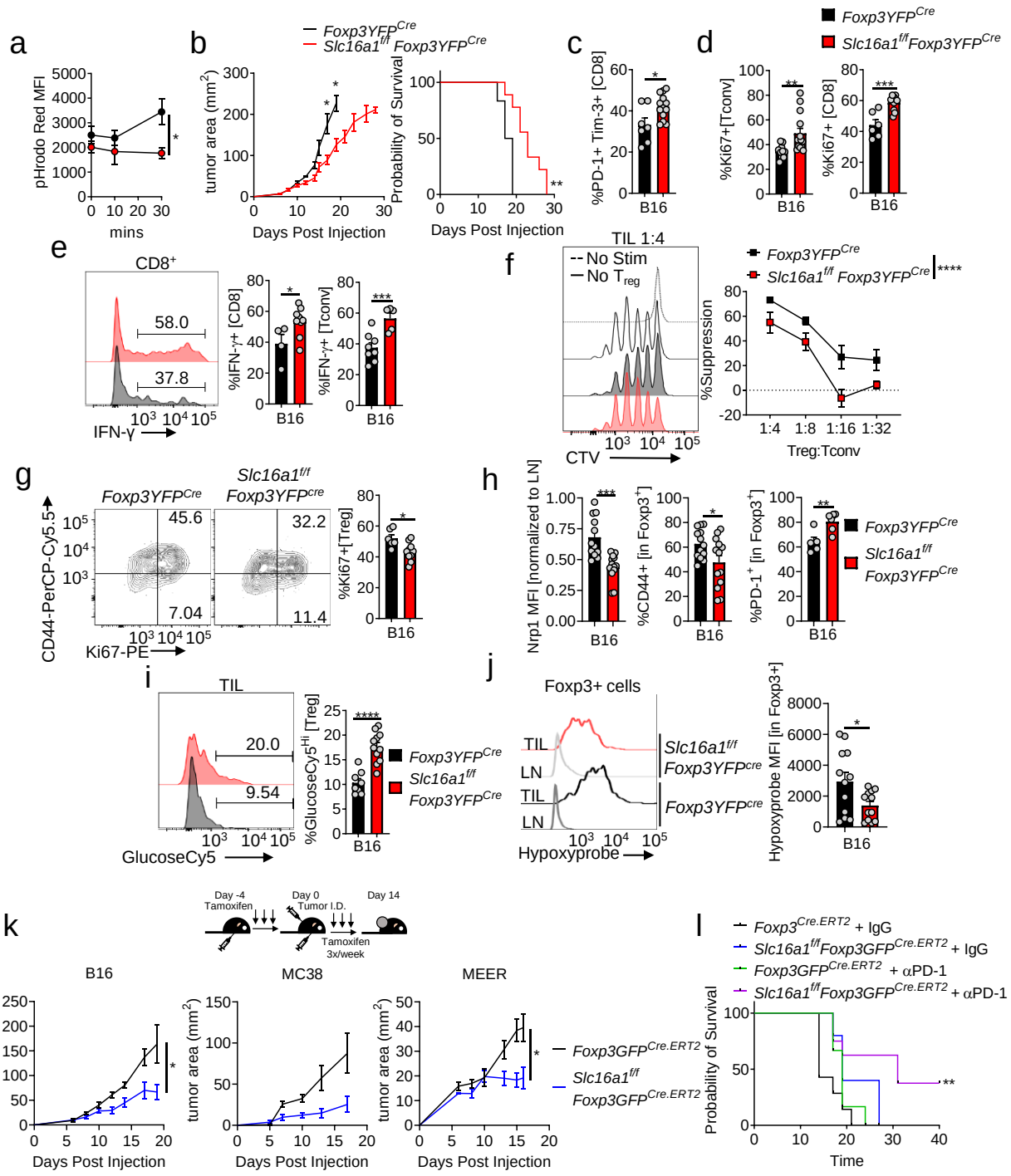

Figure 10. Tumor-infiltrating Treg cells require lactate uptake to maintain their high suppressive function.Lactate-elicited pHrodo fluorescence in Foxp3YFP-Cre or Slc16a1f/fFoxp3YFP-Cre Treg cells (*p=0.041). (b) B16 tumor growth and survival of Foxp3YFPCre and Slc16a1f/fFoxp3YFPCre mice (*p=0.016, *p=0.035, **p=0.003). (c) Percent of B16-infiltrating PD-1+Tim-3+ CD8 T cells day 14

post tumor injection in mice as in (a) (*p=0.017). (d) Proliferation of tumor infiltrating Tconv and CD8+ T cells as in (c) (p=0.009). (e) Tumor infiltrating CD8+ and Tconv cells re-stimulated with PMA/ionomycin and stained for IFN-γ (*p=0.039). (f) Capacity of WT or Slc16a1-deficient tumor-infiltrating Treg cells to suppress proliferation of CTV labeled Tconv cells. (g) Percent proliferating tumor-infiltrating Treg cells from mice as in (c). (*p=0.011). (h) Percent or MFI of WT and Slc16a1 KO Treg cells expressing Nrp1, PD-1, CD44 from B16 tumors (TIL) as in (c) (*p=0.029, **p=0.009). (i) GlucoseCy5 uptake by B16 tumor infiltrating Treg cells as in (c) (j) Pimonidazole staining of WT and Slc16a1 KO Treg cells from B16 tumors as in (c) (*p=0.029). (k) Tumor growth of B16 (melanoma, *p=0.025) MC38 (adenocarcinoma, *p=0.023), and MEER (HNSCC, *p=0.019) in tamoxifen treated Foxp3GFPCre.ERT2 and Slc16a1f/fFoxp3GFPCre.ERT2 mice. Mice were given tamoxifen 5 consecutive days prior to tumor injection then 3x per week. (l) Survival of tamoxifen treated Foxp3GFPCre.ERT2 and Slc16a1f/fFoxp3GFPCre.ERT2 mice injected with B16 and treated with IgG or anti-PD1 antibodies 3x weekly (**p=0.002). Results are representative of four (b,c,d,f,g,h(Nrp1, CD44),i,j), three (a, k(B16)), or two (h(PD-1), k(MC38, MEER),l) independent experiments. Significance (*p< 0.05, **p <0.01, ***p < 0.001, ****p<0.0001) determined by Holm-Sidak method, with alpha = 0.05 for tumor growth curve (b) or the log-rank test for survival curves (b,l) or unpaired two-tailed t test (a,c,d,e,g,h,i,j,k) or two-way ANOVA (f). Data presented as mean values ±SEM.**

To remove any unforeseen effects of MCT1 deletion on T_{reg} cell development, we interrupted MCT1 expression just prior to B16 melanoma injection using a tamoxifen-inducible model (*Slc16a1*$^{f/f}$*Foxp3*$^{GFPCre.ERT2}$) and showed similar immunologic and survival outcomes, including the development of a 'fragile'[162] T_{reg} cell phenotype in which Foxp3^{+} cells begin expressing IFN-γ (**Extended Data Fig. 11**). Induced T_{reg} deletion of MCT1 also slowed tumor growth of MC38 adenocarcinoma and MEER HNSCC (Head and neck squamous cell carcinoma) (**Fig. 10k, 11g,h**). We thus reasoned loss of lactate uptake in T_{reg} cells produced an environment conducive to immunotherapy. Triggering deletion of

MCT1 in T_{reg} cells synergized with anti-PD-1 therapy, resulting in complete regressions in 37.5% of B16-bearing mice (typically insensitive to anti-PD-1) (**Fig. 10l**). Deletion of MCT1 from T_{conv} cells using *Slc16a1*$^{f/f}$*Cd4*^{cre} mice did not impact their capacity to produce IL-2 and IFN-γ, suggesting MCT1 was not generally required for T cell function (**Fig. 9q**). Thus, MCT1 expression and consequent lactic acid uptake is dispensable for most tissue derived T_{reg} cells but required to maintain high suppressor activity in the TME.

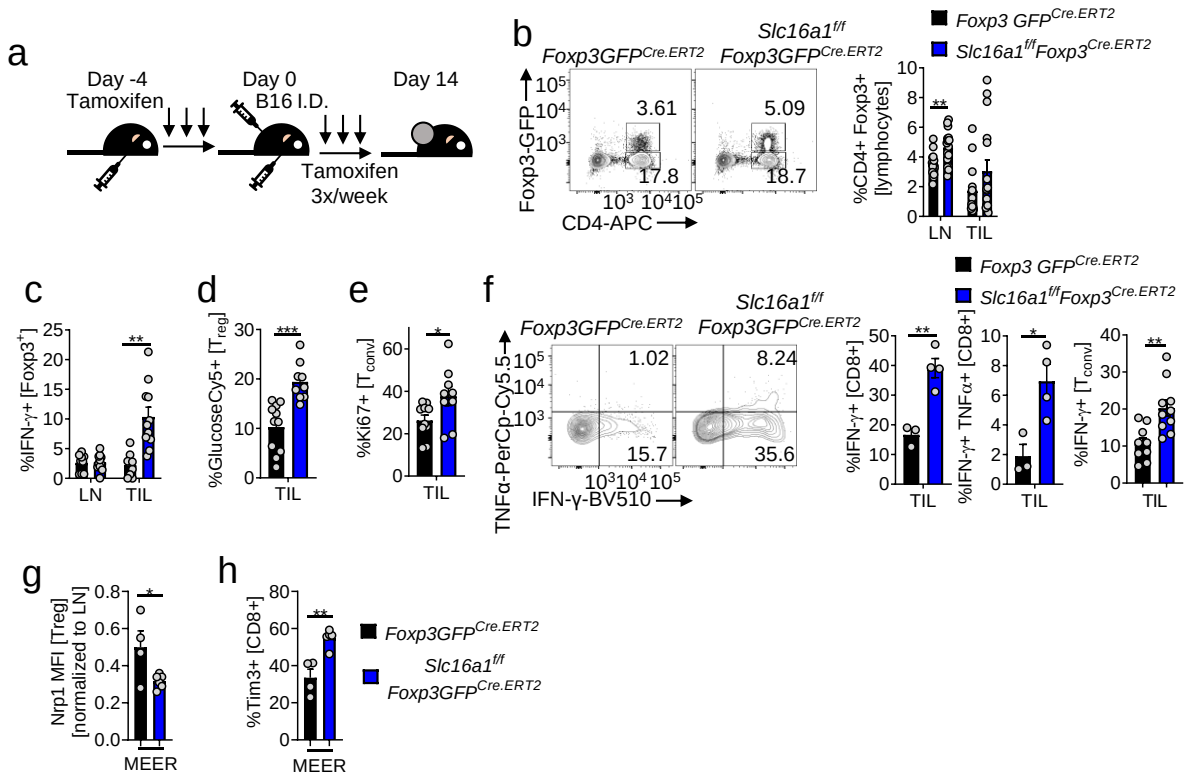

Figure 11. Acute deletion of MCT1 results in similar immunologic phenotypes in B16 melanoma and predilection towards a fragile Treg cell phenotype.Foxp3GFPCre.ERT2 and Slc16a1f/f Foxp3GFPCre.ERT2 mice were treated 5 consecutive days with tamoxifen I.P. prior to inoculation with 1.5 x 105 B16 tumor cells. Following inoculation, tamoxifen was administered I.P. 3 times a week until sacrifice at day 14. (b) Percent Foxp3+ CD4+ cells in the lymph node (LN) and tumor (TIL) as in (a) (p=0.005). (c) Tabulation of IFN-γ production by Treg cells from the LN and TIL of mice as in (a) (**p=0.002). (d) Glucose consumption by Treg cells from the TIL of mice as in (a). (e) Percent proliferating Tconv cells from the TIL of mice as in (a) (*p=0.037). (f) Representative flow plot and tabulation of IFN-γ and TNFα production by CD8 T cells from the TIL of mice as in (a) (**p=0.003, *p=0.02). Tabulation of IFN-γ production by Tconv cells from the TIL of mice as in (a) (**p=0.003). (g) Nrp1 mean fluorescence intensity on MEER intratumoral Treg cells derived from Foxp3GFPCre.ERT2 and Slc16a1f/f Foxp3GFPCre.ERT2 mice treated as in (a) (*p=0.034). (h) Tim-3 expression by MEER derived CD8 T cells from mice as in (g) (**p=0.003). Results are representative of four (b,c,d,e), or three (f), or two (g,h) independent experiments. Significance (*p< 0.05, **p <0.01) determined by unpaired two-tailed t test (b-h). Data presented as mean values ±SEM.**

In a parallel study, *Zappasodi et al.*[118] showed that glycolysis-low tumors responded better to anti-CTLA4 treatment. They observed that this increase was due to anti-CTLA4's action on T_{reg} cells, destabilizing them to produce more IFN-γ and TNFα, and lowering their CTLA4 and CD25 expression. Moreover, this loss of stability resulted in increased T_{reg} cell glucose uptake and reduced suppressive capacity. In collaboration with *Zappasodi et al.* we sought to determine whether glucose uptake was driving T_{reg} cell destabilization after anti-CTLA4 treatment. To test this, we utilized mice harboring a T_{reg} cell specific deletion of the glucose transporter Glut1 (*Glut1*$^{f/f}$ *Foxp3GFP*$^{Cre.ERT2}$) and implanted them with glycolysis-low B16 tumors (stable knockdown of LDH: B16KD). Starting on day 6 post tumor injection mice were given 4 treatments of anti-CTLA4 then harvested on day 16. T_{reg} cells with a loss of Glut1 maintained higher CTLA4 and CD25 expression upon anti-CTLA4 treatment (**Extended data Fig. 10b of [118]**). In addition, Glut1 deficient T_{reg} cells produced less IFN-γ and TNFα upon anti-CTLA4 treatment resembling T_{reg} cells treated with IgG (**Extended Data Fig 10d of [118]**). Taken together these data suggest that anti-CTLA4 impairs T_{reg} cell function by increasing their glucose uptake which can be rescued by deleting Glut1.

4.4 Discussion

It is unlikely regulatory T cells evolved to thrive in tumors; rather cancers exploit this predilection for alternative substrates to maintain an immunosuppressive environment. Lactate is not only enriched in the tumor but is elevated in immunologically distinct tissue environments such as muscle, adipose, and nervous system[183,184]. We also

suspect lactate is one of a host of alternative metabolites T_{reg} cells can utilize. MCT1 itself can also transport acetate, succinate, propionate, and butyrate, which have been shown to play roles in T_{reg} cells[38,185,186]. Indeed, our findings using transfer colitis suggest MCT1 deficiency may impact T_{reg} cell function in the gut. Notably, however, we did not observe overt gut inflammation at the steady state in *Slc16a1*$^{f/f}$*Foxp3*^{Cre} mice, suggesting both inflammation and MCT1 substrate availability play roles in maintaining T_{reg} cells in that environment.

As lactate can promote suppressive functions of other tolerogenic cell types, like tumor-associated macrophages[47], cell types sharing lactate metabolism may share suppressor activity. While this is exploited in the tumor microenvironment, causing suppressive cells to thrive, it is actionable: T_{reg} cell-specific deletion of the lactate transporter not only results in decreased tumor growth but synergy with checkpoint blockade immunotherapy. MCT1 inhibition to directly target lactate metabolism or inhibition of tumor acidity may break this metabolic symbiosis and lower the regulatory T cell barrier to cancer immunity. Currently, AstraZeneca's AZD3965 compound, an MCT1 inhibitor, has made it through Phase I testing for in-human use (NCT01791595). As described in the introduction to this thesis, preclinical work has shown AZD3965 can lower lactic acid secretion into the TME and increase natural killer and myeloid cell infiltration[123]. However, we do not understand how AZD3965 impacts T_{reg} cells as preclinical studies were performed in immunodeficient mice, and the phase I trial did not include any outcome measures to look at T_{reg} cells upon treatment. Whether pharmacologic inhibition of MCT1 recapitulates genetic deletion in T_{reg} cells is of great interest and a logical next step for these studies.

5.0 Lactic acid and glucose: possible mechanisms of support and detriment for regulatory T cells

5.1 Introduction

The previous chapters serve to describe the bulk and focus of my thesis work. I have continued to explore T_{reg} cell metabolism and how it contributes to T_{reg} cell function and identity beyond what has been described in the previous chapters. While this on-going work has yet to be published, it is my hope that these data lay the groundwork for future research within the Delgoffe lab. In this chapter I will describe my current on-going research and I will propose future directions this research could take.

5.2 Glucose avid regulatory T cells, a state or fate?

In the chapter 2 discussion the question of whether glucose avid T_{reg} cells are a state, a temporary phenotype that T_{reg} cells can freely move in and out of, or a fate, a permanent “differentiation” lineage, was posed. In chapter 2, we observed that T_{reg} cells conditioned in 25mM glucose media for three days had a decreased suppressive capacity compared to those conditioned in 5mM glucose media and wanted to determine if this was due to an increased proportion of glucose avid T_{reg} cells (**Fig. 5g**). Indeed, after 3 days of conditioning there was an increased percentage of glucose avid T_{reg} cells in the

25mM glucose compared to 0- or 5-mM (**Fig. 12a**). We next sought to determine whether the increased proportion of glucose avid T_{reg} cells was due to T_{reg} cells becoming glucose avid or if the glucose avid T_{reg} cells were being selected for. To test this, T_{reg} cells from Foxp3 reporter mice were sorted based on glucose avidity using the tracer GlucoseCy5 ($Glucose^{lo}$ and $Glucose^{hi}$) then activated overnight with CD3/CD28 and IL-2 and conditioned in 5- or 25-mM glucose media for three days (**Fig 12b**). Remarkably, 70% of $glucose^{lo}$ T_{reg} cells maintained a low glucose phenotype when conditioned in 5- and 25-mM glucose media (**Fig. 12c**). Similarly, $glucose^{hi}$ T_{reg} cells maintained their avidity for glucose (~80% $glucose^{hi}$) in both 5- and 25-mM glucose media (**Fig. 12c**).

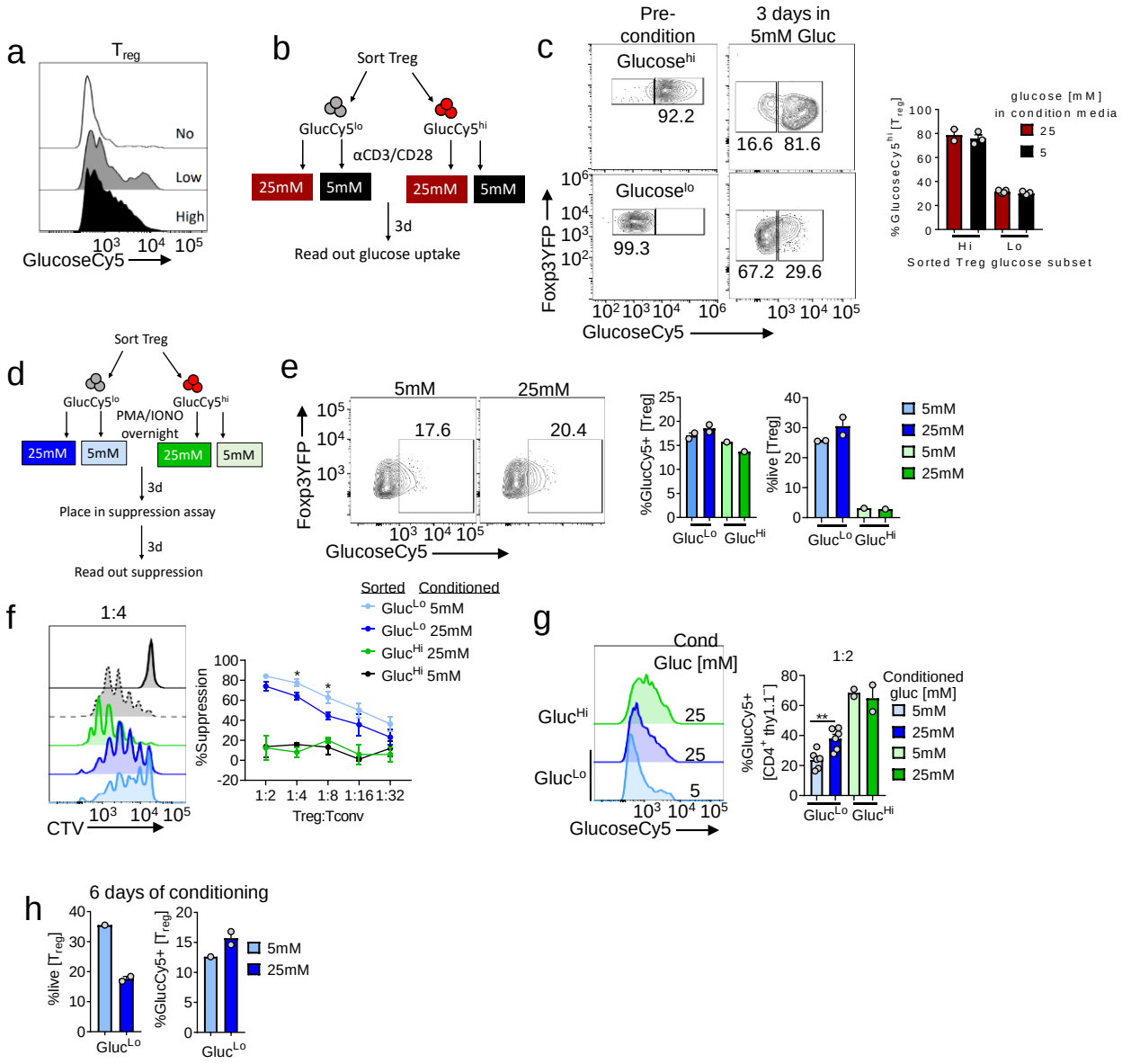

Figure 12. Extracellular glucose concentration alters glucoseLo but not glucoseHi Treg cells.Representative histogram of Treg cell glucoseCy5 uptake after 3 days in high (25 mM), low (5 mM), or no (0 mM) glucose media. (b) Diagram of experimental outline for (c). (c) Representative flow cytogram and tabulation of glucoseCy5 uptake of pre-conditioned and 3-day glucose conditioned glucoseLo/Hi Treg cells gated on CD4+ Foxp3+. Cells were activated with αCD3/CD28 and IL-2 (d) Diagram of experimental outline for (e-g). (e) Representative flow cytogram and tabulation of glucoseCy5 uptake of pre-conditioned and 3-day glucose conditioned glucoseLo/Hi Treg cells gated on CD4+ Foxp3+. Cells were activated with PMA/Iono and IL-2. (f) Capacity of

glucoseLo/Hi Treg cells conditioned in 5-or 25-mM glucose media to suppressive the proliferation of CTV labeled Tconv cells. Representative histogram depicts 1:4 Treg:Tconv cell ratio. (g) Representative histogram and tabulation of glucoseCy5 uptake from Treg cells post suppression assay as in (f). (h) Viability and glucoseCy5 uptake of glucoseLo Treg cells conditioned as in (d) for 6 days. Results are representative of two (a, e-f) or one (h) independent experiment. Significance (*p< 0.05, **p <0.01) determined by unpaired two-tailed t test (f,g). Data presented as mean values ±SEM.

As the original experiment in chapter 2 (**Fig. 5g**) activated T_{reg} cells with PMA and Ionomycin, bypassing the TCR, we repeated these experiments doing the same (**Fig 12d**). Non-TCR activation largely recapitulated the findings, with glucose^{lo} T_{reg} cells maintaining low glucose avidity when conditioned in 5- and 25-mM glucose media (**Fig 12e**). While the glucose^{hi} T_{reg} cells appear to have lost glucose avidity, this is likely due to the increased cell death after PMA/Ionomycin activation (**Fig. 12e**). We next determined whether high glucose conditioning reduced the suppressive capacity of glucose$^{lo/hi}$ T_{reg} subsets as it did with bulk T_{reg} cells (**Fig. 5g**) despite observing no overt changes in glucose uptake. Indeed, glucose^{lo} T_{reg} cells conditioned in 25 mM glucose media had a significantly reduced suppressive capacity compared to those conditioned in 5 mM glucose (**Fig 12f**). The glucose^{hi} T_{reg} subset failed to suppress altogether which, although more dramatic, is consistent with the reduced suppressive capacity of glucose^{hi} T_{reg} cells directly measured ex vivo (**Fig 12f, 5a**). The total lack of suppression may stem from the reduced viability of glucose^{hi} T_{reg} cells following PMA/Ionomycin activation. Measuring the glucose uptake of glucose$^{lo/hi}$ T_{reg} subsets post-suppression assay revealed that glucose^{lo}, but not glucose^{hi}, T_{reg} cells conditioned in 25mM glucose significantly increased their glucose uptake (**Fig. 12g**). Notably, glucose^{hi} T_{reg} cells

maintained higher glucose avidity overall than glucose^{lo} T_{reg} post suppression assay. Since T_{reg} cells post-suppression assay experienced additional time in culture we sought to determine if glucose^{lo} T_{reg} cells would become glucose avid if culture for 6 days in 25 mM glucose media. While not significant, additional time in 25 mM glucose media shifted glucose^{lo} to be slightly more glucose avid. These data suggest that culturing glucose^{lo} T_{reg} cells for 6 days is enough time to see a shift in glucose uptake.

Taken together these data suggest glucose^{hi} T_{reg} cells are more of a fate that can be "differentiated" from glucose^{lo} T_{reg} cells. Given that conditioning bulk T_{reg} cells in 25mM glucose decreases their suppressive capacity (**Fig. 5g**) and that glucose avid T_{reg} cells are poor suppressors (**Fig. 5a**), it was not surprising to observe an increase in proportion of glucose avid T_{reg} cells conditioned in 25mM glucose (**Fig. 12a**). By sorting glucose^{lo} and glucose^{hi} T_{reg} subsets we observed a majority of glucose$^{lo/hi}$ T_{reg} cells maintained their proclivities for glucose after 3 days regardless of environmental glucose concentration (**Fig. 12b,c**). However, after 3 more days of culture in a suppression assay ~40% of glucose^{lo} T_{reg} cells conditioned in 25 mM glucose became glucose avid, almost double that of 5 mM glucose condition, while the glucose^{hi} T_{reg} cells remained unchanged between conditions (**Fig. 12g**). Ultimately this suggests that environmental glucose can push glucose^{lo} T_{reg} cells to become glucose^{hi} but not the other way around. Glucose^{hi} T_{reg} cells appear to be set in their phenotype and function regardless of being in a lower glucose environment.

Prior to ultimately becoming glucose avid, glucose^{lo} T_{reg} cells conditioned in 25 mM glucose had a significant reduction in suppressive capacity (**Fig 12f**). This suggests that environmental glucose changes the function of T_{reg} cells prior to overtly changing their

glucose avidity. This would seem to suggest that environmental glucose is somehow acting as a ligand to activate signals that ultimately alter T_{reg} cell function prior to being taken up. However, more likely is that environmental glucose is being taken up by T_{reg} cells and the glucoseCy5 tracer has limitations as a glucose uptake reporter[160]. Therefore, how is glucose altering T_{reg} cell suppressive function?

Glucose has been shown to regulate the phosphorylation of Tet2, an enzyme that catalyzes the conversion of 5-methyl-cytosine (5-mC) to 5-hydroxymethyl-cytosine (5-hmC) to promote DNA demethylation[187]. In addition, aerobic glycolysis through lactate dehydrogenase A (Ldha) has been shown to maintain high levels of acetyl-CoA in activated T cells which enhanced histone acetylation and transcription of IFN-γ[188]. Thus, glucose is likely altering the epigenetic state of T_{reg} cells toward a more effector-like phenotype resulting in loss of suppressive function. As mentioned in the introduction to this thesis, NAD(H) redox balance is likely also playing a role. When glucose is fermented to pyruvate then converted to lactate, NADH is converted to NAD+. As this enzymatic reaction is reversable, conversion of lactate to pyruvate converts NAD+ to NADH. Angelin et al observed an increased NAD/NADH ratio in the presence of lactate in Foxp3+ iT_{reg} cells compared to Foxp3- T_{conv} cells[25]. Additionally, lactate influenced NAD/NADH ratio may play a role in T_{reg} suppressive function, as genetic impairment of complex I of the electron transport chain can lower NAD/NADH ratios and reduce T_{reg} suppressive function[25]. In T_{reg} cells SIRT1, a NAD dependent protein deacetylase, was shown to be an important regulator of suppressive function as deletion of SIRT1 enhanced T_{reg} cell suppressive capacity[189]. Foxp3 acetylation, which stabilizes its expression and enhances

suppressive capacity, is regulated by SIRT1[190]. Thus, the influence of glucose may also lie in its ability to alter NAD(H) redox balance and Foxp3 protein stability.

To test the hypothesis that glucose increases histone acetylation of effector T cell genes in T_{reg} cells we can do several things. Using glucoseCy5 to pulse lymph node derived T_{reg} cells from a Foxp3 reporter mouse, we would sort out glucose low and high T_{reg} subsets. During the sorting process some cells would be sorted into RNA lysis buffer to perform RNA sequencing and others would be sorted into media to perform CUT&TAG[191] for H3K9ac, a histone mark associated with active promoters, and H3K27ac, a mark associated with active enhancers. These data could be used to identify differences in H3K9ac and H3K27ac in known effector T cell genes including IFN-γ, IL-2, and Tbet between glucose low and high T_{reg} subsets and determine if glucose high T_{reg} cells have increased acetylation at these gene loci. The RNA sequencing data would be used to correlate gene expression with the histone marks. In a parallel approach, we could sort out glucose low T_{reg} cells then activate and condition them in 5- or 25-mM glucose media as we have done in **Fig. 12**. After conditioning we would perform RNA sequencing and CUT&TAG as just described but this time comparing the 5 mM to the 25 mM glucose condition. This approach would allow us to answer directly whether environmental glucose is driving increased histone acetylation of effector T cell genes.

It may be that glucose does not alter histone acetylation or that it also alters NAD/NADH ratios, SIRT1 activity and ultimately Foxp3 protein acetylation. To test this hypothesis, glucose low and high T_{reg} subsets would be sorted and NAD/NADH ratios would be compared between the two subsets. If our hypothesis is correct, we would expect to find higher NAD/NADH ratio in the glucose high T_{reg} subset which would provide

more NAD+ for SIRT1 to deacetylate Foxp3. In parallel we would measure the amount of Foxp3 acetylation by immunoprecipitation (IP for acetyl lysine and blot for Foxp3 as commercial Foxp3Ac antibody is not available). In addition, we would also sort glucose low T_{reg} cells and condition them in 5- or 25-mM glucose media then assess their NAD/NADH ratios and Foxp3 acetylation to answer whether environmental glucose can drive this. If glucose was altering Foxp3 acetylation and NAD/NADH ratios, then we could explore SIRT1 contribution by knocking out the gene via CRSPR or a SIRT1 floxed *Foxp3*Cre mouse.

Just as glucose reduces T_{reg} cell identity and suppressive function (**Fig. 3, 5**) lactic acid supports it (**Fig. 7, 10**). However, how lactic acid supports T_{reg} cell suppressive function remains unknown. Like glucose, lactic acid can alter epigenetics and the balance of NAD/NADH. The next section will discuss how lactic acid may be supporting T_{reg} cells and how to test these hypotheses.

5.3 Histone lactylation: the mechanism behind lactic acid's impact on regulatory T cells?

In figure 7i we showed T_{reg} suppressive capacity could be rescued from the detrimental effects of high glucose culture by adding lactic acid. This indicated that lactic acid is counteracting the impact of high glucose to preserve T_{reg} cell function. From a simplified viewpoint lactate is the antithesis of glucose in that it can be converted to pyruvate which depletes NAD+ and produces NADH. As discussed in the last section, depletion of NAD+ is likely beneficial for T_{reg} function as this may prevent NAD dependent

SIRT1 from deacetylating Foxp3 thus increasing suppressive capacity. However, lactate can act beyond redox balance and influence the epigenetic landscape in multiple ways. First lactate can act as a Histone Deacetylase (HDAC) inhibitor to promote transcriptional changes[192]. For already differentiated T_{reg} cells the HDAC inhibitor properties of lactate may act as a preservative, maintaining already open chromatin regions that lead to its differentiation in the first place. However, this does not explain why lactate supports the differentiation of T_{reg} cells[25].

Another way lactate can contribute to the epigenetic landscape is through lactylation. Lactylation is a histone modification derived from lactate and has distinct dynamics from acetylation[49]. Increasing histone lactylation late in M1 macrophage polarization resulted in increased Arg1 and other wound-healing associated gene expression, suggesting a shift to the immunosuppressive M2 macrophage phenotype. Lactate may contribute to T_{reg} cell lactylation in a similar way to promote T_{reg} signature genes and support suppressive capacity. However, there is some controversy surrounding the purpose of lactylation as one group found lactylation increases in macrophages preparing to die under inflammatory stress[193]. While lactylation correlated with Arg1 expression they found it was a consequence rather than a cause of macrophage activation. Therefore, it remains unclear whether lactylation can drive gene expression changes or is a marker of cell stress/death and whether lactylation plays a role in immune cells other than macrophages.

As T_{reg} cells consumed more lactic acid than Tconv cells (**Fig. 7g**), we sought to determine if they also displayed more lactylation. As H3K9ac marks active promoters we choose to investigate H3K9 lactyation (H3K9lac) as this might act similarly and total

lactylated lysine (Klac). Lymph nodes (LN) and tumors were harvested from mice bearing B16 tumors 14 days post-injection and stained for Foxp3 and lactylation markers. As expected, tumor infiltrating T_{reg} cells had significantly more H3K9lac and total Klac than their Tconv counterparts (**Fig. 13a**). This held true even within the lactate low LN compartment (**Fig. 13a**). We next sought to determine if T_{reg} cells derived from the lactate rich tumor increased H3K9lac compared to the LN. Indeed, B16 tumor infiltrating T_{reg} cells displayed significantly more H3K9lac than their LN counterparts while MEER infiltrating T_{reg} cells trended toward an increase (**Fig. 13b**). Interestingly, this increase was specific to H3K9lac as total Klac was unchanged between LN and tumor (**Fig. 13c**). As H3K9lac may promote gene expression we sought to determine a correlation between H3K9lac and T_{reg} signature gene expression. Gating on the top 30-40% of H3K9lac expressing T_{reg} cells revealed H3K9lac^{hi} cells expressed significantly more Foxp3 in both the LN and the tumor than their H3K9lac^{lo} counterparts (**Fig. 13d**). Indeed this held true with other T_{reg} signature genes such as Nrp1, Helios (trending toward increase), ICOS, and Ki67 (**Fig. 13e,f**).

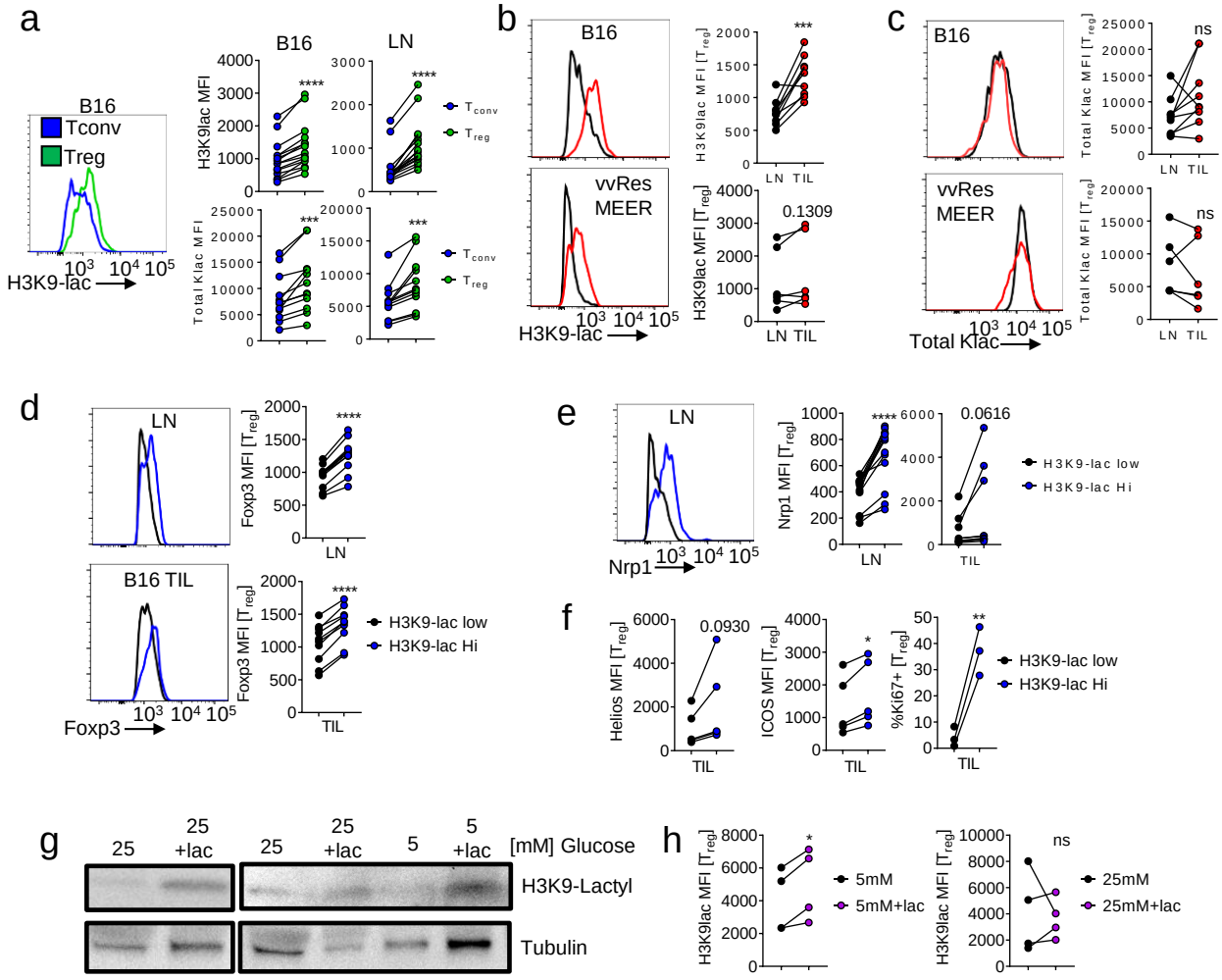

Figure 13. Lactic acid increases H3K9 lactylation and correlates with increased signature gene expression in Treg cells. (a) Representative histogram and tabulation of mean fluorescence intensity (MFI) of H3K9lac and total lactylated lysine (Klac) in Treg and Tconv cells derived from B16 tumors and lymph nodes (LN). (b) Representative histograms and tabulation of H3K9lac in Treg cells derived from B16 or oncolytic vaccinia resistant MEER (vvRes MEER) tumors and LN. (c) Representative histograms and tabulation of Klac as in (b). (d) Representative histograms and tabulation of Foxp3 expression in Treg cells with high or low H3K9lac derived from B16 tumors or LN. (e) Representative histogram and tabulation of Nrp1 expression as in (d). (f) Tabulation of Helios, ICOS, and Ki67 as in (d). (g) Western blot for H3K9lac in Treg cells conditioned for three days in 5- or 25-mM glucose media ±10 mM lactic acid. (h) Tabulation of flow staining for H3K9lac in Treg cells as in (g). Results are representative of four (a, b (B16), c (B16), d, e), two (b (MEER), c

(MEER), f (Helios, ICOS), g) and one (f (Ki67), h) independent experiments. Significance (*p< 0.05, **p <0.01, ***p < 0.001, ****p<0.0001) determined by paired two-tailed t test (a-f, g).

While we know B16 tumors are enriched for lactic acid (**Fig. 7a**) we sought to determine if environmental lactic acid could increase H3K9lac. T_{reg} cells from a Foxp3 reporter mouse were sorted then activated overnight with PMA/Ionomycin and IL-2 then conditioned for three days in 5- or 25-mM glucose plus or minus 10 mM lactic acid. Addition of lactic acid to the 5 mM glucose condition increased H3K9lac by western blot and by flow cytometry (**Fig. 13g, h**). Addition of lactic acid to the 25 mM glucose condition increased H3K9lac by western blot but it was only trending toward increased by flow cytometry. Taken together these data suggest that environmental lactic acid can contribute to T_{reg} H3K9lac and increased H3K9lac correlates with higher T_{reg} signature gene expression.

While these data are interesting much work needs to be done to figure out how or if lactylation drives T_{reg} cell function and identity. To help identify if H3K9lac correlates more globally with T_{reg} signature gene expression and whether this enrichment occurs in the lactate rich tumor, we could perform RNA sequencing and CUT&TAG for H3K9lac as well as H3K9ac from T_{reg} cells derived from the LN and B16 tumors. In fact, we have conducted this experiment, but preliminary analysis does not show any enrichment in H3K9lac or H3K9ac between tumor and LN derived T_{reg} cells (Data not shown). Either these data are correct, or the CUT&TAG assay did not perform as expected. Given that there were no differences in H3K9ac it is likely the CUT&TAG assay failed in some manner. These experiments will have to be repeated to confirm whether this is the case. It may be that lactylation is marking cells that are under stress and about to die[193] and is

just a consequence of T_{reg} activity rather than a driver. While our data show T_{reg} that appear to be healthy and stable (**Fig. 13**) it will be important to determine if H3K9lac marks cells about to die. This can be determined by including markers such as Bcl2, cleaved caspase3, and annexin5 in the flow panels.

Beyond lactylation, lactate may also be altering histone acetylation through its HDAC activity or changing NAD/NADH ratios. Like what was described in the last section for glucose, CUT&TAG for H3K9ac and H3K27ac could be performed on T_{reg} cells conditioned in media with or without lactic acid. These data could be used to identify differences in H3K9ac and H3K27ac in known T_{reg} cell genes determine if lactic acid conditioned T_{reg} cells have increased acetylation at these gene loci. Alternatively, NAD/NADH ratios from T_{reg} cells conditioned with or without lactic acid could be measured along with Foxp3 protein acetylation. Since we know T_{reg} take up lactic acid and convert it to pyruvate (**Fig. 7g**) NAD+ is being converted into NADH which could deactivate SIRT1 allowing for increased Foxp3 acetylation and function. In this experiment we could utilize MCT1 KO T_{reg} cells which don't take up lactic acid (**Fig. 10a**) to demonstrate that changes in Foxp3 acetylation and NAD/NADH ratio are dependent on import of lactic acid.

6.0 Future Directions

6.1 Summary of findings

Throughout this thesis we have revealed that regulatory T cell function is tuned by a glucose/lactate axis that is exploited within the tumor microenvironment. In chapter 2, we demonstrate that T_{reg} cells display a distinct glucose metabolism compared to T_{conv} cells. T_{reg} cells display lower glucose avidity than T_{conv} cells even when they share a TCR and are activated in vivo with the same antigen (**Fig. 3**). This limited glucose uptake translates into reduced engagement in glycolysis even directly following TCR stimulation (**Fig. 3d, 4c**)**.** Despite an overall reduced glucose avidity, a subset of T_{reg} cells was glucose avid. Functional assays revealed that high glucose avidity T_{reg} cells from the lymph node and tumor were significantly less suppressive than their low glucose avidity counterparts (**Fig. 5a**). This held true even in a transfer colitis model, with mice receiving high glucose avidity T_{reg} cells displaying significantly more colitis (**Fig. 5d**). RNA sequencing of glucose^{lo} and glucose^{hi} T_{reg} cells revealed a reduction in T_{reg} cell signature gene expression in the glucose^{hi} T_{reg} cells and an enrichment of lactate metabolism genes in glucose^{lo} T_{reg} cells (**Fig 5b,h**). Taken together these data suggest glucose avidity can predict T_{reg} cell function and phenotype and that glucose^{lo} T_{reg} cells can possibly engage in lactate metabolism rather than glycolysis.

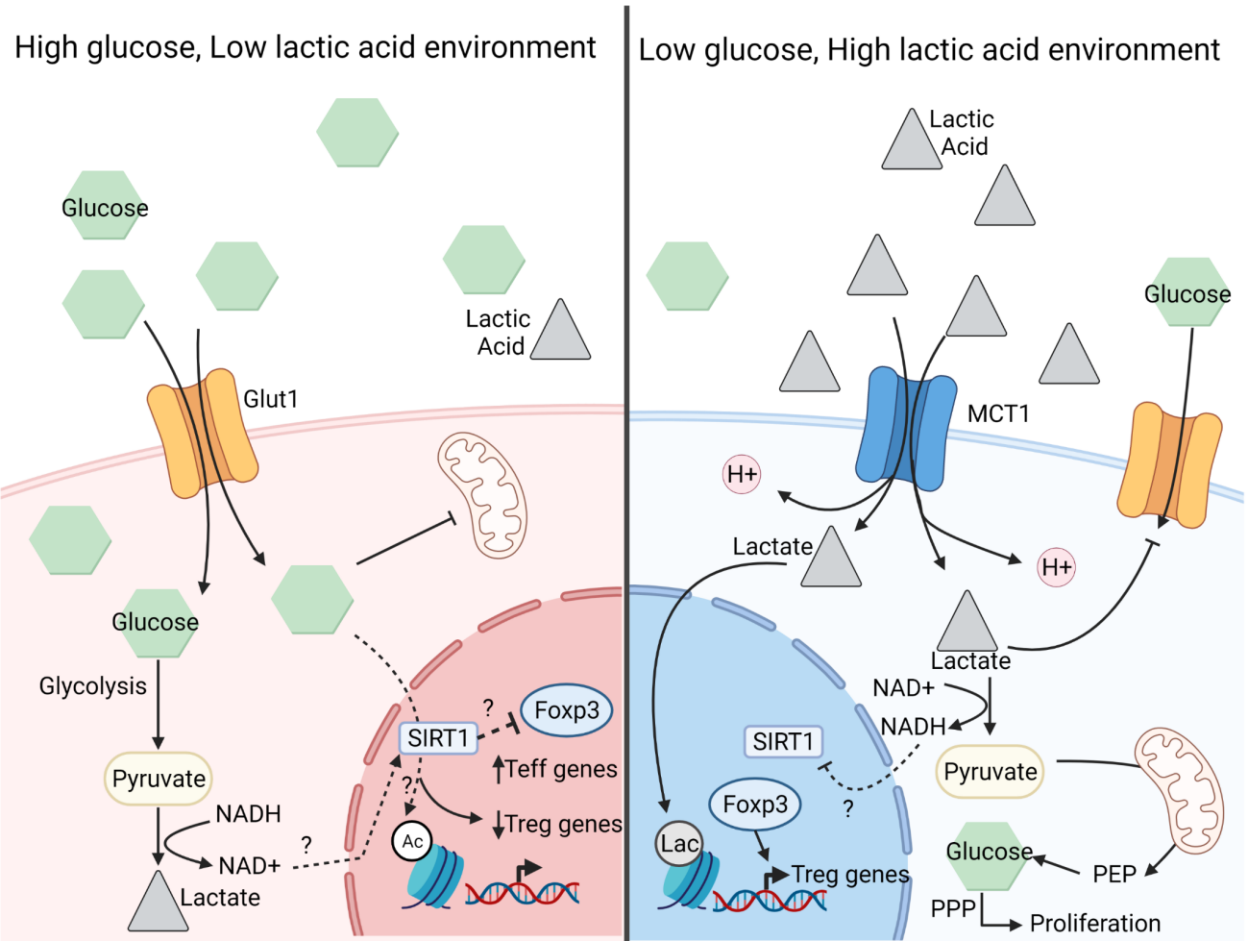

Figure 14. Model of glucose and lactic acid's impact on Treg cells. (left) High glucose environments lead Treg cells to increase glucose uptake and decrease their suppressive capacity. One potential mechanism for this may be an accumulation of NAD+ as pyruvate derived from glucose is converted to lactate. Increased NAD+ may enhance protein deacetylases like SIRT1 which have been shown to deacetylate Foxp3 and reduce its function. Alternatively, glucose has been shown to contribute to the acetyl-CoA pool in CD8 T cells, increasing histone acetylation resulting in increased effector T cell gene expression. This event may also be driving effector T cell genes in Treg cells. High glycolytic rates can dampen mitochondrial metabolism which has been shown to be critical for Treg cell function. (right) Environments with high levels of lactic acid, such as the tumor, lead to increased lactic acid uptake by Treg cells. Proton assisted transport shuttles extracellular lactic acid into the cell as lactate and H+ and correlates with decreased glucose uptake by Treg cells. Lactate is converted to pyruvate, regenerating NADH and depleting NAD+, potentially inhibiting

NAD+ dependent SIRT1 allowing for increased Foxp3 protein acetylation and therefore expression of Treg cell signature genes. In addition, Treg cells can utilize lactate to create higher order glycolytic intermediates such as phosphoenolpyruvate (PEP), a key substrate for gluconeogenesis, which is likely converted to glucose then shunted into the pentose phosphate pathway (PPP) to support intratumoral Treg cell proliferation. Lactate can also play a role in histone lactylation which correlates with increased Treg signature gene expression and increases as Treg cells enter the lactic acid rich tumor. (Created with Biorender.com)

In chapter 3 we demonstrate that T_{reg} cells can metabolize lactic acid to support their proliferation and suppressor function. Using an intracellular pH dye, we demonstrate that T_{reg} cells take up more lactic acid than their T_{conv} cell counterparts (**Fig. 7b**). The ability to uptake lactic acid was heterogenous between various tissue derived T_{reg} cells and inversely correlated with T_{reg} cell glucose uptake from these same tissues (**Fig. 3g, 7c**). In contrast to glucose uptake, T_{reg} cells that took up lactic acid displayed increased Nrp1 and CD44 expression (**Fig. 7e**). Using heavy carbon tracing and mass spectrometry we confirmed that T_{reg} cells took up more lactic acid than T_{conv} cells and that they generated TCA cycle intermediates and PEP whose formation was critical to maintain intratumoral T_{reg} cell proliferation (**Fig 7f-h, j-l**). Lactic acid also supported T_{reg} cell suppressive function as it could rescue the detrimental impact of high glucose culturing on T_{reg} cell suppressive capacity (**Fig. 7i**).

In chapter 4 we demonstrate that tumor infiltrating regulatory T cells require lactate uptake to maintain their high suppressive function. Using mice harboring a T_{reg} cell specific deletion of the lactate transporter MCT1, we demonstrate that loss of lactic acid uptake by T_{reg} cells significantly slows tumor growth and extends survival in several different tumor models. Moreover, tumor infiltrating MCT1 knockout (KO) T_{reg} cells had a

significantly reduced suppressive capacity resulting in increased proliferation and IFN-γ production by $CD8^+$ T and T_{conv} cells (**Fig. 10a-f, k**). Consistent with blocking the production of lactate derived PEP, tumor infiltrating MCT1 KO T_{reg} cells displayed reduced proliferation (**Fig. 10g**). As MCT1 KO T_{reg} cells could no longer take up lactic acid they switched to taking up glucose, excluding them from hypoxic regions of the tumor (**Fig. 10a, i, j**). Importantly, MCT1 KO T_{reg} cells were still competent to suppress in non-tumor tissues and did not cause any overt autoimmunity (**Fig. 9**). When combined with anti-PD-1 immunotherapy, T_{reg} cell loss of MCT1 resulted in ~40% of mice bearing B16 tumors to become tumor free (**Fig. 10l**). Taken together these data suggest T_{reg} cells require lactic acid uptake within the tumor microenvironment to maintain their proliferation and function and this could be translated to the clinic by combing MCT1 inhibitors with anti-PD1 immunotherapy.

In the first half of chapter 5 we explore whether glucose avid T_{reg} cells are a state or a fate. Here we define state as a temporary character that T_{reg} cells can freely move into and out of given the proper signals. In contrast, we define fate as a more permanent and terminal character that T_{reg} cells "differentiate" into and stay for the rest of the cell's existence. We observed that high glucose culturing led to an increase in glucose avid T_{reg} cells (Fig. 12a). However, when $glucose^{lo}$ and $glucose^{hi}$ T_{reg} cells were sorted out then placed in a high or low glucose media we observed that the $glucose^{hi/lo}$ T_{reg} cell subsets maintained their proclivity for glucose and were not altered between the high and low glucose media conditions. For example, ~70% of T_{reg} sorted as $glucose^{lo}$ stayed glucose low in both the 5- and 25-mM glucose media and about 80% of the $glucose^{hi}$ T_{reg} cells stayed $glucose^{hi}$ in both conditions (**Fig. 12c**). Interestingly, after conditioning in high

glucose media then putting them into a suppression assay, the glucose^{lo} T_{reg} cells had a reduced suppressive capacity and higher glucose uptake than glucose^{lo} T_{reg} cells conditioned in low glucose media (**Fig. 12f**). Interestingly glucose^{hi} T_{reg} cell regardless of conditioning media failed to suppress and did not alter their glucose avidity (**Fig. 12f**). These data suggest that glucose^{hi} T_{reg} cells are more of a fate that is not easily changed, at least by environmental glucose concentration, whereas glucose^{lo} T_{reg} cells are more malleable and act as a precursor to the glucose^{hi} fate.

The second half of chapter 5 explores histone lactylation as a potential mechanism of lactate to bolster and preserve T_{reg} cell function. Lactylation is a histone modification derived from lactate that was suggested to control gene expression in macrophages. We demonstrate that T_{reg} cells have increased total lacylation (lac) and H3K9lac compared to T_{conv} cells, consistent with their increased lactate uptake (**Fig. 7g, 13a**). Moreover, T_{reg} cells that infiltrate the lactic acid rich TME have increased H3K9lac which correlates with increased T_{reg} cell signature genes (**Fig. 13b-f**). This observed increase in lactylation is likely due to increased environmental lactic acid as conditioning T_{reg} cells in media with 10mM lactic acid increased H3K9lac (**Fig 13g, h**).

Taken together, these data suggest T_{reg} cell function, phenotype, and proliferation are tuned by a glucose/lactate axis which is exploited within the TME. Environmental glucose acts to dampen T_{reg} cell function and can push glucose^{lo} T_{reg} cells to a glucose^{hi} fate. Lactic acid can counteract the detrimental impact of high environmental glucose on T_{reg} cell function and may act to stabilize T_{reg} cell signature gene expression and thus function, especially within lactic acid rich environments such as the tumor. While lactic acid is not required at steady state by T_{reg} cells in non-tumor tissues, it likely plays a role

in tuning T_{reg} function given the nutrient milieu and context of various tissues both at homeostasis and during inflammation.

6.2 Future directions: glucose and T_{reg} cells

Many questions remain as it pertains to glucose and T_{reg} cells. A major question, which was posed in chapters 2 and 5.2, is what is the purpose of glucose$^{hi/lo}$ T_{reg} cell subsets? As already discussed, glucose^{hi} T_{reg} cells exhibit a decreased suppressive capacity and T_{reg} cell gene signature, and this seems to be a fate (more a differentiation path) than a state (a transient way of being). One experiment that could be done to elucidate the purpose of glucose$^{hi/lo}$ T_{reg} subsets would be to identify the overlap in T cell receptor (TCR) expression between these subsets. It may be that glucose^{hi} T_{reg} cells have an entirely distinct TCR repertoire compared to glucose^{lo} T_{reg} cells. If true, this would suggest that TCR stimulation through particular antigens may be a driver for the difference in glucose uptake. It may also indicate the origins of these subsets as glucose^{lo} T_{reg} cells may be thymically derived and glucose^{hi} T_{reg} cells may be peripherally derived, such as those T_{reg} cells that recognize microbial antigens in the gut. It also may be that glucose$^{lo/hi}$ T_{reg} cell subsets have no distinction in TCR expression. This possibility is equally as interesting as this would suggest TCR specificity was not the driver of glucose uptake in T_{reg} cells. Ruling out the contribution of TCR specificity would be key in discovering the purpose of these subsets. This finding would indicate all T_{reg} cells regardless of antigen specificity can be both glucose^{lo} and glucose^{hi} pointing to some other mechanism driving this difference.

Another remaining question is how are glucose^{lo} and glucose^{hi} T_{reg} cell subsets formed? An obvious place to investigate would be the T_{reg} cell's ability to sense glucose. Sensing glucose is a relatively complex as there aren't direct receptors for glucose molecules. Glucose is transported into T_{reg} cells by Glut1 (expressed more highly on glucose^{hi} T_{reg} **Fig. 5h**) and by Glut3 (expressed more highly glucose^{lo} T_{reg}). As a rate limiting step for glucose is driven by hexokinase (Hk), it may be that differing HK expression (**Fig. 5h**) drives T_{reg} cells toward a glucose$^{hi/lo}$ fate. Those T_{reg} cells with high Hk expression may "sense" glucose more strongly and be fated to become glucose^{hi}. Using mice with a conditional Hk knockout in T_{reg} cells then investigating whether this eliminates glucose^{hi} T_{reg} cells or culturing Hk knockout T_{reg} cells in a high glucose environment and observing whether they increase glucose uptake could help to answer this question. Alternatively, glucose could be sensed by the mTOR pathway. While mTOR signaling in T_{reg} cells is complex, there is strong evidence that hyperactivation of mTOR can be linked to T_{reg} cell dysfunction in autoimmunity, and that lack of mTOR signaling can promote T_{reg} cell differentiation[194]. It would be interesting to investigate if mTOR signaling was higher in glucose^{hi} T_{reg} cells and whether rapamycin treatment could rescue the suppressive and phenotypic defect in glucose^{hi} T_{reg} cells.

6.3 Future directions: MCT1 and its substrates

The gut plays a large role in shaping T_{reg} cell biology. As non-self gut microbes are key for overall health and homeostasis, T_{reg} cells must protect these microbes from effector cells while still allowing for inflammation when there are pathogenic invaders.

This finely tuned state, in part, is driven by metabolites produce by gut microbes. In particular, short chain fatty acids (SCFA) such as butyrate, propionate, and acetate have been show to support T_{reg} function within the gut[185,186]. Interestingly, these SCFAs are also substrates of MCT1[38], the lactate transporter we showed to be crucial for T_{reg} function and proliferation in the tumor (**Fig. 10**). In our transfer colitis model, we observed that mice receiving MCT1 knockout (KO) T_{reg} cells had significantly more colitis compared to those receiving WT T_{reg} cells (**Fig. 9o**). While the colitis was not as severe as mice receiving 2NBDG^{hi} T_{reg} cells, this suggests a defect in MCT1 KO T_{reg} cells in the gut when inflammation is present. Therefore, do T_{reg} cells require MCT1 to robustly function under gut inflammation in an immunocompetent environment? To test this, we could use MCT1 f/f Foxp3Cre mice and dose them with Dextrane Sulfate Sodium (DSS) to induce colitis, then measure weight loss, colitis histology, and immune cell make up within the gut. Under these conditions we may see a loss of a subset of T_{reg} cells, such as RORγt+ T_{reg} cells[195], when MCT1 is knocked out. It may be that MCT1 KO T_{reg} cells allow for an outgrowth of specific microbes or allow for increased invasiveness of microbes into the gut tissue leading to increased inflammation. Sequencing of 16s from WT and MCT1 KO mice guts after DSS and immunofluorescence staining of the gut mucosal layer could determine bacterial species differences and potential invasiveness of these species. If MCT1 KO T_{reg} cells allow for an outgrowth of a specific bacterial species or phyla this may indicate a difference in TCR specificity. It would be interesting to investigate TCR specificity between MCT1 KO T_{reg} and WT T_{reg} in the gut (or if enough cells cannot be obtained from the gut, we could take it from the mesenteric LN and Peyers patches). In addition, we could investigate the TCR specificity between WT T_{reg} cells that have high

versus low lactic acid uptake using the pHrodo red assay to sort out these subsets. All these experiments would increase our understanding of T_{reg} cell metabolism within the gut especially as it pertains to SCFAs.

Appendix: Methods

MATERIALS AND METHODS

In Vitro Tissue Culture

B16-F10 were obtained from ATCC. MC38 cells were obtained from Dario Vignali (commercially available from Kerafast). Clone24 was produced in house by single cell sorting melanoma tumors arising from Ptenf/f BrafLSL-V600E TyrCre.ER mice. MEER cells were obtained from Robert Ferris (originally from[196]). B16 cell line was authenticated in 2018 by independent sequencing. MC38 cells were authenticated in 2016 by independent sequencing. Clone24 cell line was authenticated via metabolic profiling and tumor growth compared to Melan-A (normal melanocytes) in 2019[5]. MEER cells were authenticated in 2013 via western blot to show E6/E7 and Ras overexpression in MTEC cells. MC38 and MEER were confirmed mycoplasma free in 2016, B16 were confirmed in 2018, Clone24 in 2019. Both primary and immortalized cell lines were maintained in lab-made R10 media [RPMI1640, 10%FBS, 2mM L-glut, PenStrep, NEAA, 1mM Sodium pyruvate, 5mM HEPES, β-ME]. Cultures were incubated in temperature and partial pressure-stable conditions at 37ºC and 5% CO_2. For in vitro conditioning experiments, isolated T_{reg} or T_{conv} cells were activated in complete R10 media with 0.1 ug/mL Phorbol 12-myristate 13-acetate (PMA) and 1ug/mL ionomycin (Sigma-Aldrich) with 1000U/mL IL-2 for ~20 hours at 37ºC then placed in the conditions indicated in the figure with IL-2. For *in vitro* 3-mercaptopicolinic acid (3MP, Cayman Chemical) experiments a 250 μM concentration was used.

In Vivo Mice Studies

Sample sizes were not statistically predetermined but were chosen based on previous work in T_{reg} cell functional assays[8,162] and tumor immunology[4,5,8,32,162]. These sample sizes are sufficient because they allowed for the determination of statistical significance between groups and minimized the number of animals or replicates needed for each experiment. Mice were placed into experimental group by nature of their genotype and/or if receiving treatment were randomized within a genotype. For experiments not involving mice, cells were randomized into experimental groups. Blinding was not possible as most of the data acquisition and analysis was done by a single person. Blinding would have required at least two individuals for every experiment which was not feasible during the course of our study. C57BL/6J-*Foxp3*$^{YFP\text{-}cre}$, -*Foxp3*$^{GFP.Cre.ERT2}$, -*Rag1*$^{-/-}$, and -*Thy1*^{a} (Thy1.1 congenic) were purchased from The Jackson Laboratory. *Slc16a1*$^{f/f}$ mice were a gift from Jeffrey Rothstein and Brett Morrison[197] used to generate *Slc16a1*$^{f/f}$*Foxp3*$^{GFP.Cre.ERT2}$ and *Slc16a1*$^{f/f}$*Foxp3*$^{YFP.Cre}$ mice. *Foxp3*$^{\text{FlpO Ametrine}}$ mice were a gift from Dario AA Vignali. Spleens of OT-II Foxp3RFP Thy1.1 mice were a gift from Geoffrey Camirand. Animal work was done in accordance with the Institutional Animal Care and Use Committee of the University of Pittsburgh (protocol #17071235). All mice were housed in specific pathogen free conditions at an ambient temperature 20-26°C and humidity of 30-70% with a 12:12 hour light:dark cycle prior to use. The maximal tumor size of 15 mm in any direction was not exceed in any experiment. Both male and female mice were used in studies, from five (5) to ten (10) weeks of age.

Flow Sorting and Cytometric Analysis

Single-cell suspensions from murine tumors (day 14 post tumor inoculation), lymph node, liver, thymus, or spleen were derived through mechanical separation and 70 μM filter (Fisherbrand) passage. For hypoxia detection, mice were injected intravenously with pimonidazole (80mg/kg, Hypoxyprobe) in PBS 1.0 hour before sacrifice. Tumors dissolution was aided through lab-made tumor lysis buffer [2mg/mL Collagenase Type IV (Gibco), 2U/mL Dispase in Hanks' Balanced Salt Solution (Stemcell Technologies), 10U/mL Deoxyribonuclease I (Sigma), serum free RPMI medium] injected with a 20G needle and incubated for 30 minutes at 37°C. Prior to sort tumor suspensions were purified by negative selection with MojoSort magnetic bead separation (BioLegend) and biotin-conjugated anti-mouse antibodies to CD105 (MJ7/18, Cat# 120403, Lot# B266720, BioLegend).The skin (ears of mice were used), were finely minced using scissors and resuspended in RPMI1640 (Gibco, Grand Island, NY) with 2.5 mg/mL collagenase XI (Sigma-Aldrich), 0.25 mg/mL hyaluronidase (Sigma-Aldrich), 0.1 mg/mL DNase (Sigma-Aldrich), 0.01 M HEPES (Sigma-Aldrich), and 10% FBS followed by incubation in a shaking incubator for 1 h at 37C at 250 rpm. Following incubation skin was subjected to mechanical separation and passed through a 70 μM filter. Similarly, muscles (quadriceps were used) were finely minced using scissors then resuspended in 0.05% type II collagenase (ThermoFisher) in HBSS for 30 min at 37 °C under constant agitation. Islets were isolated as previously described[198]. Pimonidazole was visualized using anti-pimonidazole antibodies (Hypoxyprobe, Cat# HP7-100, Lot# 5914) after 5 minutes of 4% PFA fixation followed by the FoxP3 Fix/perm kit (Biolegend). Staining for expression markers was performed with anti-mouse specific antibodies obtaining from the following

companies; Biolegend: anti-CD4 (GK1.5, Cat# 100412, Lot# B184560, dil 1:1000), CD8 (53-6.7, Cat# 100707, Lot# B171971, dil 1:1000), CD39 (Duha59, Cat# 143806, Lot# B186014, dil 1:500), CD44 (IM7, Cat# 103032, Lot# B267976, dil 1:500), CD73 (TY/11.8, Cat# 127215, Lot# B260585, dil 1:500), CD279 (PD-1, 29F.1A12, Cat# 135221, Lot# B194160, dil 1:250), HAVcr-2 (TIM-3, RMT3-23, Cat# 119705, Lot# B224472, dil 1:250), Helios (22F6, Cat# 137220, Lot# B155089, dil 1:250), IFNγ (XMG1.2, Cat# 505842, Lot# B270630, dil 1:250), Ki67 (16A8, Cat# 652403, Lot# B208445, dil 1:250), CD304 (Nrp-1, 3E12, Cat# 145212, Lot# B175814 dil 1:200), TNFα (MP6-XT22, Cat# 506322, Lot# B218553, dil 1:500). BD Horizon: CD62L (MEL-14, Cat# 564109, Lot# 7341887, dil 1:500). eBioscience: FoxP3 (FJK-16s, Cat# 53-5773-82, Lot#2011698, dil 1:250). Intracellular staining was performed using FoxP3 Fix/Perm buffer set (BioLegend) as per manufacturer's protocol and staining was performed on overnight at 4°C. PTM Biolabs: Lactyl-histone H3 (Lys9) (13H2L1, Cat# PTM-1419RM, dil 1:250 flow and 1:1000 western blot). Stained cells were analyzed on a LSRFortessa (BD). Cell doublets were excluded by comparison of side-scatter and forward-scatter width to area. Flow cytometry data and proliferation modeling were analyzed with FlowJo v10 software (Tree Star) and figures were produced in Prism v8 (GraphPad).

Glucose Uptake Assay

Single cell suspensions of tumor and lymph node and other tissues of ~1 million cells/mL were placed in serum free RPMI containing 40 µM 2NBDG or 0.4 µM Glucose-Cy5 for 25 minutes at 37°C. Glucose-Cy5, a Cy5-linked 1-amino-glucose tracer was synthesized in collaboration with Dr. Marcel Bruchez[161]. For OT-II experiments, $CD4^+$ T cells were isolated via negative selection using magnetic bead separation as previously

described[4] then injected retroorbital into C57BL/6J mice. Simultaneously, recipient mice were injected I.P. with 1 x 10^6 vaccinia-OVA viral particles and harvested 5 days later.

Microsuppression & Proliferation Assays

In vitro microsuppression assays were performed as previously described[162]. Briefly T_{reg} cells ($CD4^+FoxP3^+$) populations were isolated via flow assisted sorting from tumor or lymph node from C57BL/6J-*Foxp3*$^{GFP.Cre.ERT2}$, -*Foxp3*$^{YFP.Cre}$ mice or mice crossed to these strains. Responder cells ($CD4^+Foxp3^-$ T_{conv}) and antigen presenting cells ($CD4^-CD8^-$ APCs) were isolated via flow assisted sorting from the spleen of a C57BL/6J-*Thy1*^{a} mouse. T_{reg} cells were co-cultured for 72 hours at 37ºC with APCs and CellTrace Violet (CTV, ThermoFisher Scientific) labeled responder cells at ratios from 1:2 (T_{reg}:responder) to 1:32 in complete RPMI media with 1ug/mL anti-CD3. Proliferation assays were performed by labeling isolated T_{reg}, T_{conv}, and CD8 T cells with CTV then activating at 1 million cells/mL using anti-CD3/CD28 Dynabeads according to the manufacture's protocol (ThermoFisher Scientific) and IL-2 in complete RPMI media containing 0 to 10mM lactic acid (Fisher Bioreagents). Cell proliferation of responding cell populations was modeled using FlowJo v10 software (Tree Star).

RT-qPCR

Total RNA was extracted using Trizol reagent (Invitrogen) and cDNA was transcribed using a High Capacity cDNA Reverse Transcription Kit (Applied Biosystems), according to manufacturer protocol. Transcript levels were measured with SybrGreen (ThermoFisher Scientific) and using primers specific to genes of interest, including; *Slc16a1*: FWD 5'-GCAGTGTTAGTCGGAGCC-3' REV 5'-GCGATCATTACTGGACGGC-3', *Ldha*: FWD 5'-AGCTTCCATTTAAGGCCCCG-3' REV 5'-

TCTTTTGAGACCGCTAGTGC-3' cDNA concentration was normalized per samples relative to β-actin. All experiments were performed in technical triplicates.

Cytokine Production Assay

Cell suspensions were stimulated in complete R10 media with 0.1 ug/mL Phorbol 12-myristate 13-acetate (PMA) and 1ug/mL ionomycin (Sigma-Aldrich) for ~20 hours at 37ºC. Five hours prior to antibody staining, Golgi-Plug (BD Biosciences) was added to the samples. Cells were surfaced stained and then intracellular stained using FoxP3 Fix/Perm buffer set (Invitrogen) as per manufacturer's protocol. Unstimulated controls were used to determine gating strategies.

Interstitial Lactate Quantification

Tumor and spleen were harvested and placed in empty 15mL conical tubes. Tissues were cut up with scissors then wrapped with a 5-micron Nylon filter paper (Sterlitech) and stuffed filter down into a 1.5 mL conical tube making sure the tissue did not touch the bottom. Tissues were centrifuged at 4000 rpm for 2 hours. Interstitial fluid was assayed for L-lactate concentration using a colorimetric detection kit according to manufacturer's protocol (abcam).

Isotopic Flux Analysis

Cell suspensions at 1 million cells/mL in complete RPMI media were stimulated for 24 hours at 37ºC with plate-bound anti-mouse CD3ε (10 μg for T_{reg}, 3 μg for Tconv, clone 145-2C11, Cat#100239, Lot# B306297, Biolegend) and soluble anti-mouse CD28 (2 μg/mL, clone 37.51, Cat#102115, Lot#B283231, Biolegend) and IL-2 (1000U/mL T_{reg} 50U/mL T_{conv}). After activation media was exchanged for complete RPMI with 5mM uniformly labeled ^{13}C-L-Lactate (Sigma Aldrich) and IL-2. For some experiments PEPCK

inhibitor, 3-mercaptopicolinic acid (3MP, Cayman Chemical) was added at 250 μM. Media was then titrated to pH 6.88 with 1 N HCl. Suspensions were pulsed for 25 hours then washed 2x with room temperature PBS then resuspended in ice cold 80% methanol.

Metabolic quenching and polar metabolite pool extraction was performed using ice cold 80% methanol in water with 0.1% formic acid at a ratio of 400µL per 100µL. Deuterated (D4)-taurine and (D3)-lactate (Sigma-Aldrich) was added to the sample lysates as an internal standard for a final concentration of 100µM. The supernatant was cleared of protein by centrifugation at 16,000xg. 5µL of cleared supernatant was subjected to online LC-MS analysis.

Analyses were performed by untargeted LC-HRMS. Briefly, Samples were injected via a Thermo Vanquish UHPLC and separated over a reversed phase Phenomenex Kinetex C18+ column (2.1×100mm, 1.7µm particle size) maintained at 40°C. For the 20 minute LC gradient, the mobile phase consisted of the following: solvent A (1.5mM ammonium fluoride) and solvent B (100% acetonitrile). The gradient was the following: 0-12.0 min 5% B, to 1000% B, 12.0-15.0 min hold at 100% B, 15.0-15.1100% to 5% B, 15.1-20.0 min 5%B. The Q Exactive mass spectrometer was operated in polarity switching mode, using both positive and negative ion mode, scanning in Full MS mode (2 µscans) from 66.7 to 1000 m/z at 70,000 resolution with an AGC target of 3e6. Source ionization settings were 4.5/3.0 kV spray voltage respectively for positive and negative mode. Source gas parameters were 20 sheath gas, 10 auxiliary gas at 250°C, and 4 sweep gas. Calibration was performed prior to analysis using the PierceTM Positive and Negative Ion Calibration Solutions (Thermo Fisher Scientific). Integrated peak areas were then extracted manually using Quan Browser (Thermo Fisher Xcalibur ver. 2.7).

Fully untargeted analysis was completed by using Thermo Compound Discoverer 3.0 software suite to extract and align molecular features. Graphs and statistical analyses (either t-test or ANOVA) were prepared with GraphPad Prism 7.0 (GraphPad Software, Inc., La Jolla, CA, USA).

In Vivo Tumor Growth and Therapy

Slc16a1$^{f/f}$*Foxp3*$^{YFP\text{-}cre}$ *or Foxp3*$^{YFP\text{-}cre}$ mice were inoculated with 1.5 x 10^5 B16-F10 cells in complete RPMI media. To monitor tumor growth, tumors area was determined 3x weekly using digital calipers and stopped once tumors reached 15mm in any direction. For 3MP treated mice, *Foxp3*$^{YFP\text{-}cre}$ or *Foxp3*$^{GFP.Cre.ERT2}$ mice were inoculated with 1.5 x 10^5 B16-F10 cells. Starting on day 10 or 12 post tumor inoculation mice were treated daily either with water or 25 mg/kg 3MP (Caymen Chemical) via intraperitoneal (I.P.) injection. On day 14 one hour prior to sacrifice, mice were given a final dose of 25 mg/kg 3MP or water. For 3MP tumor growth, treatment started day 7 post tumor injection and continued daily with 25 mg/kg 3MP or H_2O I.P. until tumors reached 15mm in any direction.

For the inducible deletion of MCT1 (*Slc16a1*) *Slc16a1*$^{f/f}$*Foxp3*$^{GFP.Cre.ERT2}$ or *Foxp3*$^{GFP.Cre.ERT2}$ mice were treated I.P. or P.O. with 1 mg of Tamoxifen (T5648, Sigma) in corn oil (C8267, Sigma) from day –4 to 0. On day 0, mice were inoculated intradermally with 2.5x10^5 B16-F10, MC38, or MEER cells in complete RPMI media and given a dose of 1mg Tamoxifen. Tamoxifen treatment continued 3x weekly until the conclusion of the experiment. On day 7, when tumors reached 1-10 mm^2 mice were treated with 0.2mg anti–PD-1 or hamster IgG isotype control (Bio X Cell) 3x weekly until the conclusion of the experiment.

pHrodo Red Lactic Acid Uptake Assay

Cell suspensions from lymph nodes and day 14 B16-F10 tumors were loaded with pHrodo Red AM (ThermoFisher Scientific) according to manufacturer's protocol in a 20mM HEPES in PBS solution. Cells were surfaced stained for multicolor flow cytometry following the normal protocol in 20mM HEPES/PBS buffer. At the flow cytometer, lactic acid was spiked into each sample at a final concentration of 5mM pH ~6.7. Samples were read at 0, 10, and 30 mins after addition of lactic acid.

Extracellular flux analysis

Isolated T_{reg} and T_{conv} cells were plated on Cell-Tak coated Seahorse culture plates (250,000/well) in media consisting of minimal, unbuffered DMEM supplemented with 2mM glutamine. Basal rates were taken for 30 min, and then streptavidin-complexed anti-$CD3^{biotin}$ at 3 µg/mL was injected and readings continued for 3 hrs. 2µM oligomycin and 10mM 2-DG were injected to obtain maximal and minimal ECAR values, respectively. Similarly, isolated T_{reg} and T_{conv} cells were activated using plate bound anti-CD3 (5 µg/mL) and soluble anti-CD28 (2 µg/mL) with 250 U/mL IL-2 for 48hrs then plated on Cell-Tak coated Seahorse culture plates (100,000/well) in media consisting of minimal, unbuffered DMEM supplemented with 2mM glutamine. Basal extracellular acidification rates were taken for 30 mins. Cells were stimulated with 10mM Glucose, 2µM oligomycin, 10mM 2-DG.

Transfer Colitis

The transfer colitis model was performed as previously described[199]. Briefly, $2NBDG^{hi}$ and $2NBDG^{lo}$ T_{reg} cells from Foxp3-Ametrine reporter mice or T_{reg} cells from *Slc16a1*$^{f/f}$*Foxp3*$^{YFP\text{-}cre}$ or *Foxp3*$^{YFP\text{-}cre}$ were isolated via flow assisted sorting ($CD4\text{-}APC^{+}$

Foxp3-reporter^{+}). T_{conv} cells (CD4^{+} CD25^{-}) from C57BL/6J-*thy1^{a}* were isolated via flow assisted sorting. Rag1$^{-/-}$ mice were simultaneously given 2 x 10^4 sorted T_{reg} cells and 1 x 10^5 thy1.1^{+} T_{conv} cells via retroorbital injection. Mice were weighed once a week for 7 weeks (experiment end). Sections of colons were fixed in 10% formalin and paraffin embedded. Slides were stained with hematoxylin and eosin by the University of Pittsburgh Pathology Department, and histology scores were blindly determined using criteria previously described[199].

Tumor Histology

After pimonidazole pulsing, tumors were dissected and frozen at -80 deg C in Optimal Cutting Temperature Compound (OCT) (Tissue-Tek) and sectioned (Cryostat microtome). Tissue was fixed in histology-grade acetone (Fisher) at -20 deg C, then rehydrated in staining buffer, stained with hypoxyprobe (Hypoxyprobe, catalog# HP7-100Kit), and DAPI (Life Technologies), and mounted with ProLong Diamond AntifadeMountant (Life Technologies). Sections were imaged with an Olympus IX83 microscope and analyzed with ImageJ and NIS-Elements Imaging Software.

RNA Sequencing

1000 low glucose and high glucose consuming T_{reg} cells were sorted directly into lysis buffer in a 96-well plate. Immediately after sorting cDNA was generated using SMART-seq HT kit (Cat # 634456 Clontech) using 1000 cells. cDNA product was checked by Tape Station D5000 from Agilent technologies 2200 to make sure cDNA was successfully generated. Library construction was done using Nextrera XT kit # 15031942 from Illumina. 1ng cDNA was used in total volume 5ul. Sequencing was done using

NextSeq 500 System. High Output 75 Cycles kit with run Parameter Paired Read 150 cycles (2X75).

Sequencing reads were trimmed for adapters using Cutadapt[200] prior to being aligned to Mus musculus reference genome (mm10) using the RNA-seq aligner HISAT2. Subread's featureCounts function was used for gene level quantification and results were normalized to Transcripts Per Kilobase Million (TPM). Using the raw quantification, differential genes were found with the R package DESeq2 and statistical cutoffs of q-value <0.05 and |log2foldchange|>1.5.

Western Blot

Immunoblotting was performed as previously described[201]. Isolated T_{reg} or T_{conv} cells were activated in complete R10 media with 0.1 ug/mL Phorbol 12-myristate 13-acetate (PMA) and 1ug/mL ionomycin (Sigma-Aldrich) with 500U/mL IL-2 for ~20 hours at 37ºC then placed in the conditions indicated in the figure with IL-2. H3K9-lactyl antibody was obtained from PTM Biolabs and used at 1:1000. IBs were detected via standard secondary detection and chemiluminescent exposure in a chemidoc (Biorad).

Statistical Analysis

The data presented in the figures are mean ± standard error of the mean (S.E.M.). Multiple group comparison in *in vivo* and *ex vivo* assays was accomplished with one- or two-way analysis of variance (ANOVA). For single comparison, unpaired two-tailed Student's t test was used, unless otherwise denoted. In cases of non-Gaussian distribution, nonparametric t-test was used. Survival and tumor growth in *in vivo* implantable tumor models are presented as Kaplan–Meier survival curves and plotted tumor area with respect to time and were statistically analyzed using log rank test. All

analysis was completed with on Prism v5 software (GraphPad). A value of $P < 0.05$ is statistically significant. In the figures, standard designations of significance were given; *$p < 0.05$; **$p < 0.01$; ***$p < 0.001$ and ****$p < 0.0001$. The specific analysis used per figure in the manuscript can be found within the legends.

Data availability

RNA sequencing data that support the findings of this study (Fig. 5b, h) have been deposited in GEO with the GSE158801 accession code. The authors declare that the data supporting the findings of this study are available within the paper and its supplementary information files.

Bibliography

1. Wang, H., Franco, F. & Ho, P.-C. Metabolic regulation of tregs in cancer: opportunities for immunotherapy. *Trends Cancer* **3,** 583–592 (2017).

2. *Sakaguchi, S., Yamaguchi, T., Nomura, T. & Ono, M. Regulatory T cells and immune tolerance. Cell **133,** 775–787 (2008).*

3. *Hanahan, D. & Weinberg, R. A. Hallmarks of cancer: the next generation. Cell **144,** 646–674 (2011).*

4. *Scharping, N. E. et al. The tumor microenvironment represses T cell mitochondrial biogenesis to drive intratumoral T cell metabolic insufficiency and dysfunction. Immunity **45,** 374–388 (2016).*

5. *Najjar, Y. G. et al. Tumor cell oxidative metabolism as a barrier to PD-1 blockade immunotherapy in melanoma. JCI Insight **4,** (2019).*

6. *Ho, P.-C. et al. Phosphoenolpyruvate Is a Metabolic Checkpoint of Anti-tumor T Cell Responses. Cell **162,** 1217–1228 (2015).*

7. *Wang, D. et al. Targeting EZH2 reprograms intratumoral regulatory T cells to enhance cancer immunity. Cell Rep. **23,** 3262–3274 (2018).*

8. *Delgoffe, G. M. et al. Stability and function of regulatory T cells is maintained by a neuropilin-1-semaphorin-4a axis. Nature **501,** 252–256 (2013).*

9. *Michalek, R. D. et al. Cutting edge: distinct glycolytic and lipid oxidative metabolic programs are essential for effector and regulatory CD4+ T cell subsets. J. Immunol. **186,** 3299–3303 (2011).*

10. *Gerriets, V. A. et al. Foxp3 and Toll-like receptor signaling balance T reg cell anabolic metabolism for suppression. Nat. Immunol. **17,** 1459 (2016).*

11. *Weinberg, S. E. et al. Mitochondrial complex III is essential for suppressive function of regulatory T cells. Nature **565,** 495–499 (2019).*

12. *Kim, J. & Dang, C. V. Cancer's molecular sweet tooth and the Warburg effect. Cancer Res. **66,** 8927–8930 (2006).*

13. *Warburg, O. On the Origin of Cancer Cells. Science **123,** 309–314 (1956).*

14. *Lunt, S. Y. & Vander Heiden, M. G. Aerobic glycolysis: meeting the metabolic requirements of cell proliferation. Annu. Rev. Cell Dev. Biol. **27,** 441–464 (2011).*

15. *Romero-Garcia, S., Lopez-Gonzalez, J. S., Báez-Viveros, J. L., Aguilar-Cazares, D. & Prado-Garcia, H. Tumor cell metabolism: an integral view. Cancer Biol. Ther.* ***12,*** *939–948 (2011).*

16. *Kim, J. & DeBerardinis, R. J. Mechanisms and implications of metabolic heterogeneity in cancer. Cell Metab.* ***30,*** *434–446 (2019).*

17. *Reznik, E. et al. A Landscape of Metabolic Variation across Tumor Types. Cell Syst.* ***6,*** *301–313.e3 (2018).*

18. *Walenta, S. et al. High lactate levels predict likelihood of metastases, tumor recurrence, and restricted patient survival in human cervical cancers. Cancer Res.* ***60,*** *916–921 (2000).*

19. *Brizel, D. M. et al. Elevated tumor lactate concentrations predict for an increased risk of metastases in head-and-neck cancer. Int. J. Radiat. Oncol. Biol. Phys.* ***51,*** *349–353 (2001).*

20. *Cheung, S. M. et al. Lactate concentration in breast cancer using advanced magnetic resonance spectroscopy. Br. J. Cancer* ***123,*** *261–267 (2020).*

21. *Blatt, S. et al. Lactate as a predictive marker for tumor recurrence in patients with head and neck squamous cell carcinoma (HNSCC) post radiation: a prospective study over 15 years. Clin. Oral Investig.* ***20,*** *2097–2104 (2016).*

22. *Fulham, M. J. et al. Mapping of brain tumor metabolites with proton MR spectroscopic imaging: clinical relevance. Radiology* ***185,*** *675–686 (1992).*

23. *Yokota, H. et al. Lactate, choline, and creatine levels measured by vitro 1H-MRS as prognostic parameters in patients with non-small-cell lung cancer. J. Magn. Reson. Imaging* ***25,*** *992–999 (2007).*

24. *Hui, S. et al. Glucose feeds the TCA cycle via circulating lactate. Nature* ***551,*** *115–118 (2017).*

25. *Angelin, A. et al. Foxp3 Reprograms T Cell Metabolism to Function in Low-Glucose, High-Lactate Environments. Cell Metab.* ***25,*** *1282–1293.e7 (2017).*

26. *Watson, M. J. et al. Metabolic support of tumour-infiltrating regulatory T cells by lactic acid. Nature (2021).*

27. *Ma, E. H. et al. Metabolic profiling using stable isotope tracing reveals distinct patterns of glucose utilization by physiologically activated CD8+ T cells. Immunity* ***51,*** *856–870.e5 (2019).*

28. *Sun, S., Li, H., Chen, J. & Qian, Q. Lactic Acid: No Longer an Inert and End-Product of Glycolysis. Physiology (Bethesda)* ***32,*** *453–463 (2017).*

29. *Morita, N. et al. GPR31-dependent dendrite protrusion of intestinal CX3CR1+ cells by bacterial metabolites. Nature **566,** 110–114 (2019).*

30. *Garrote, G. L., Abraham, A. G. & Rumbo, M. Is lactate an undervalued functional component of fermented food products? Front. Microbiol. **6,** 629 (2015).*

31. *Fischer, K. et al. Inhibitory effect of tumor cell-derived lactic acid on human T cells. Blood **109,** 3812–3819 (2007).*

32. *Menk, A. V. et al. Early TCR signaling induces rapid aerobic glycolysis enabling distinct acute T cell effector functions. Cell Rep. **22,** 1509–1521 (2018).*

33. *Chang, C.-H. et al. Posttranscriptional control of T cell effector function by aerobic glycolysis. Cell **153,** 1239–1251 (2013).*

34. *Cham, C. M., Driessens, G., O'Keefe, J. P. & Gajewski, T. F. Glucose deprivation inhibits multiple key gene expression events and effector functions in CD8+ T cells. Eur. J. Immunol. **38,** 2438–2450 (2008).*

35. *Wang, T. et al. Inosine is an alternative carbon source for CD8+-T-cell function under glucose restriction. Nat. Metab. **2,** 635–647 (2020).*

36. *Sukumar, M. et al. Inhibiting glycolytic metabolism enhances CD8+ T cell memory and antitumor function. J. Clin. Invest. **123,** 4479–4488 (2013).*

37. *Quinn, W. J. et al. Lactate limits T cell proliferation via the NAD(H) redox state. Cell Rep. **33,** 108500 (2020).*

38. *Halestrap, A. P. & Wilson, M. C. The monocarboxylate transporter family--role and regulation. IUBMB Life **64,** 109–119 (2012).*

39. *Brand, A. et al. LDHA-Associated Lactic Acid Production Blunts Tumor Immunosurveillance by T and NK Cells. Cell Metab. **24,** 657–671 (2016).*

40. *Andrienko, T. N., Pasdois, P., Pereira, G. C., Ovens, M. J. & Halestrap, A. P. The role of succinate and ROS in reperfusion injury - A critical appraisal. J. Mol. Cell Cardiol. **110,** 1–14 (2017).*

41. *Prag, H. A. et al. Mechanism of succinate efflux upon reperfusion of the ischaemic heart. Cardiovasc. Res. **117,** 1188–1201 (2021).*

42. *Wu, J.-Y. et al. Cancer-Derived Succinate Promotes Macrophage Polarization and Cancer Metastasis via Succinate Receptor. Mol. Cell **77,** 213–227.e5 (2020).*

43. *Dalla Pozza, E. et al. Regulation of succinate dehydrogenase and role of succinate in cancer. Semin. Cell Dev. Biol. **98,** 4–14 (2020).*

44. *Reinfeld, B. I. et al. Cell-programmed nutrient partitioning in the tumour microenvironment. Nature **593,** 282–288 (2021).*

45. *Macintyre, A. N. et al. The glucose transporter Glut1 is selectively essential for CD4 T cell activation and effector function. Cell Metab. **20,** 61–72 (2014).*

46. *Lim, S. A. et al. Lipid signalling enforces functional specialization of Treg cells in tumours. Nature **591,** 306–311 (2021).*

47. *Colegio, O. R. et al. Functional polarization of tumour-associated macrophages by tumour-derived lactic acid. Nature **513,** 559–563 (2014).*

48. *Duan, Z. & Luo, Y. Targeting macrophages in cancer immunotherapy. Signal Transduct. Target. Ther. **6,** 127 (2021).*

49. *Zhang, D. et al. Metabolic regulation of gene expression by histone lactylation. Nature **574,** 575–580 (2019).*

50. *Routy, J.-P., Routy, B., Graziani, G. M. & Mehraj, V. The Kynurenine Pathway Is a Double-Edged Sword in Immune-Privileged Sites and in Cancer: Implications for Immunotherapy. Int. J. Tryptophan Res. **9,** 67–77 (2016).*

51. *Moffett, J. R. & Namboodiri, M. A. Tryptophan and the immune response. Immunol. Cell Biol. **81,** 247–265 (2003).*

52. *Suzuki, S. et al. Expression of indoleamine 2,3-dioxygenase and tryptophan 2,3-dioxygenase in early concepti. Biochem. J. **355,** 425–429 (2001).*

53. *Britan, A., Maffre, V., Tone, S. & Drevet, J. R. Quantitative and spatial differences in the expression of tryptophan-metabolizing enzymes in mouse epididymis. Cell Tissue Res. **324,** 301–310 (2006).*

54. *Haber, R., Bessette, D., Hulihan-Giblin, B., Durcan, M. J. & Goldman, D. Identification of tryptophan 2,3-dioxygenase RNA in rodent brain. J. Neurochem. **60,** 1159–1162 (1993).*

55. *Ball, H. J. et al. Characterization of an indoleamine 2,3-dioxygenase-like protein found in humans and mice. Gene **396,** 203–213 (2007).*

56. *Qian, F. et al. Effects of 1-methyltryptophan stereoisomers on IDO2 enzyme activity and IDO2-mediated arrest of human T cell proliferation. Cancer Immunol. Immunother. **61,** 2013–2020 (2012).*

57. *Merlo, L. M. F. & Mandik-Nayak, L. IDO2: A pathogenic mediator of inflammatory autoimmunity. Clin. Med. Insights Pathol. **9,** 21–28 (2016).*

58. *Metz, R. et al. IDO2 is critical for IDO1-mediated T-cell regulation and exerts a non-redundant function in inflammation. Int. Immunol. **26,** 357–367 (2014).*

59. *Cheng, C.-W. et al. Indoleamine 2,3-dioxygenase, an immunomodulatory protein, is suppressed by (-)-epigallocatechin-3-gallate via blocking of gamma-interferon-induced JAK-PKC-delta-STAT1 signaling in human oral cancer cells. J. Agric. Food Chem.* ***58,*** *887–894 (2010).*

60. *Currier, A. R. et al. Tumor necrosis factor-alpha and lipopolysaccharide enhance interferon-induced antichlamydial indoleamine dioxygenase activity independently. J. Interferon Cytokine Res.* ***20,*** *369–376 (2000).*

61. *Robinson, C. M., Hale, P. T. & Carlin, J. M. The role of IFN-gamma and TNF-alpha-responsive regulatory elements in the synergistic induction of indoleamine dioxygenase. J. Interferon Cytokine Res.* ***25,*** *20–30 (2005).*

62. *Wang, X.-F. et al. The role of indoleamine 2,3-dioxygenase (IDO) in immune tolerance: focus on macrophage polarization of THP-1 cells. Cell Immunol.* ***289,*** *42–48 (2014).*

63. *Munn, D. H. et al. Prevention of allogeneic fetal rejection by tryptophan catabolism. Science* ***281,*** *1191–1193 (1998).*

64. *Munn, D. H. et al. GCN2 kinase in T cells mediates proliferative arrest and anergy induction in response to indoleamine 2,3-dioxygenase. Immunity* ***22,*** *633–642 (2005).*

65. *Fallarino, F. et al. The combined effects of tryptophan starvation and tryptophan catabolites down-regulate T cell receptor zeta-chain and induce a regulatory phenotype in naive T cells. J. Immunol.* ***176,*** *6752–6761 (2006).*

66. *Barroso, A., Mahler, J. V., Fonseca-Castro, P. H. & Quintana, F. J. Therapeutic induction of tolerogenic dendritic cells via aryl hydrocarbon receptor signaling. Curr. Opin. Immunol.* ***70,*** *33–39 (2021).*

67. *Ravishankar, B. et al. The amino acid sensor GCN2 inhibits inflammatory responses to apoptotic cells promoting tolerance and suppressing systemic autoimmunity. Proc. Natl. Acad. Sci. USA* ***112,*** *10774–10779 (2015).*

68. *Quintana, F. J. et al. Control of T(reg) and T(H)17 cell differentiation by the aryl hydrocarbon receptor. Nature* ***453,*** *65–71 (2008).*

69. *Mezrich, J. D. et al. An interaction between kynurenine and the aryl hydrocarbon receptor can generate regulatory T cells. J. Immunol.* ***185,*** *3190–3198 (2010).*

70. *Dagenais-Lussier, X. et al. Kynurenine Reduces Memory CD4 T-Cell Survival by Interfering with Interleukin-2 Signaling Early during HIV-1 Infection. J. Virol.* ***90,*** *7967–7979 (2016).*

71. *Brochez, L., Chevolet, I. & Kruse, V. The rationale of indoleamine 2,3-dioxygenase inhibition for cancer therapy. Eur. J. Cancer* ***76,*** *167–182 (2017).*

72. *Wei, L. et al. High Indoleamine 2,3-Dioxygenase Is Correlated With Microvessel Density and Worse Prognosis in Breast Cancer. Front. Immunol.* ***9,*** *724 (2018).*

73. *Meireson, A. et al. Peritumoral endothelial indoleamine 2, 3-dioxygenase expression is an early independent marker of disease relapse in colorectal cancer and is influenced by DNA mismatch repair profile. Oncotarget* ***9,*** *25216–25224 (2018).*

74. *Yu, C.-P. et al. The Clinicopathological and Prognostic Significance of IDO1 Expression in Human Solid Tumors: Evidence from a Systematic Review and Meta-Analysis. Cell Physiol. Biochem.* ***49,*** *134–143 (2018).*

75. *Kim, D., Kim, J. M., Kim, J.-S., Kim, S. & Kim, K.-H. Differential Expression and Clinicopathological Significance of HER2, Indoleamine 2,3-Dioxygenase and PD-L1 in Urothelial Carcinoma of the Bladder. J Clin Med* ***9,*** *(2020).*

76. *Liu, Y. et al. Tumor-Repopulating Cells Induce PD-1 Expression in CD8+ T Cells by Transferring Kynurenine and AhR Activation. Cancer Cell* ***33,*** *480–494.e7 (2018).*

77. *Sinclair, L. V., Neyens, D., Ramsay, G., Taylor, P. M. & Cantrell, D. A. Single cell analysis of kynurenine and System L amino acid transport in T cells. Nat. Commun.* ***9,*** *1981 (2018).*

78. *Hascitha, J. et al. Analysis of Kynurenine/Tryptophan ratio and expression of IDO1 and 2 mRNA in tumour tissue of cervical cancer patients. Clin. Biochem.* ***49,*** *919–924 (2016).*

79. *Triplett, T. A. et al. Reversal of indoleamine 2,3-dioxygenase-mediated cancer immune suppression by systemic kynurenine depletion with a therapeutic enzyme. Nat. Biotechnol.* ***36,*** *758–764 (2018).*

80. *Muz, B., de la Puente, P., Azab, F. & Azab, A. K. The role of hypoxia in cancer progression, angiogenesis, metastasis, and resistance to therapy. Hypoxia (Auckl)* ***3,*** *83–92 (2015).*

81. *Szatrowski, T. P. & Nathan, C. F. Production of large amounts of hydrogen peroxide by human tumor cells. Cancer Res.* ***51,*** *794–798 (1991).*

82. *Vijayan, D., Young, A., Teng, M. W. L. & Smyth, M. J. Targeting immunosuppressive adenosine in cancer. Nat. Rev. Cancer* ***17,*** *709–724 (2017).*

83. *Sena, L. A. & Chandel, N. S. Physiological roles of mitochondrial reactive oxygen species. Mol. Cell* ***48,*** *158–167 (2012).*

84. *Sabharwal, S. S. & Schumacker, P. T. Mitochondrial ROS in cancer: initiators, amplifiers or an Achilles' heel? Nat. Rev. Cancer* ***14,*** *709–721 (2014).*

85. *Reczek, C. R. & Chandel, N. S. The two faces of reactive oxygen species in cancer. Annu. Rev. Cancer Biol.* ***1,*** *79–98 (2017).*

86. *Blay, J., White, T. D. & Hoskin, D. W. The extracellular fluid of solid carcinomas contains immunosuppressive concentrations of adenosine. Cancer Res.* ***57,*** *2602–2605 (1997).*

87. *Busse, M. & Vaupel, P. Accumulation of purine catabolites in solid tumors exposed to therapeutic hyperthermia. Experientia* ***52,*** *469–473 (1996).*

88. *Stagg, J. & Smyth, M. J. Extracellular adenosine triphosphate and adenosine in cancer. Oncogene* ***29,*** *5346–5358 (2010).*

89. *Ohta, A. A metabolic immune checkpoint: adenosine in tumor microenvironment. Front. Immunol.* ***7,*** *109 (2016).*

90. *Flannagan, R. S., Cosío, G. & Grinstein, S. Antimicrobial mechanisms of phagocytes and bacterial evasion strategies. Nat. Rev. Microbiol.* ***7,*** *355–366 (2009).*

91. *Hattori, H. et al. Small-molecule screen identifies reactive oxygen species as key regulators of neutrophil chemotaxis. Proc. Natl. Acad. Sci. USA* ***107,*** *3546–3551 (2010).*

92. *Rutault, K., Alderman, C., Chain, B. M. & Katz, D. R. Reactive oxygen species activate human peripheral blood dendritic cells. Free Radic. Biol. Med.* ***26,*** *232–238 (1999).*

93. *Kantengwa, S., Jornot, L., Devenoges, C. & Nicod, L. P. Superoxide anions induce the maturation of human dendritic cells. Am. J. Respir. Crit. Care Med.* ***167,*** *431–437 (2003).*

94. *Oberkampf, M. et al. Mitochondrial reactive oxygen species regulate the induction of CD8+ T cells by plasmacytoid dendritic cells. Nat. Commun.* ***9,*** *2241 (2018).*

95. *Sena, L. A. et al. Mitochondria are required for antigen-specific T cell activation through reactive oxygen species signaling. Immunity* ***38,*** *225–236 (2013).*

96. *Gelderman, K. A. et al. Macrophages suppress T cell responses and arthritis development in mice by producing reactive oxygen species. J. Clin. Invest.* ***117,*** *3020–3028 (2007).*

97. *Pizzolla, A. et al. CD68-expressing cells can prime T cells and initiate autoimmune arthritis in the absence of reactive oxygen species. Eur. J. Immunol.* ***41,*** *403–412 (2011).*

98. *Kobayashi, S. D. et al. Gene expression profiling provides insight into the pathophysiology of chronic granulomatous disease. J. Immunol.* ***172,*** *636–643 (2004).*

99. *Scharping, N. E., Menk, A. V., Whetstone, R. D., Zeng, X. & Delgoffe, G. M. Efficacy of PD-1 Blockade Is Potentiated by Metformin-Induced Reduction of Tumor Hypoxia. Cancer Immunol Res* ***5,*** *9–16 (2017).*

100. *Scharping, N. E. et al. Mitochondrial stress induced by continuous stimulation under hypoxia rapidly drives T cell exhaustion. Nat. Immunol.* ***22,*** *205–215 (2021).*

101. *Nagaraj, S. et al. Altered recognition of antigen is a mechanism of CD8+ T cell tolerance in cancer. Nat. Med.* ***13,*** *828–835 (2007).*

102. *Kraaij, M. D. et al. Induction of regulatory T cells by macrophages is dependent on production of reactive oxygen species. Proc. Natl. Acad. Sci. USA* ***107,*** *17686–17691 (2010).*

103. *Yu, X. et al. SENP3 maintains the stability and function of regulatory T cells via BACH2 deSUMOylation. Nat. Commun.* ***9,*** *3157 (2018).*

104. *Ohl, K. & Tenbrock, K. Reactive Oxygen Species as Regulators of MDSC-Mediated Immune Suppression. Front. Immunol.* ***9,*** *2499 (2018).*

105. *Ohl, K. et al. Nrf2 Is a Central Regulator of Metabolic Reprogramming of Myeloid-Derived Suppressor Cells in Steady State and Sepsis. Front. Immunol.* ***9,*** *1552 (2018).*

106. *Corzo, C. A. et al. Mechanism regulating reactive oxygen species in tumor-induced myeloid-derived suppressor cells. J. Immunol.* ***182,*** *5693–5701 (2009).*

107. *Synnestvedt, K. et al. Ecto-5'-nucleotidase (CD73) regulation by hypoxia-inducible factor-1 mediates permeability changes in intestinal epithelia. J. Clin. Invest.* ***110,*** *993–1002 (2002).*

108. *Kong, T., Westerman, K. A., Faigle, M., Eltzschig, H. K. & Colgan, S. P. HIF-dependent induction of adenosine A2B receptor in hypoxia. FASEB J.* ***20,*** *2242–2250 (2006).*

109. *Tak, E. et al. Protective role of hypoxia-inducible factor-1α-dependent CD39 and CD73 in fulminant acute liver failure. Toxicol. Appl. Pharmacol.* ***314,*** *72–81 (2017).*

110. *Ohta, A. & Sitkovsky, M. Role of G-protein-coupled adenosine receptors in downregulation of inflammation and protection from tissue damage. Nature* ***414,*** *916–920 (2001).*

111. *Ohta, A. et al. A2A adenosine receptor protects tumors from antitumor T cells. Proc. Natl. Acad. Sci. USA* ***103,*** *13132–13137 (2006).*

112. *Vecchio, E. A. et al. Ligand-Independent Adenosine A2B Receptor Constitutive Activity as a Promoter of Prostate Cancer Cell Proliferation. J. Pharmacol. Exp. Ther.* ***357,*** *36–44 (2016).*

113. *Canale, F. P. et al. CD39 Expression Defines Cell Exhaustion in Tumor-Infiltrating CD8+ T Cells. Cancer Res.* ***78,*** *115–128 (2018).*

114. *Vignali, D. A. A., Collison, L. W. & Workman, C. J. How regulatory T cells work. Nat. Rev. Immunol.* ***8,*** *523–532 (2008).*

115. *Petrelli, F. et al. Prognostic and predictive role of elevated lactate dehydrogenase in patients with melanoma treated with immunotherapy and BRAF inhibitors: a systematic review and meta-analysis. Melanoma Res* ***29,*** *1–12 (2019).*

116. *Hodi, F. S. et al. Nivolumab plus ipilimumab or nivolumab alone versus ipilimumab alone in advanced melanoma (CheckMate 067): 4-year outcomes of a multicentre, randomised, phase 3 trial. Lancet Oncol.* ***19,*** *1480–1492 (2018).*

117. *Larkin, J. et al. 3303 Efficacy and safety in key patient subgroups of nivolumab (NIVO) alone or combined with ipilimumab (IPI) versus IPI alone in treatment-naïve patients with advanced melanoma (MEL) (CheckMate 067). Eur. J. Cancer* ***51,*** *S664–S665 (2015).*

118. *Zappasodi, R. et al. CTLA-4 blockade drives loss of Treg stability in glycolysis-low tumours. Nature* ***591,*** *652–658 (2021).*

119. *Cascone, T. et al. Increased tumor glycolysis characterizes immune resistance to adoptive T cell therapy. Cell Metab.* ***27,*** *977–987.e4 (2018).*

120. *Gottfried, E. et al. New aspects of an old drug--diclofenac targets MYC and glucose metabolism in tumor cells. PLoS One* ***8,*** *e66987 (2013).*

121. *Renner, K. et al. Restricting glycolysis preserves T cell effector functions and augments checkpoint therapy. Cell Rep.* ***29,*** *135–150.e9 (2019).*

122. *Lin, X., Xiao, Z., Chen, T., Liang, S. H. & Guo, H. Glucose metabolism on tumor plasticity, diagnosis, and treatment. Front. Oncol.* ***10,*** *317 (2020).*

123. *Beloueche-Babari, M. et al. Monocarboxylate transporter 1 blockade with AZD3965 inhibits lipid biosynthesis and increases tumour immune cell infiltration. Br. J. Cancer* ***122,*** *895–903 (2020).*

124. *Corbet, C. et al. Interruption of lactate uptake by inhibiting mitochondrial pyruvate transport unravels direct antitumor and radiosensitizing effects. Nat. Commun.* ***9,*** *1208 (2018).*

125. *Draoui, N. et al. Antitumor activity of 7-aminocarboxycoumarin derivatives, a new class of potent inhibitors of lactate influx but not efflux. Mol. Cancer Ther.* ***13,*** *1410–1418 (2014).*

126. *Benjamin, D. et al. Dual Inhibition of the Lactate Transporters MCT1 and MCT4 Is Synthetic Lethal with Metformin due to NAD+ Depletion in Cancer Cells. Cell Rep.* ***25,*** *3047–3058.e4 (2018).*

127. *Yang, M., Zhong, X. & Yuan, Y. Does baking soda function as a magic bullet for patients with cancer? A mini review. Integr. Cancer Ther.* ***19,*** *1534735420922579 (2020).*

128. *Pötzl, J. et al. Reversal of tumor acidosis by systemic buffering reactivates NK cells to express IFN-γ and induces NK cell-dependent lymphoma control without other immunotherapies. Int. J. Cancer* ***140,*** *2125–2133 (2017).*

129. *Pilon-Thomas, S. et al. Neutralization of tumor acidity improves antitumor responses to immunotherapy. Cancer Res.* ***76,*** *1381–1390 (2016).*

130. *Walton, Z. E. et al. Acid Suspends the Circadian Clock in Hypoxia through Inhibition of mTOR. Cell* ***174,*** *72–87.e32 (2018).*

131. *Röhrig, U. F., Majjigapu, S. R., Vogel, P., Zoete, V. & Michielin, O. Challenges in the Discovery of Indoleamine 2,3-Dioxygenase 1 (IDO1) Inhibitors. J. Med. Chem.* ***58,*** *9421–9437 (2015).*

132. *Holmgaard, R. B., Zamarin, D., Munn, D. H., Wolchok, J. D. & Allison, J. P. Indoleamine 2,3-dioxygenase is a critical resistance mechanism in antitumor T cell immunotherapy targeting CTLA-4. J. Exp. Med.* ***210,*** *1389–1402 (2013).*

133. *Spranger, S. et al. Mechanism of tumor rejection with doublets of CTLA-4, PD-1/PD-L1, or IDO blockade involves restored IL-2 production and proliferation of CD8(+) T cells directly within the tumor microenvironment. J. Immunother. Cancer* ***2,*** *3 (2014).*

134. *Sarrouilhe, D. & Mesnil, M. Serotonin and human cancer: A critical view. Biochimie* ***161,*** *46–50 (2019).*

135. *Wu, H., Denna, T. H., Storkersen, J. N. & Gerriets, V. A. Beyond a neurotransmitter: The role of serotonin in inflammation and immunity. Pharmacol. Res.* ***140,*** *100–114 (2019).*

136. *Afzal, M. Z., Mercado, R. R. & Shirai, K. Efficacy of metformin in combination with immune checkpoint inhibitors (anti-PD-1/anti-CTLA-4) in metastatic malignant melanoma. J. Immunother. Cancer* ***6,*** *64 (2018).*

137. *Horikawa, N. et al. Expression of Vascular Endothelial Growth Factor in Ovarian Cancer Inhibits Tumor Immunity through the Accumulation of Myeloid-Derived Suppressor Cells. Clin. Cancer Res.* ***23,*** *587–599 (2017).*

138. *Lee, W. S., Yang, H., Chon, H. J. & Kim, C. Combination of anti-angiogenic therapy and immune checkpoint blockade normalizes vascular-immune crosstalk to potentiate cancer immunity. Exp Mol Med* ***52,*** *1475–1485 (2020).*

139. *Huang, Y. et al. Vascular normalizing doses of antiangiogenic treatment reprogram the immunosuppressive tumor microenvironment and enhance immunotherapy. Proc. Natl. Acad. Sci. USA **109,** 17561–17566 (2012).*

140. *Rini, B. I. et al. Pembrolizumab plus Axitinib versus Sunitinib for Advanced Renal-Cell Carcinoma. N. Engl. J. Med. **380,** 1116–1127 (2019).*

141. *Cheng, A. L., Qin, S. & Ikeda, M. Efficacy and safety results from a ph III study evaluating atezolizumab (atezo)+ bevacizumab (bev) vs sorafenib (Sor) as first treatment (tx) for patietns (pts) ….*

142. *Deng, H. et al. Targeted scavenging of extracellular ROS relieves suppressive immunogenic cell death. Nat. Commun. **11,** 4951 (2020).*

143. *Reisman, S. A., Lee, C.-Y. I., Meyer, C. J., Proksch, J. W. & Ward, K. W. Topical application of the synthetic triterpenoid RTA 408 activates Nrf2 and induces cytoprotective genes in rat skin. Arch Dermatol Res **306,** 447–454 (2014).*

144. *Reisman, S. A. et al. Topical application of the synthetic triterpenoid RTA 408 protects mice from radiation-induced dermatitis. Radiat Res **181,** 512–520 (2014).*

145. *Probst, B. L. et al. RTA 408, A Novel Synthetic Triterpenoid with Broad Anticancer and Anti-Inflammatory Activity. PLoS One **10,** e0122942 (2015).*

146. *Churov, A. & Zhulai, G. Targeting adenosine and regulatory T cells in cancer immunotherapy. Hum. Immunol. (2021). doi:10.1016/j.humimm.2020.12.005*

147. *Geoghegan, J. C. et al. Inhibition of CD73 AMP hydrolysis by a therapeutic antibody with a dual, non-competitive mechanism of action. MAbs **8,** 454–467 (2016).*

148. *Kashyap, A. S. et al. Antisense oligonucleotide targeting CD39 improves anti-tumor T cell immunity. J. Immunother. Cancer **7,** 67 (2019).*

149. *Wei, J. et al. Targeting REGNASE-1 programs long-lived effector T cells for cancer therapy. Nature **576,** 471–476 (2019).*

150. *Cantor, J. R. The rise of physiologic media. Trends Cell Biol. **29,** 854–861 (2019).*

151. *Slack, M., Wang, T. & Wang, R. T cell metabolic reprogramming and plasticity. Mol. Immunol. **68,** 507–512 (2015).*

152. *Nabe, S. et al. Reinforce the antitumor activity of CD8+ T cells via glutamine restriction. Cancer Sci. **109,** 3737–3750 (2018).*

153. *Ramsdell, F. Foxp3 and natural regulatory T cells: key to a cell lineage? Immunity **19,** 165–168 (2003).*

154. *Tanaka, A. & Sakaguchi, S. Regulatory T cells in cancer immunotherapy. Cell Res.* ***27,*** *109–118 (2017).*

155. *Rubtsov, Y. P. et al. Regulatory T cell-derived interleukin-10 limits inflammation at environmental interfaces. Immunity* ***28,*** *546–558 (2008).*

156. *Rubtsov, Y. P. et al. Stability of the regulatory T cell lineage in vivo. Science* ***329,*** *1667–1671 (2010).*

157. *Pacholczyk, R., Ignatowicz, H., Kraj, P. & Ignatowicz, L. Origin and T cell receptor diversity of Foxp3+CD4+CD25+ T cells. Immunity* ***25,*** *249–259 (2006).*

158. *Lee, H.-M., Bautista, J. L., Scott-Browne, J., Mohan, J. F. & Hsieh, C.-S. A broad range of self-reactivity drives thymic regulatory T cell selection to limit responses to self. Immunity* ***37,*** *475–486 (2012).*

159. *Apostolou, I., Sarukhan, A., Klein, L. & von Boehmer, H. Origin of regulatory T cells with known specificity for antigen. Nat. Immunol.* ***3,*** *756–763 (2002).*

160. *Sinclair, L. V., Barthelemy, C. & Cantrell, D. A. Single cell glucose uptake assays: A cautionary tale. Immunometabolism* ***2,*** *e200029 (2020).*

161. *Xu, H. et al. Cyanine-based 1-amino-1-deoxyglucose as fluorescent probes for glucose transporter mediated bioimaging. Biochem. Biophys. Res. Commun.* ***474,*** *240–246 (2016).*

162. *Overacre-Delgoffe, A. E. et al. Interferon-γ Drives Treg Fragility to Promote Anti-tumor Immunity. Cell* ***169,*** *1130–1141.e11 (2017).*

163. *D'Alise, A. M., Ergun, A., Hill, J. A., Mathis, D. & Benoist, C. A cluster of coregulated genes determines TGF-beta-induced regulatory T-cell (Treg) dysfunction in NOD mice. Proc. Natl. Acad. Sci. USA* ***108,*** *8737–8742 (2011).*

164. *Li, L. et al. TLR8-Mediated Metabolic Control of Human Treg Function: A Mechanistic Target for Cancer Immunotherapy. Cell Metab.* ***29,*** *103–123.e5 (2019).*

165. *Procaccini, C. et al. The proteomic landscape of human ex vivo regulatory and conventional T cells reveals specific metabolic requirements. Immunity* ***44,*** *406–421 (2016).*

166. *Priyadharshini, B. et al. Cutting Edge: TGF-β and Phosphatidylinositol 3-Kinase Signals Modulate Distinct Metabolism of Regulatory T Cell Subsets. J. Immunol.* ***201,*** *2215–2219 (2018).*

167. *Gorby, C. et al. Engineered IL-10 variants elicit potent immunomodulatory effects at low ligand doses. Sci. Signal.* ***13,*** *(2020).*

168. *Oft, M. Immune regulation and cytotoxic T cell activation of IL-10 agonists - Preclinical and clinical experience. Semin. Immunol.* ***44,*** *101325 (2019).*

169. *Johanns, T. M., Ertelt, J. M., Rowe, J. H. & Way, S. S. Regulatory T cell suppressive potency dictates the balance between bacterial proliferation and clearance during persistent Salmonella infection. PLoS Pathog.* ***6,*** *e1001043 (2010).*

170. *Varanasi, S. K., Donohoe, D., Jaggi, U. & Rouse, B. T. Manipulating Glucose Metabolism during Different Stages of Viral Pathogenesis Can Have either Detrimental or Beneficial Effects. J. Immunol.* ***199,*** *1748–1761 (2017).*

171. *Zheng, Y. et al. Role of conserved non-coding DNA elements in the Foxp3 gene in regulatory T-cell fate. Nature* ***463,*** *808–812 (2010).*

172. *Simpson, I. A. et al. The facilitative glucose transporter GLUT3: 20 years of distinction. Am. J. Physiol. Endocrinol. Metab.* ***295,*** *E242–53 (2008).*

173. *Zhao, M. & Zhang, Z. Glucose transporter regulation in cancer: A profile and the loops. Crit. Rev. Eukaryot. Gene Expr.* ***26,*** *223–238 (2016).*

174. *Romero-Garcia, S., Moreno-Altamirano, M. M. B., Prado-Garcia, H. & Sánchez-García, F. J. Lactate contribution to the tumor microenvironment: mechanisms, effects on immune cells and therapeutic relevance. Front. Immunol.* ***7,*** *52 (2016).*

175. *Liu, C. et al. Lactate inhibits lipolysis in fat cells through activation of an orphan G-protein-coupled receptor, GPR81. J. Biol. Chem.* ***284,*** *2811–2822 (2009).*

176. *Jackson, V. N. & Halestrap, A. P. The kinetics, substrate, and inhibitor specificity of the monocarboxylate (lactate) transporter of rat liver cells determined using the fluorescent intracellular pH indicator, 2',7'-bis(carboxyethyl)-5(6)-carboxyfluorescein. J. Biol. Chem.* ***271,*** *861–868 (1996).*

177. *Zhang, X., Yang, S., Chen, J. & Su, Z. Unraveling the regulation of hepatic gluconeogenesis. Front. Endocrinol. (Lausanne)* ***9,*** *802 (2018).*

178. *O'Neill, L. A. J., Kishton, R. J. & Rathmell, J. A guide to immunometabolism for immunologists. Nat. Rev. Immunol.* ***16,*** *553–565 (2016).*

179. *Robinson, B. H. & Oei, J. 3-Mercaptopicolinic acid, a preferential inhibitor of the cytosolic phosphoenolpyruvate carboxykinase. FEBS Lett.* ***58,*** *12–15 (1975).*

180. *Raffin, C., Vo, L. T. & Bluestone, J. A. Treg cell-based therapies: challenges and perspectives. Nat. Rev. Immunol.* ***20,*** *158–172 (2020).*

181. *Gómez-Valadés, A. G. et al. Overcoming diabetes-induced hyperglycemia through inhibition of hepatic phosphoenolpyruvate carboxykinase (GTP) with RNAi. Mol. Ther.* ***13,*** *401–410 (2006).*

182. *Lowther, D. E. et al. PD-1 marks dysfunctional regulatory T cells in malignant gliomas. JCI Insight **1,** (2016).*

183. *Consoli, A., Nurjhan, N., Reilly, J. J., Bier, D. M. & Gerich, J. E. Contribution of liver and skeletal muscle to alanine and lactate metabolism in humans. Am. J. Physiol. **259,** E677–84 (1990).*

184. *Proia, P., Di Liegro, C. M., Schiera, G., Fricano, A. & Di Liegro, I. Lactate as a metabolite and a regulator in the central nervous system. Int. J. Mol. Sci. **17,** (2016).*

185. *Arpaia, N. et al. Metabolites produced by commensal bacteria promote peripheral regulatory T-cell generation. Nature **504,** 451–455 (2013).*

186. *Smith, P. M. et al. The microbial metabolites, short-chain fatty acids, regulate colonic Treg cell homeostasis. Science **341,** 569–573 (2013).*

187. *Wu, D. et al. Glucose-regulated phosphorylation of TET2 by AMPK reveals a pathway linking diabetes to cancer. Nature **559,** 637–641 (2018).*

188. *Peng, M. et al. Aerobic glycolysis promotes T helper 1 cell differentiation through an epigenetic mechanism. Science **354,** 481–484 (2016).*

189. *Beier, U. H. et al. Sirtuin-1 targeting promotes Foxp3+ T-regulatory cell function and prolongs allograft survival. Mol. Cell. Biol. **31,** 1022–1029 (2011).*

190. *Kwon, H.-S. et al. Three novel acetylation sites in the Foxp3 transcription factor regulate the suppressive activity of regulatory T cells. J. Immunol. **188,** 2712–2721 (2012).*

191. *Kaya-Okur, H. S. et al. CUT&Tag for efficient epigenomic profiling of small samples and single cells. Nat. Commun. **10,** 1930 (2019).*

192. *Latham, T. et al. Lactate, a product of glycolytic metabolism, inhibits histone deacetylase activity and promotes changes in gene expression. Nucleic Acids Res. **40,** 4794–4803 (2012).*

193. *Dichtl, S. et al. Lactate and IL6 define separable paths of inflammatory metabolic adaptation. Sci. Adv. **7,** (2021).*

194. *Chapman, N. M. & Chi, H. mTOR signaling, Tregs and immune modulation. Immunotherapy **6,** 1295–1311 (2014).*

195. *Yang, B. H. et al. Foxp3(+) T cells expressing RORγt represent a stable regulatory T-cell effector lineage with enhanced suppressive capacity during intestinal inflammation. Mucosal Immunol. **9,** 444–457 (2016).*

196. *Jung, Y.-S. et al. CD200: association with cancer stem cell features and response to chemoradiation in head and neck squamous cell carcinoma. Head Neck **37,** 327–335 (2015).*

197. *Jha, M. K. et al. Monocarboxylate transporter 1 in Schwann cells is critical for maintenance of sensory nerve myelination during aging. BioRxiv (2019). doi:10.1101/686832*

198. *Lennon, G. P. et al. T cell islet accumulation in type 1 diabetes is a tightly regulated, cell-autonomous event. Immunity **31,** 643–653 (2009).*

199. *Ostanin, D. V. et al. T cell transfer model of chronic colitis: concepts, considerations, and tricks of the trade. Am. J. Physiol. Gastrointest. Liver Physiol. **296,** G135–46 (2009).*

200. *Martin, M. Cutadapt removes adapter sequences from high-throughput sequencing reads. EMBnet j. **17,** 10 (2011).*

201. *Delgoffe, G. M., Kole, T. P., Cotter, R. J. & Powell, J. D. Enhanced interaction between Hsp90 and raptor regulates mTOR signaling upon T cell activation. Mol. Immunol. **46,** 2694–2698 (2009).*